Modelling and Control of an Electrode System for a Three-Phase Electric Arc Furnace

by

Marius Peens

Submitted in partial fulfillment of the requirements for the degree

Master of Engineering (Electronic Engineering)

in the

Faculty of Engineering, the Built Environment and

Information Technology

UNIVERSITY OF PRETORIA

December 2004

Abstract

Title:	Modelling and Control of an Electrode System for a Three-phase Electric Arc Furnace
By:	Marius Peens
Supervisor:	Professor I.K. Craig
Department:	Department of Electrical, Electronic and Computer Engineering
Degree:	Master of Engineering(Electronic Engineering)

This dissertation investigates the control of the electrical energy input to a three-phase electric arc furnace (EAF). Graphite electrodes are used to convert electrical energy into heat via three-phase electric arcs. Constant arc length is desirable as it implies steady energy transfer from the graphite electrodes to the metallic charge in the furnace bath. With the charge level constantly changing, the electrodes must be able to adjust for the arc length to remain constant. In this dissertation electric arc current is used as the control variable. This is the most often used control variable in the electric arc furnace industry and implies fast adjustments of short circuits between the electrode tips and the metallic charge.

The motivation behind the modelling of the electrode system for a three-phase electric arc furnace is to extend an existing EAF model developed at the University of Pretoria. The existing model investigates the control of the electric arc furnace process itself and it is assumed that the applied electrical energy input is constant.

Proportional-Integral-Derivative (PID) control as well as Model-Predictive-Control (MPC) is applied to the electrode system. Time delays on the outputs of the hydraulic actuators makes it necessary to include approximations of time delays on the outputs of the linear model, which is needed for controller design. A well known general control problem is followed in this dissertation. All models are derived from first principles, and complete controller design is carried out. Most available literature lack in at least one of these fields.

Keywords: Electrodes, Electric Arc, Modelling, Hydraulic Actuator, Energy Input, Arc impedance, Arc current.

Contents

1 Introduction **1**
1.1 Background . . . 2
1.2 Dissertation Motivation . . . 4
1.3 Aims and Contributions . . . 6
1.4 Organization of the Dissertation . . . 8

2 Process Description **10**
2.1 Introduction . . . 10
2.2 Steel Production Overview . . . 11
2.2.1 Basic Steel Production Route . . . 11
2.2.2 Steel Production Statistics . . . 12
2.3 The Electric Arc Furnace Process . . . 12
2.3.1 Overview . . . 12
2.3.2 The Furnace Transformer and the Electrical Supply System . . . 15
2.3.3 Motivation and Background for Electrode Control . . . 18
2.3.4 Voltage and Current Measurements . . . 21
2.4 Electric Arc Furnace Production Flow . . . 22
2.4.1 Furnace Charging . . . 24
2.4.2 Melting . . . 25
2.4.3 Refining . . . 26
2.5 Conclusion . . . 27

3 Modelling **28**
3.1 Introduction . . . 28
3.2 The Electrical System . . . 29
3.2.1 The Electric Arc . . . 29
3.2.1.1 Physics of a High Current Electric Arc . . . 29
3.2.1.2 Radius Model for an Electric Arc . . . 30
3.2.1.3 Impedance Model for an Electric Arc . . . 32
3.2.2 The Electrical Supply System . . . 34
3.2.3 State Definitions and the Complete Electrical Model . . . 35
3.3 The Hydraulic Actuator . . . 38
3.4 Conclusion . . . 42

4 Model Simulation Results **44**
4.1 Introduction . . . 44
4.2 The Electrical System . . . 45
4.2.1 Constant Arc Length . . . 46
4.2.2 Variable Arc Length on a Single Phase . . . 50
4.2.3 Variable Arc Length on Multiple Phases . . . 55
4.3 The Hydraulic Actuator . . . 57
4.4 Electric and Hydraulic Models Connected Together . . . 60
4.5 Conclusion . . . 65

5 Linear Model Derivation **66**
5.1 Introduction . . . 66
5.2 The General Linearisation Problem . . . 67
5.2.1 State Space Models . . . 67
5.2.2 Obtaining the Linear Model . . . 67
5.3 Re-modelling and Adjustments on the Electrical Model . . . 69
5.3.1 Validation of Adjusted Electric Model . . . 71
5.3.1.1 Constant Arc Length . . . 72
5.3.1.2 Variable Arc Length on a Single Phase . . . 73
5.3.1.3 Variable Arc Length on Multiple Phases . . . 73
5.4 Re-modelling the Hydraulic Model . . . 75
5.5 The Linear Arc Furnace Model . . . 77
5.5.1 Simulation Results and Validation of the Linear Model . . . 78
5.6 Conclusion . . . 80

6 Controller Design **82**
6.1 Introduction . . . 82
6.2 PID Control . . . 83
6.2.1 PID Synthesis by Using Pole Assignment . . . 86
6.2.2 Controller Implementation on the Linear Model . . . 90
6.2.3 PID Controller Implementation on the Nonlinear Model . . . 93
6.2.3.1 Initial Controller Implementation . . . 93
6.2.3.2 PID Controller Tuning . . . 97
6.2.3.2.1 Frequency Domain Analysis . . . 97
6.2.3.2.2 Direct Inclusion of the Time Delay . . . 97
6.3 Model Predictive Control . . . 100
6.3.1 Background on Model Predictive Control . . . 100
6.3.2 Applying Model Predictive Control to the Three-phase Electric Arc Furnace Model . . . 101
6.4 Conclusion . . . 104

7 Industrial Measurements and Comparisons **107**
7.1 Introduction . . . 107
7.2 The Industrial Experiment . . . 108
7.3 Simulations . . . 111

8 Conclusion and Recommendations **118**
8.1 Introduction 118
8.2 Conclusion 118
8.3 Recommendations 120

A Controller Tuning and Controller Inputs and Outputs **129**
A.1 Initial PID Controller Outputs 129
A.2 Controller Tuning via Frequency Domain Analysis 129
A.3 Inputs and Outputs for the Tuned PID Controllers 135
A.4 Model Predictive Controller Outputs without Disturbance Rejection 136
A.5 Model Predictive Controller Outputs with Disturbance Rejection 142

Chapter 1

Introduction

This dissertation deals with the modelling and control of an electrode system for a three-phase electric arc furnace (EAF). Electric arc furnaces are used to produce steel by melting scrap together with some other raw materials using an electrical supply as the main energy input [1]. The graphite electrodes, connected to the electrical supply, are used to convert electrical energy into extensive heat by means of high current electric arcs drawn between the electrode tips and the metallic charge [2]. The electric arcs cause the solid scrap to be transformed into the liquid state [3]. The molten steel is then converted to a specified grade with the addition of chemical substances by means of oxygen blowing and carbon injection.

The main objective in an electric arc furnace industry is maximum production of high quality steel at the lowest possible cost ([4] and [5]). Electric current in the graphite electrodes will remain constant if the lengths of the electric arcs are constant [6]. Tap changes on the furnace transformer are the main source for controlling electrical power. However, constant arc lengths imply that the power input to the arc furnace load is stable around the set-point determined by the tap changer, which results in effective production. The electrode system under investigation in this dissertation is mainly responsible for the vertical adjustments of the electrode tip displacement according to specified set-points, to ensure that the arc lengths remain as constant as possible [7]. Arc current is mainly used as the control variable in an industrial electric arc furnace because of its direct relation with the lengths of the electric arcs and some other advantages.

Electric arc furnaces are normally characterized by the maximum capacity of steel, in tonnes, being produced during a single production phase [8]. Other parameters that characterize the electric arc furnace are power input capacity (MVA) and the type of electrical supply being used. EAF's are classified as either AC (Alternating-Current) or DC (Direct-Current) arc furnaces, depending on the type of electrical supply [9]. This dissertation focus mainly on AC arc furnaces or simply three-phase electric arc furnaces.

The remainder of this chapter outlines the motivation and contributions behind the modelling and control of an electrode system for a three-phase electric arc furnace. Some background on the electric arc furnace process and its development are also presented.

1.1 Background

The production of steel via electric arc furnaces started way back in 1800 when Humphrey Davy discovered a phenomenon called the carbon arc [10]. The first electric steel heat was cast by R. Lindenberg in Remcheid in 1906. This was the beginning of steel production via the electrical arc furnace route.

Capacities of the first three-phase electric arc furnaces were either a 5 ton or a 6 ton furnace [10]. The rated specific transformer capacity for these furnaces was only 170 to 230 kVA. In those days electricity and electrodes were highly expensive and low carbon steel was rarely produced via the electric arc furnace route. Alloy steels were the only products produced by EAF's almost until the end of the 1930's. Since then, steel production via electric arc furnaces has expanded dramatically. Some modern furnace capacities are rated above 100MW [11]. Electric arc furnaces with extremely high capacities are called ultra high electric arc furnaces and require up to 165MVA of electric power, with capacities of around 400 tonnes.

Over capacity of steel production has introduced much more industrial competition and factors, such as the quality of the produced steel, distinguish steel producers from each other [12]. With the emphasis of steel production shifting towards quality, advanced

control systems are becoming more and more popular in various sections in an electric arc furnace process.

The significant development seen in the electric arc furnace industry over the years is mainly due to greater demands for higher quality steel products [13]. Further expansion of the electric arc furnace process will occur [10], and this is resulting in a significant increase in research being undertaken in electric arc furnaces, specially in the field of control and automation.

Various factors have to be considered when automation is applied to the electric arc furnace process [14]. Some of the critical factors are:

- efficient usage of energy,
- efficient usage of the raw materials, and
- quality of the product.

Note that automatic control of the electrical energy input is only a single field in the arc furnace process in which research is currently taking place.

In the past few years the demand for environmentally friendly operation of electric arc furnaces has increased [15]. Current research in the automation of electric arc furnace off-gas processes is currently running where carbon and silicon content is the major concern when aiming to achieve specified steel grades. The blowing of oxygen and the injection of carbon is mainly used to help achieve these desired steel grades and research is strongly focussing on the automation of this process [16]. This dissertation, however, is focussing on the automatic control of the electrical energy input via adjustments of the electrode tip displacements above the scrap steel. The positions of the electrodes are adjusted via hydraulic actuators and arc current is used as the control variable for this purpose [17].

1.2 Dissertation Motivation

The electrical energy input to a three-phase electric arc furnace is regarded as the most important measure of effective production [10]. An arc furnace process can simply not function without automatic control of the electrical energy input. This is mostly due to the random nature of the arc furnace load. Short circuits are very common during meltdown and without the implementation of automatic control, unacceptable damage will occur to the electrodes and other expensive components. Falling scrap will cause the electrical power input to vary significantly and this is the main reason for electrode breakage. The main objective of the controlled electrode system is thus, to maintain constant distances between the electrode tips and the metallic charge [18]. Electrode breakage will then be minimized and production will be more effective.

In an existing electric arc furnace model, developed at the University of Pretoria, a controlled electrical energy input is assumed ([16] [19] and [20]). This is of course a simplifying assumption given the complex and unpredictable nature of the furnace operation. This introduces the need for an additional model, representing the control of the electrode system for a three-phase electric arc furnace, to be added to the existing model. The controlled energy output of the electrode system will serve as the electrical power input to the existing model. This will eliminate the assumption made in the existing three-phase electric arc furnace model.

Owing to the characteristics of electric arc phenomena, electric arc furnace loads can result in serious electrical disturbances on a power system [21]. Most literature, in connection with electrical energy input to a three-phase electric arc furnace process, focus on quality aspects regarding the rejection of these disturbances. Some of the most common quality aspects considered in an arc furnace industry is voltage flicker and harmonic distortion [22] and [23]. The improvement of these quality aspects falls outside the scope of this dissertation.

Limited literature is available on the automatic control of the electrical energy input to a three-phase electric arc furnace. The available literature, relating directly to the

control of the electrodes and where modelling is done from first principles alone is very old [24]. In modern derived arc furnace models, relating to electrode control, various subsection are modelled with system identification. The subsections modelled with system identification is regarded as black box models where descriptions about the internal states are limited. An electrode system, modelled entirely from first principles, will give a more complete technical description regarding the electrical behavior of a three-phase electric arc furnace [7].

Older models, specially in the 1970's, did not use any control system design techniques, such as PID (Proportional, Derivative and Integral) control, to automatically control the electric arc lengths. The entire control of the electrode positions was constructed from power electronic components [1] and the tuning of such controllers were very difficult. A typical arrangement was a amplidyne rotating amplifier together with a Ward-Leonard drive to move the electrodes up or down. Most modern three-phase electric arc furnaces make use of some form of feedback control strategy for the automatic control of the electrical energy input. The complete design of feedback control strategies, for the purpose of electrode control, is very limited in literature. Most electrode systems in the industry use PID control to adjust the lengths of the electric arcs relative to some set-point. Multi-variable control strategies are not commonly used in the arc furnace industry for the regulation of the electrical energy input. Comparisons between multi-variable control and single-input-single-output (SISO) techniques, such as PID control, will be valuable to choose the most effective control strategy.

The construction of a complete dynamic model for an electrode system, via first principles, together with detailed controller design, is required to investigate the properties of a three-phase electric arc furnace process. Literature, relating to the modelling of the electric arc furnace in this dissertation, is limited but not completely lacking. Literature on various subsections in this dissertation is available. These subsections include the hydraulic actuator, the physics of high current electric arcs, the three-phase electrical supply system and the controller design strategies.

1.3 Aims and Contributions

The main aim in this dissertation is to provide a mathematical model that generate a controlled electrical energy input to a three-phase electric arc furnace. This model is derived from first principles.

The electrode system for a three-phase electric arc furnace typically consists of three identical hydraulic actuator systems to adjust the vertical positions of each graphite electrode. A three-phase electrical supply serves as the electrical energy input, where each phase is connected to a separate graphite electrode. Electric arcs, generated between the tips of the electrodes and the metallic charge, cause the scrap steel and other raw materials to melt. The aim is to derive first principle models for each subsystem in the electrode system as outlined above.

Linear controller design are far more developed than nonlinear control methods. PID control and Model Predictive Control (MPC) are good examples of control strategies where the linear model is used for design purposes before implementing the controllers on the nonlinear model. Both are investigated in this dissertation to compare various control strategies for a three-phase electric arc furnace. PID control is commonly used in the industry and MPC is a well known multi-variable technique for systems with input or/and output constraints. A linear approximation of the highly nonlinear electric arc furnace model is necessary to design and implement the proposed controller techniques for the regulation of the electrical energy input to the arc furnace. A very important step towards obtaining a linear approximation of the model is the choice of steady state operating points. The electric arc furnace under study in this dissertation is three-phase (no steady states), which proposes the need for a second arc furnace model where only signal amplitudes are considered.

This dissertation can be divided into the following contributory steps:

- Development of models for the three-phase electrical supply system, the high current electric arcs and the hydraulic actuators, from first principles.
- Combine all models to illustrate the behavior of a complete electrode system.

- Obtaining a linear approximation of the complete model for the purpose of controller design.
- Design and implementation of both, PID control and Model Predictive Control on the linear plant model.
- Apply and tune the designed controllers on the nonlinear plant model.
- Validate the complete electrode system with the use of industrial tests and measurements. Simulations will be conducted similar to the operation of the industrial process to compare certain parameters.
- Evaluate the closed loop performance of the system with respect to the initial objectives.

These contributory steps follow the guidelines of a well known General Control Problem (GCP) [25]. Figure 1.1 illustrates a graphical representation of the GCP that was used in this dissertation. However, the "Real World" section in figure 1.1 is outside the scope of this dissertation.

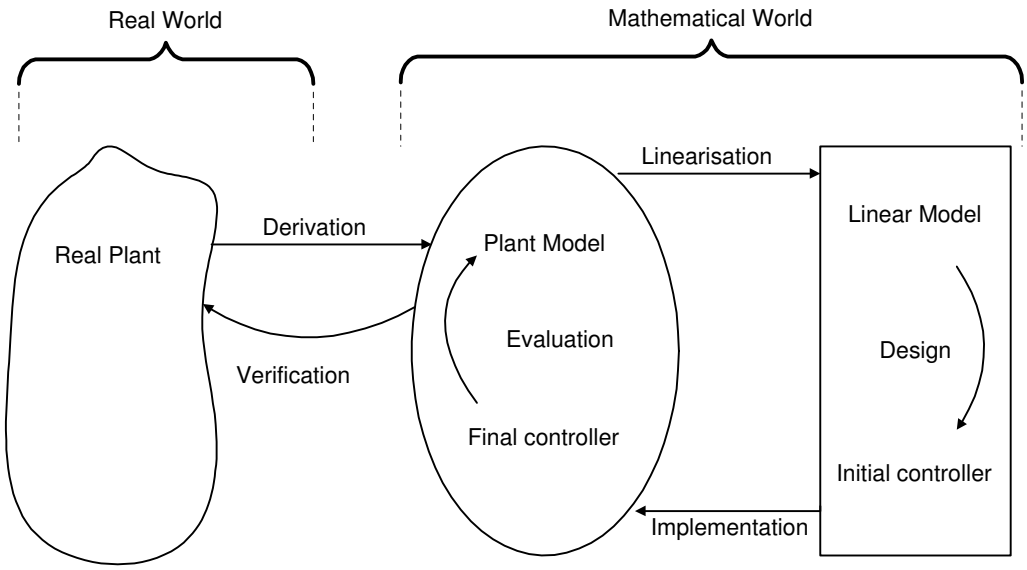

Figure 1.1: Flow diagram for the general control problem used in this dissertation [25].

1.4 Organization of the Dissertation

The organization of the dissertation is as follow:

- Chapter 1: A general introduction to the steel industry and the electric arc furnace process is given. The motivation behind the dissertation, together with the aims and contributions, are given.

- Chapter 2: This section discusses some general background on steel production to show where the electric arc furnace fits into the industry. A general overview and discussion of the technical aspects regarding an arc furnace process is given. The general production route for steel via an electric arc furnace is also discussed to illustrate the importance of the electrode system.

- Chapter 3: Nonlinear models for all the subsections of the electrode system for a three-phase electric arc furnace are derived from first principles. The models include the hydraulic actuators, the three phase electrical supply and the high current electric arc. Technical aspects, regarding the electrode system, are discussed in more detail.

- Chapter 4: The separate models in chapter 3 are simulated and discussed. The models are then simulated when connected together to show the response of the complete open loop system.

- Chapter 5: Some adjustments are made to the nonlinear model which need to be validated. The adjusted version of the nonlinear model is approximated by an linear model for the purpose of controller design. Some background on the method used for linearization is given. The linear model is simulated and compared with the nonlinear model.

- Chapter 6: The linear approximation of the arc furnace model are then used to design appropriate controllers for the positioning of the electrodes. PID control and MPC are used to compare different techniques with each other. The complete electrode system is then simulated and discussed.

- Chapter 7: The complete electrode system is validated with the help of industrial measurements.

- Chapter 8: The content of the dissertation is summarized and conclusions are drawn.

Chapter 2

Process Description

2.1 Introduction

In this chapter a general process description for a three-phase electric arc furnace is presented. A general and short overview on the production route for steel is also given to illustrate where an electric arc furnace fits in.

The focus of this dissertation is on electrode control for a three-phase electric arc furnace. The electric arc furnace is normally not the only process in a steel plant that requires large amounts of electrical power. This gives rise to the typical power transformation used in a steel plant which will also be discussed in this chapter.

An electrode system for a three-phase electric arc furnace can typically be separated into an electrical and hydraulic actuator process. A detail description of both sections is given in this chapter. The electrical input specifications of the electrode system differs during production. General production flow for an electric arc furnace process is discussed in this chapter to illustrate the effect it has on the operation of the electrode system.

World steel production statistics are given to illustrate the enormous growth in the industry over the years. This imply the strong competition which exist in the steel industry and technology has to be at the highest levels to succeed.

2.2 Steel Production Overview

2.2.1 Basic Steel Production Route

The production of steel can typically be characterized into three areas where processing takes place namely, Iron Manufacturing, Steelmaking and Rolled products [12].

Iron production can be defined as the extraction of metallic iron from iron ore via a reductant such as coal or natural gas. Two well known products resulting from this process is pig iron and direct reduced iron (DRI).

Steelmaking can be defined as the purification of the products resulting from the iron production phase to yield desired steel grades. Two well known processes are typically used during this phase to melt raw materials and produce specified steel grades. The first is a Blast Furnace together with a Basic Oxygen Furnace (BOF). The second is an Electric Arc Furnace (sometimes together with a Blast Furnace) which is also the focus of this dissertation. Electric furnaces are mainly used when steel is produced with solid metallic iron (such as DRI or scrap) as feed.

Steelmaking also consists of a secondary process where the molten steel is tapped and transferred to a ladle furnace. The necessary alloys are added, degassing is performed and sometimes powder reagents are injected as required. The molten steel, with desired steel grade and temperature, is now transferred to a continuous caster for the final steel production processing step.

Molten steel is poured into a tundish, which acts as a reservoir, at the top of the caster. It is then fed through a water cooled mould and sprayed with water to produce a continuous slab, billet or bloom depending on the mould size and shape. These steel products are then further treated and shaped according to customer requirements.

2.2.2 Steel Production Statistics

World steel production is constantly growing and competitiveness, in terms of larger production at lower cost, is also increasing [26]. Table 2.1 illustrates the steel production growth, worldwide as well as in South-Africa. World crude steel production via specific routes are illustrated in table 2.2.

Table 2.1: Continuously-Cast steel outputs, worldwide and in South-Africa, (Million Metric Tons per Annum).

Location	**2001**	**2002**	**2003**
World	730.9	793.4	846.1
South-Africa	8.7	9.0	9.4

Table 2.2: Steel production via different production routes, 2003/2004.

Location	**Million Metric Tons**	**Oxygen**	**Electrical**	**Open Hearth**
World	963.1	63.3%	33.1%	3.6%
South-Africa	9.5	54.6%	45.4%	0%

Figure 2.1 illustrates the percentage production of crude steel per continent for 2003/2004. Asia is by far the biggest producer of steel in the world, as almost half of all steel is produced there. However, South-Africa dominates steel production in Africa with Egypt being the second biggest producer. This illustrate the importance of steel production in South-Africa. To keep competing against the rest of the world and dominating in its own continent, South-African steel manufacturers have to be up the date with technology.

2.3 The Electric Arc Furnace Process

2.3.1 Overview

A large amount of energy is required in the steel industry to convert scrap steel and other raw materials into liquid and to achieve specified steel grades [27]. The energy inputs

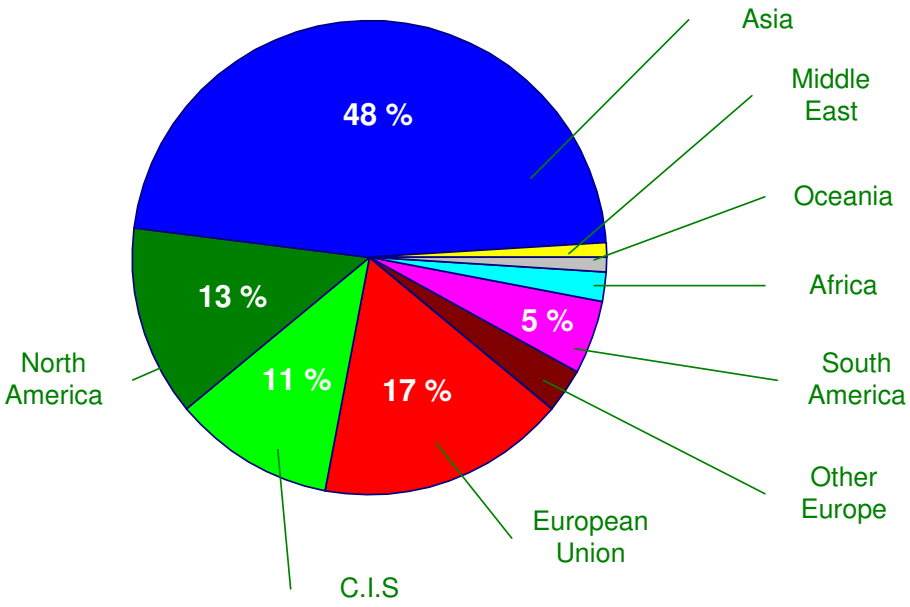

Figure 2.1: World crude steel production, 2003/2004.

to an electric arc furnace process are either electrical or chemical [10]. Two types of electrical supplies can be used for an electric arc furnaces process [28] and [29]. The first is a direct-current (DC) supply, which consists of a single electrical phase. A furnace supplied in this way is known as a DC Arc Furnace. The second is an alternating-current (AC) supply, which consists of three electrical phases. Such a furnace is called an AC Arc Furnace or simply a three-phase electric arc furnace. DC Arc Furnaces use less power and fewer electrodes to operate than a three-phase electric arc furnaces, but they are more expensive to install. This dissertation, however, focus mainly on Three-phase Electric Arc Furnaces and the control of its electrical energy input.

The fundamental problem in the arc furnace industry is to maximize the production of specified steel quality while achieving lowest possible production costs [3]. The electric arc furnace energy inputs are highly variable and need to be controlled with the aim being effective production of high quality steel. The increasing demand for high quality steel also provides a need for improved efficiency of the energy inputs to remain competetive.

In a three-phase electric arc furnace, each of the three electrical phases is connected to a separate graphite electrode [30]. The graphite electrodes are placed above the metallic

charge inside the furnace bath. Figure 2.2 illustrates the basic configuration for a three-phase electric arc furnace process. The connection between the furnace bath and roof together with the three graphite electrodes E_1, E_2 and E_3 and the electrical energy input is illustrated. Also illustrated is the connection of the electrical supply with the electrode position control system. In practice, three identical electrode position control systems are used to position each electrode individually [3]. The electrode position control systems consist of an automatic controller AC together with an actuator M to move the electrodes up and down.

Electrical energy is supplied to the graphite electrodes via a heavy duty three-phase furnace transformer, T. The transformer is connected to the electrodes via flexible bus-bars, C, to allow for vertical movements. The objective behind the vertical movements of the electrodes is to control the lengths of the electric arcs.

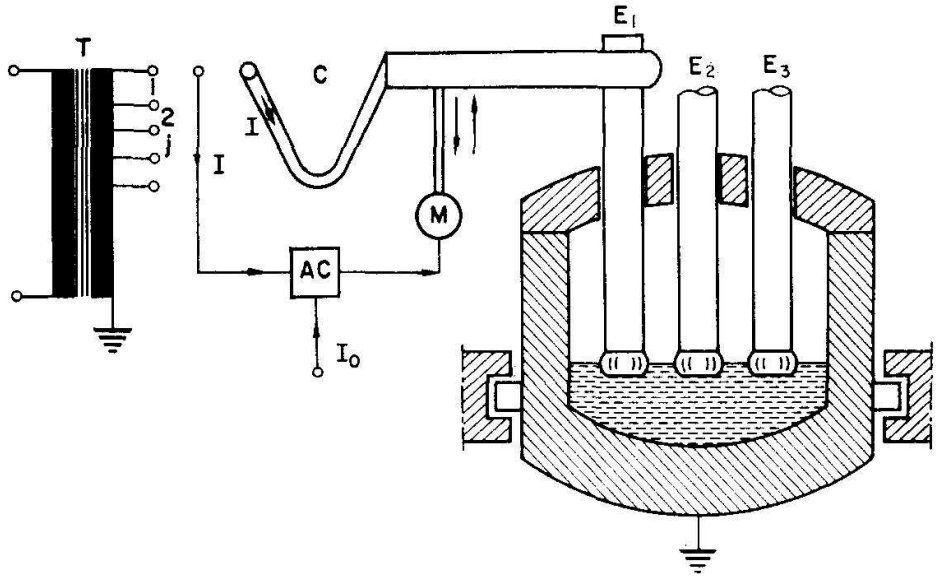

Figure 2.2: A typical three-phase electric arc furnace configuration [30].

With raw material loaded into the furnace bath and electrical energy being supplied to the graphite electrodes, the furnace operation then is based on heat transfer via electric arcs drawn between the tips of the electrodes and the metallic charge [10]. The electrodes

are thus used to convert electrical energy into heat to melt the scrap steel and other raw materials inside the furnace bath and also to increase temperature when tapping is required. The graphite electrodes enter the furnace through the middle of a furnace roof in a triangular configuration. The electrodes arc mainly in the middle of the bath and chemical energy, such as oxygen lancing, enters through the sides of the furnace bath (numbered 1 to 7 in figure 2.3) [10]. This configuration assures even power distribution to the arc furnace load and is illustrated in figure 2.3.

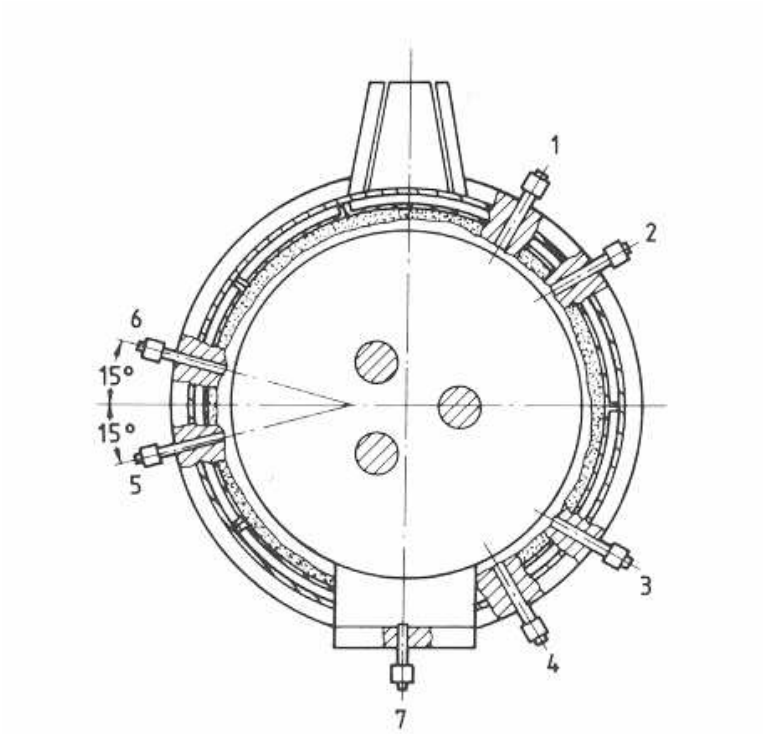

Figure 2.3: Top view of a furnace bath, with the triangular configuration of the graphite electrodes in the center. Also visible is auxiliary burners through the sides of the bath [10], pp. 120b.

2.3.2 The Furnace Transformer and the Electrical Supply System

Complete analysis of the power supply system in an electric arc furnace are not discussed in this dissertation and various simplifications and assumptions were used. Complete

studies and simulations have been carried out in literature ([31], [32] and [33]).

The furnace transformer supplies electrical energy to the entire electric arc furnace plant. A very important feature of the furnace transformer is the different tap settings on the transformer primary winding [34]. The tap settings enable the transformer to operate at various power specifications which are very important in electric arc furnace production. The device which enables the transformer to have different tap settings and various choices of secondary voltages is called the tap changer [17]. The basic principle behind the tap changer is to change the number of coil rotations on the primary side of the furnace transformer. The primary winding deals with lower currents, which makes is much simpler to change the number of turns on this coil rather than the high current secondary coil. A schematic diagram of the tap changer connected to the primary coil is illustrated in figure 2.4. Two basic methods are used in the steel industry to change the number of rotations on the transformer primary winding. This is either done with an off-load tap-changer or with on-load switching. On-load switching, where the tap settings are changed with the furnace in operation, is a very heavy duty technique because of the extensive currents being used. With off-load tap changing the steel producer has to break the electric circuit by lifting the electrodes. This is regarded as off-time, which is very undesirable in an arc furnace process, and might have an effect on the efficiency of the production.

In a three-phase electric arc furnace process, the transformer is typically connected in a wye-delta configuration [35]. This configuration is commonly used to step down from higher to lower voltages, and can deal effectively with the high currents required in the furnace operation. A typical configuration for the secondary coil connections on a furnace transformer is illustrated in figure 2.5.

It is regarded as standard practice to place the furnace transformer together with some other related equipment in a separate building, which is called the transformer house. This is because of a slight risk that the transformer oil may be a fire hazard.

The furnace transformer is usually not the only transformer connected to the utility

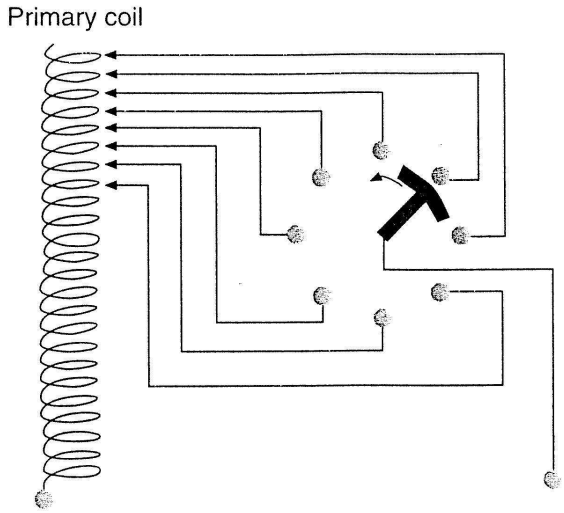

Figure 2.4: Schematic arrangement of a tap changer connected to the primary winding of the furnace transformer [17].

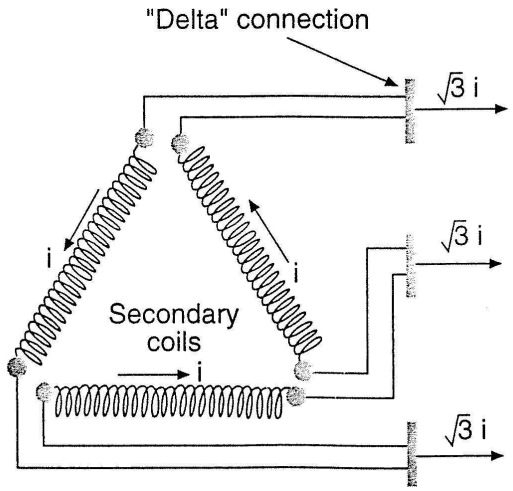

Figure 2.5: Delta-connection on the secondary windings of the three-phase furnace transformer ($\sqrt{3}i$ denotes the transformation from the primary to the secondary side) [17].

supply [36] and [37]. Other sectors in a steel plant which requires require electric power are a caster and a rolling mill [38]. This makes it common to have a small substation within a steel plant. For this reason the transformation from utility to arc furnace is normally done in two steps, using a double-transformer configuration. Such a configuration is illustrated in figure 2.6. Note that this configuration might be different from one steel plant to another and the voltage supplies might also differ from one country to another.

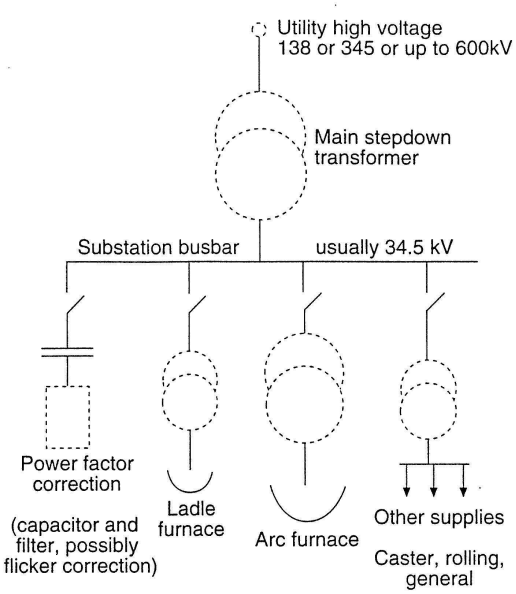

Figure 2.6: Typical power transformation from the high voltage line to the arc furnace and other sectors in a steel plant [17].

2.3.3 Motivation and Background for Electrode Control

With energy applied to the arc furnace the position of raw material and scrap steel inside the bath is highly heterogeneous and will cause irregular variations in the lengths of the electric arcs [39]. This will cause the electrical energy input to vary significantly if the electrodes are kept static. Figure 2.7 illustrates the random change in the arc furnace load due to meltdown of the scrap steel and also the effect it has on the lengths of the electric arcs.

Automatic and manual control of the electric power is necessary to achieve effective production of high quality steel [41]. Manual control is carried out by adjusting the tap settings on the furnace transformer primary windings. The reason for this is different electrical energy specifications needed during the production of a single bath of molten steel [42]. Worked out electrical specification, according the the required steel grade, is normally used to determine the tap settings for each period within a single tap. Automatic regulation is then used to control the electrode tip positions and to minimize the variations in the lengths of the electric arcs. The lengths of the electric arcs are defined

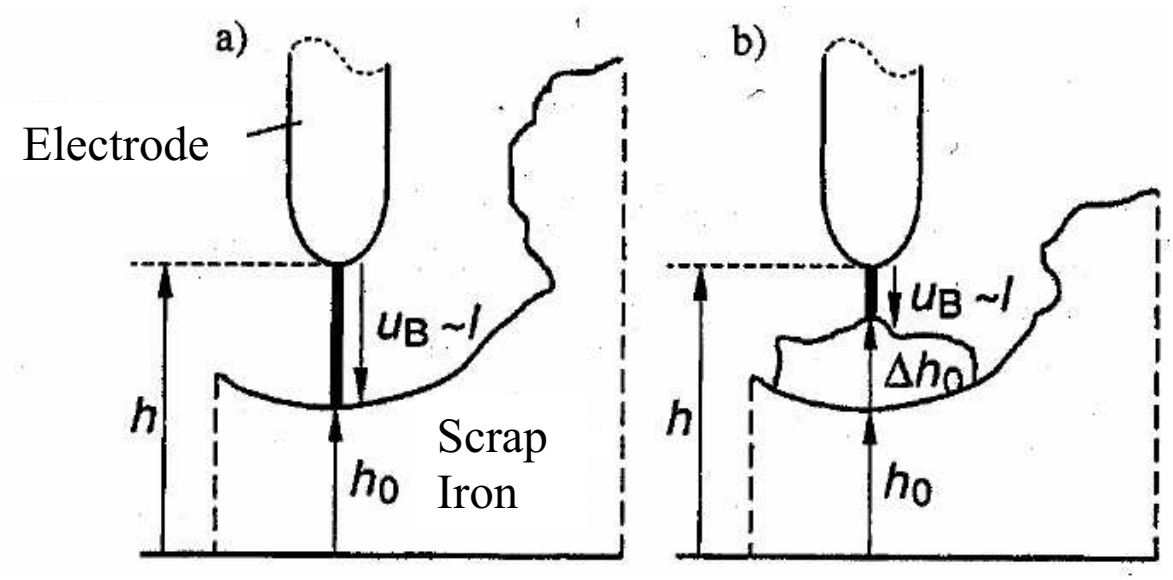

Figure 2.7: A typical step change in the arc length caused by the melting of scrap steel [40]. If h remains constant and h_0 increases with Δh_0, then the arc length, u_B, will change accordingly.

as the distances between the electrode tips and the metallic charge in the furnace bath. Hence, constant arc lengths will help to ensure that the electrical energy input remain constant at some reference value.

The arc lengths are controlled by vertically adjusting the electrode positions whenever it differs from the specified reference values [6]. The system responsible for the automatic control of the electric arc lengths are known as the electrode system. This is the focus point of this dissertation and a basic configuration of such a system is illustrated in figure 2.8.

Each of the three electrodes is connected to its own actuator system, which acts according to an error input signal, to move it up or down [1]. The most common actuators are either hydraulic or electromechanical (both systems achieve similar results) [10]. It is stated by Trenkler and Krieger (1985) that 50% of industrial actuators used to move

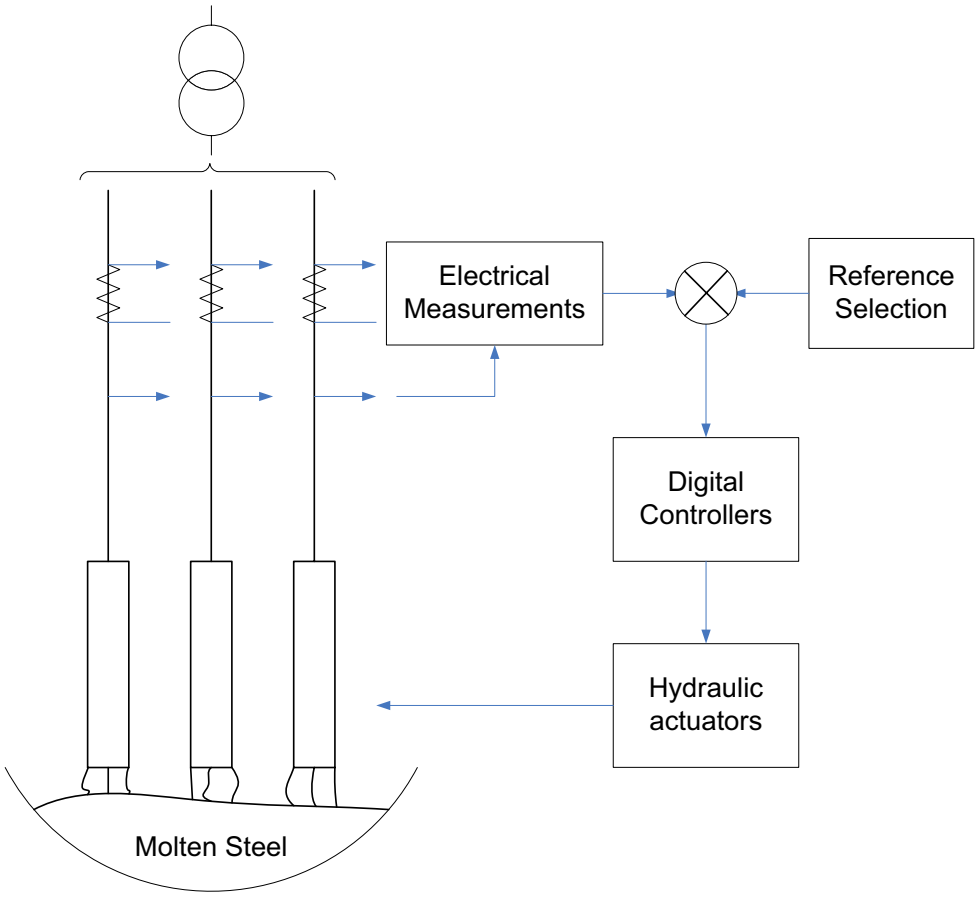

Figure 2.8: Electrode position control system to move the electrodes up or down.

electrodes are hydraulic and 50% are electromechanical. However, a greater percentage of hydraulic electrode control systems are in use for larger furnaces with large capacities. Other uses of hydraulic systems in an arc furnace process include the tilting of the furnace for tapping purposes and lifting and swinging out of the furnace roof. All the hydraulic equipment for an electric arc furnace process are usually installed together in a single room.

This dissertation focus mainly on electrode control systems which use hydraulic actuators for the movement of the graphite electrodes. A hydraulic spool valve is used to control the flow of inflammable fluid to a mast cylinder ([43] and [44]). The main spool valve is driven by an amplifying valve which operate with lubricating oil which is under pressure. A low-level electric signal is applied to this amplifying valve which has the effect of moving the piston in the mast cylinder up or down. The mast cylinder is connected to the graphite electrode. Note that three separate actuators are used for a three-phase

electric arc furnace, one for each phase/electrode.

With the graphite electrodes being oxidised and production being almost continuous, the lengths of the electrodes will decrease with time. The electrodes are clamped into electrode arms (figure 2.9), and they can be slipped down manually by an operator while energy is being supplied to the furnace. This ensure longer electrodes lifetimes with resulting monetary savings [45]. This phenomenon is another source of manual control in the electric arc furnace process.

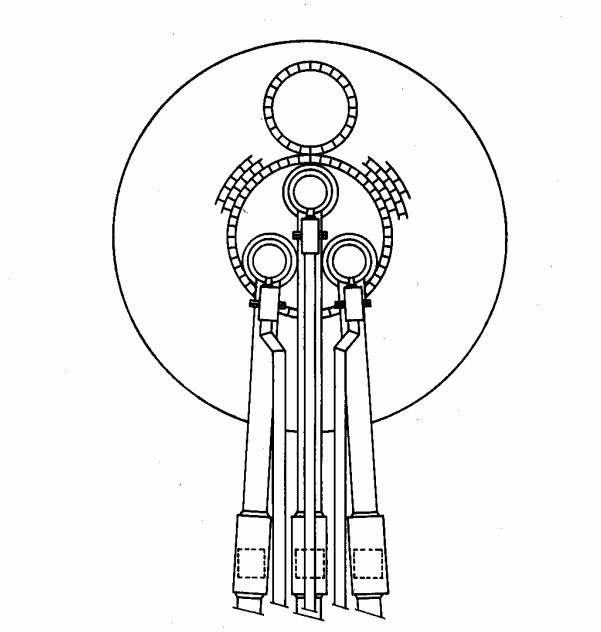

Figure 2.9: Schematic representation of the electrode arms connected to the graphite electrodes [10], pp. 101b.

2.3.4 Voltage and Current Measurements

Another important aspect in the electrode system for a three-phase electric arc furnace is the current and voltage measurements. All electrode control systems start by measuring at the furnace (transformer secondary side) the current and voltage of each phase, which must have a certain ratio [1]. The measurements are usually done with step down current and voltage transformers and then evaluated to determine the necessary control signal to

be applied to the input of the actuator. Accuracy of these measurements is very important to assure that the complete system is functioning effectively. A possible circuit for the measurements of the electrical quantities is illustrated in figure 2.10.

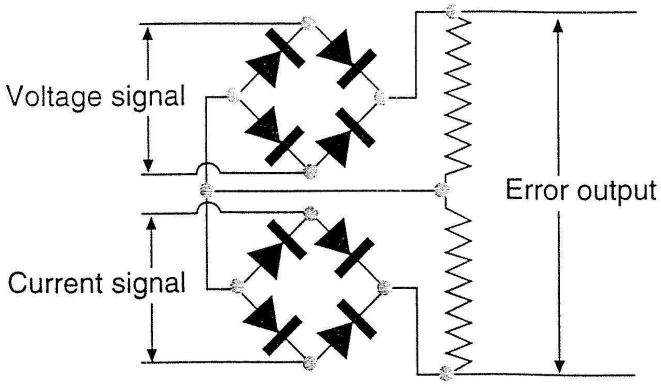

Figure 2.10: Typical configuration used for voltage and current measurements in a three-phase electric arc furnace [17].

2.4 Electric Arc Furnace Production Flow

Each batch of molten steel is called a heat [10]. It takes one operating cycle, which is called the tap-to-tap cycle, to produce a single heat. A tap-to-tap cycle is typically less than an hour and is made up of several different operations as illustrated by the flow diagram in figure 2.11. Energy specifications and the charge of raw materials are different for each melting period within a heat and need to be considered by the electrode system.

The first step in the production of steel via a three-phase electric arc furnace is to charge the furnace bath with scrap steel and other raw materials [10]. The charging of an arc furnace can be either continuous or discontinuous. In a furnace with continuous charging the raw materials are loaded into the bath without turning off the power. This dissertation, however, focus mainly on the latter arc furnace where power is turned off while the furnace is charged with raw materials.

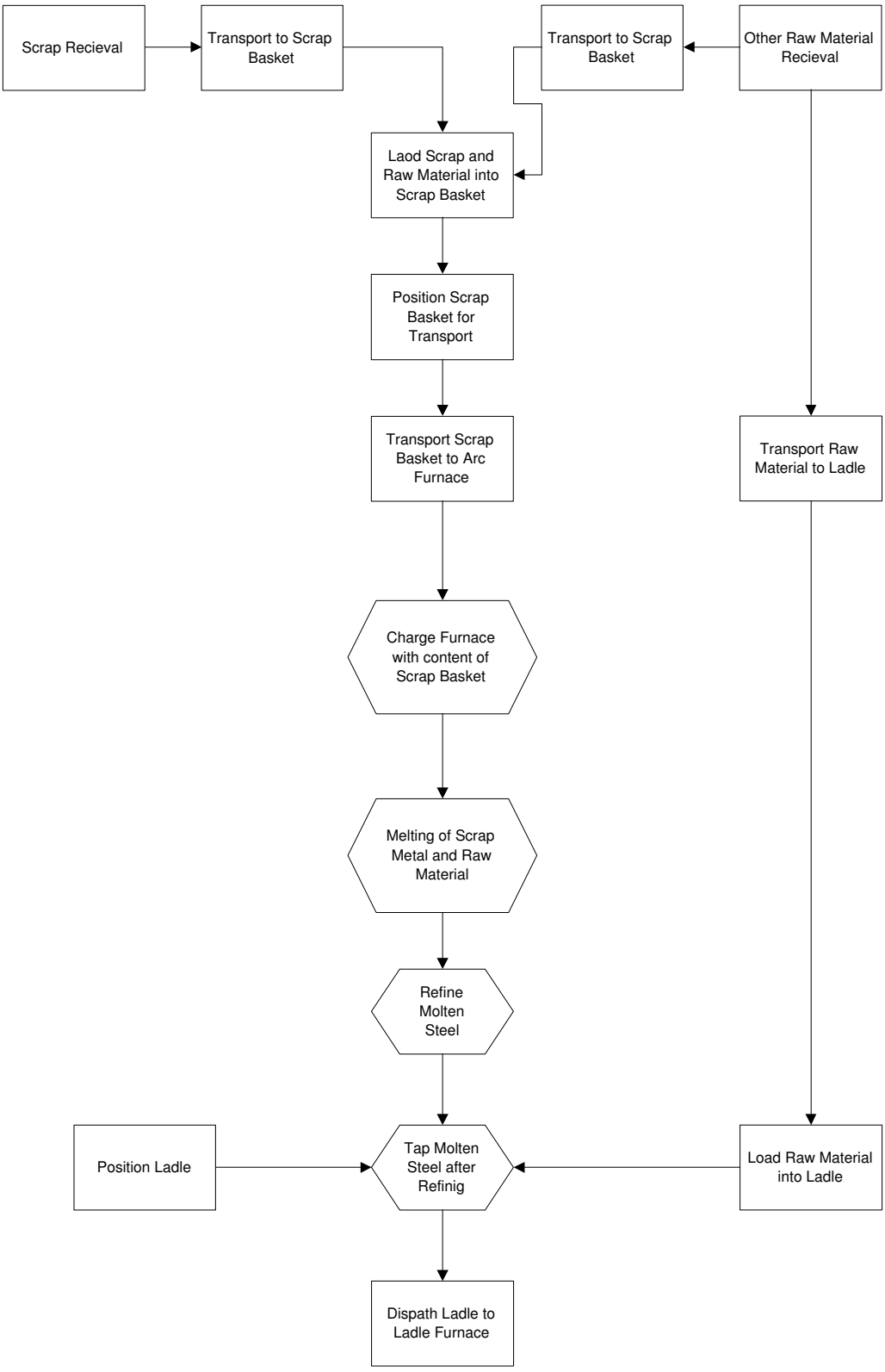

Figure 2.11: Typical flow diagram for a single electric arc furnace heat (constructed from an industrial training manual).

The remainder of this section describes the most important operations as illustrated in the flow diagram in figure 2.11.

2.4.1 Furnace Charging

A very important step in the production of any heat is to define the required steel grade. This will determine the specifications of the scrap and other raw materials needed for efficient melting. The furnace power is off for the duration of this period and power-off times must be minimized to ensure effective production. Note that furnace charging is often repeated within a heat until enough scrap has been converted into liquid. Another common practice during the charging of an electric arc furnace is to use a small amount of molten steel, left over from the previous heat called the hot heel, to ensure effective initial meltdown [15].

Preparing the charge bucket is also very important to ensure proper melt-in chemistry and good melting conditions. The scrap must be layered in the bucket according to size and density to promote rapid transformation to liquid steel. This will also minimize scrap cave-ins which will lower the risk of electrode breakage.

The following are examples of different types of scrap used in the industry [10]:

- General yard scrap,
- Shredded scrap,
- Shavings,
- Pig Iron, and
- Direct Reduced Iron, also called sponge iron.

Other raw material used for the charging of the arc furnace or the ladle furnace can typically be divided into either alloys or fluxes.

Some alloys being used in an arc furnace process are:

- Ferro manganese,
- Ferro silicon,
- Vanadium,
- Carbon,
- Boron wire, and
- CaSi wire.

Some types of fluxes used are:

- Burnt lime,
- Burnt dolomite,
- Fluorspar, and
- Anthracite.

The scrap basket is weighed and checked before transfer to the arc furnace. When charging the furnace the electrodes and the furnace roof are raised and swung to the side. A crane then moves a full bucket of scrap over the furnace bath. The bucket opens by retracting two segments on the bottom of the bucket which causes the scrap to fall into the furnace bath. The furnace roof is then closed and the electrodes are lowered after which power is applied.

2.4.2 Melting

The melting period is the heart of the arc furnace operation. When energy is supplied to the furnace, electric arcs ignite from the electrode tips, converting electrical energy into heat. This causes the metallic charge to convert to the liquid state.

The melting phase can typically be divided into periods as follow [10] [17] [2] and [42]:

- Arc ignition period: This is the instant when energy is initially applied to the furnace. With no penetration into the charge, the arcs are very unstable and the applied arc current must be kept relatively low for this duration. Other important conditions for this period is to protect the furnace roof from arc radiation and to rapidly submerge the electrode tips into the scrap.

- Boring period: After arc ignition the electrode tips will penetrate into the scrap without causing a short circuit. With the electrodes now being surrounded by scrap the arcs are relatively stable and power can be increased. The aim is to achieve the maximum boring speed possible.

- Molten steel formation period: After a while molten steel will begin to form at the bottom of the furnace bath. The electrode tips will penetrate completely through the scrap and arc onto the molten steel. With only a small amount of steel in the liquid state it is important to protect the furnace bottom from arc spot (damage due to direct contact with electric arc).

- Main melting period: The electrodes will now continue to arc onto the increasing liquid bath at the bottom of the furnace. With the arc at its most stable condition, maximum power is now applied to rapidly transform all the scrap into the liquid state. The furnace sidewalls are exposed to intense radiation from the arcs during this period. As a result, the voltage must be reduced. Creation of a foamy slag will allow the arcs to be buried and hence, the sidewalls will be protected from radiation. The energy transfer from the electrode tips to the molten steel will then be more efficient. With the majority of the first charge now being in the liquid state, a second furnace charge is sometimes necessary to ensure the desired amount of liquid steel.

2.4.3 Refining

The refining period can typically be divided into pre-refining period and the main refining period. These are described below.

- Pre-refining period: Once the final scrap charge is fully melted, flat bath conditions

are reached. A sample is taken from the bath to analyze the liquid steel. Measurements obtained from this period are evaluated and process adjustments are made for the purpose of the refining period.

- Refining period: Arcing continues as adjustments are made to achieve the desired specifications of the steel. Oxygen and carbon burners are used to adjust the composition and temperature of the steel as required. As soon as the correct specifications and temperature are reached, preparation for tapping will be performed. Tapping of the steel concludes an electric arc furnace heat and the next production step is refining of the steel in the ladle furnace. This refining is much more specific and accurate.

2.5 Conclusion

This chapter provided some background on a three-phase electric arc furnace process. The technical aspects involving such a process together with the typical flow of production were discussed. Motivations for control of the electrical energy inputs were given together with a proposed method to achieve this. The control of the electrode tip displacements is the main focus of this dissertation. The system under investigation mainly consists of a hydraulic actuator and a electrical supply system. These subsystems were separately discussed in this chapter.

In the following chapter, the derivation of nonlinear models necessary to simulate a controlled arc furnace process are derived and discussed. The mathematical models are derived from first principles to deliver maximum information regarding the arc furnace process.

Chapter 3

Modelling

3.1 Introduction

This chapter deals with the mathematical modelling of an electrode system for a three-phase electric arc furnace. The entire electrode system can be divided into four main section. These are the electrical supply system, the hydraulic actuators, the electric arc and the controllers. The design and implementation of the controllers are not discussed in this chapter. Mathematical models for the other three sections of the electrode system are however derived from first principles. The models are all represented as first order nonlinear differential equations as this is the general method of modelling for the purpose of controller design and implementation.

Various control variables, e.g. arc impedance, have been used to control the electrical energy input to a three-phase electric arc furnace [1]. The most common control variable used in the industry is arc current, which will also be the control variable in this dissertation. This strategy is known as current control and the main disadvantage is inherent interaction between the three phases. When disturbances occur on one of the electrode positions, all the arc currents will change. However, with current control, the disturbances are rejected much faster than in the case when other control variables are used. This is very desirable in an arc furnace industry, specially if the electrode tips make connection with the metallic charge and short circuits occur.

In deriving the models for the electrode control systems, the following assumptions are made:

- The furnace transformer is ideal and delivers specified power to the three graphite electrodes (Mutual inductances and all other phase dependent aspects are neglected).
- Quality aspects like harmonic distortion and voltage flicker are compensated for or simply neglected (This will assure smooth calculated waveforms which are desirable to analyze the arc impedance properties).
- When energy is supplied to the furnace, electric arcs are present at all three electrodes. (This assumption is only valid when the electrode positions are such that the distances between electrode tips and metallic charge are below or equal to the minimum distance necessary for an electric arc to occur).
- For simplification it is assumed that for the entire duration of the simulation the transformer tap position remains constant.

3.2 The Electrical System

The connection for the electrical system of an electrode system is such that separate models can be derived for the high current electric arc and the three-phase electrical supply system.

3.2.1 The Electric Arc

3.2.1.1 Physics of a High Current Electric Arc

An electric arc is defined as discharging gas between two electrodes (anode and cathode) which are connected to a voltage source [11], [39] and [46]. In an electric arc furnace process, the main electrode consists of graphite material. The electrical energy input will be applied to the graphite electrodes. The scrap metal and other raw materials to be melted constitutes the other electrode. The discharging arc is also known as plasma and consists of negatively charged electrons and positive gas ions [47]. A photograph of an electric arc

burning in an electric arc furnace process during flat bath conditions is illustrated in [48].

The electric arc is the main nonlinearity in the arc furnace process [49] and [50]. In a three-phase arc furnace the electric arcs must be ignited in every half wave due to the zero crossings on the AC supply signals [51]. Once the arc vanishes, it is necessary to increase the voltage applied across the electrodes until it reaches the minimum value required to re-establish the arc. The polarity of the graphite electrode with reference to the metallic charge also has a significant effect on the stability of the electric arc, which introduces further nonlinearity into the process, as shown in figure 3.1. With a negative connection of the graphite electrode (cathode half-wave) a discharging gas is formed in a cylindrical shape. The gas is stabilized by a gas stream (jet) which is caused by a higher current density at the cathode bottom. In contrast to the cathode half-wave, the stabilizing jet is not present at the anode half-wave, such that the plasma column exhibits unstable discharging.

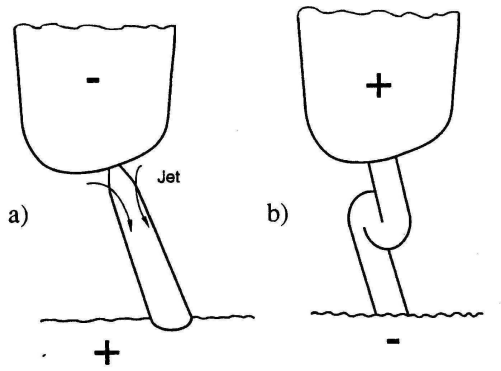

Figure 3.1: Arcs discharging with a) cathode half-wave and b) anode half-wave. This illustrates the extreme nonlinearity in an electric arc furnace process due to the relative polarity of the electrodes [40].

3.2.1.2 Radius Model for an Electric Arc

Various methods are available in the literature to model a three-phase electric arc [7], [11], [52] and [53]. A comprehensive arc model, developed for harmonic studies of electric furnaces , is given and discussed in [11]. This general dynamic arc model is in the form of

a differential equation based on the fundamental principle of conservation of energy. The power balance equation for the arc is presented by

$$p_1 + p_2 = p_3, \tag{3.1}$$

where

- p_1 represents the power transmitted in the form of heat to the external environment.
- p_2 represents the power which increases the internal energy in the arc.
- p_3 represents the total power developed in the arc which converts into heat.

The different power components in 3.1 are each represented by

$$p_1 = k_1 r^n, \tag{3.2}$$

$$p_2 = k_2 r \frac{dr}{dt} \tag{3.3}$$

and

$$p_3 = vi = ((k_3/r^m)/r^2)i. \tag{3.4}$$

The arc radius is represented by r and the arc voltage and current by v and i respectively. k_1, k_2 and k_3 are constants. If the environment around the arc is hot the cooling of the arc may not depend on its radius at all, so that in this case $n = 0$. If this is not the case and the arc is long, then the cooling area is mainly its lateral surface, so that $n = 1$. If the arc is short, then the cooling is proportional to its cross-section at the electrodes. In such a case, $n = 2$. m is used to indicate the dependance between arc voltage and arc radius (typically $m = 0$). Substituting equations 3.2, 3.3 and 3.4 into 3.1 gives the differential equation for an AC electric arc in terms of its radius:

$$k_1 r^n + k_2 r \frac{dr}{dt} = ((k_3/r^{(m)})/r^2)i. \tag{3.5}$$

This equation can be solved in the time domain, using a Runga-Kutta approximation or in the frequency domain using Newton's law [54]. Good voltage/current characteristics for an electric arc were obtained with this model. However, for the purpose of this dissertation, a model represented in terms of arc resistance will more advantageous.

3.2.1.3 Impedance Model for an Electric Arc

A three-phase electric arc furnace can be modelled as an electric circuit with the arc being represented by a variable resistance [55] and [56]. Such a model will be very advantageous for the use of this dissertation because the highly nonlinear electric arc has to function as a variable three-phase load.

Two well known and widely used arc impedance models are the Mayr model, which is a suitable representation of an arc for low currents, and the Cassie model, which yields good results for arcs with high currents [49]. These models are usually expressed in conductance rather than arc resistance because of extremely low values for arc resistance [57].

The Cassie equation is given by

$$G_C = \frac{vi}{E_0^2} - \theta \frac{dG_C}{dt} \tag{3.6}$$

and the Mayr equation by

$$G_M = \frac{i^2}{P_0} - \theta \frac{dG_M}{dt} \tag{3.7}$$

The variables in 3.6 and 3.7 are described as follow:

- E_0 - momentarily constant steady-state arc voltage,
- θ - arc time constant,
- P_0 - momentarily power loss,
- i - arc current, and

- v - arc voltage.

These relatively simple differential equation models are based on simplifications of principal power-loss mechanisms and energy storage in the arc column. They provide a qualitative understanding of the phenomenon that determine arc striking or extinction in energy-balance systems [58]. In this dissertation, a combined Cassie and Mayr model, derived by Wang and Vilathgamuwa (1997), is used to represent the arc impedance characteristics. The two models are combined into a single model by defining a transition current I_0. Cassie's model will dominate when the arc current is bigger than I_0, and when the arc current is smaller than I_0, Mayr's model dominates. However, to allow for smooth transition between the two models, a transition function $\sigma(i)$ is defined, which is a function of the arc current such that the final arc conductance is given by

$$G = [1 - \sigma(i)]G_C + \sigma(i)G_M, \tag{3.8}$$

where G_C and G_M are the conductances given by (3.6) and (3.7), respectively. The transition factor varies between zero and unity and should be a monotonically decreasing function when arc current i increases. The transition factor is given by

$$\sigma(i) = exp(-\frac{i^2}{I_0^2}). \tag{3.9}$$

When the arc current i is small, the value of σ is close to unity and G is dominated by the Mayr conductance G_M. When i is large, σ is negligible and, therefore, G is dominated by the Cassie conductance G_C. (3.8) and (3.9) are combined to generate the complete Cassie-Mayr arc impedance model for a single electric arc as follow:

$$G = G_{min} + [1 - exp(-\frac{i^2}{I_0^2})]\frac{vi}{E_0^2} + [exp(-\frac{i^2}{I_0^2})]\frac{i^2}{I_0^2} - \theta\frac{dG}{dt} \tag{3.10}$$

and

$$i = Gv \tag{3.11}$$

G_{min} is the conductance between any two electrodes when the electric arc is absent. When

an arc is igniting or extinguishing, the energy stored per unit volume is large compared with the energy loss per unit volume. Thus, θ should be a function of the arc current i. When the arc stabilizes, θ is small and can be represented as follow:

$$\theta = \theta_0 + \theta_1 exp(-\alpha|i|), \tag{3.12}$$

where $\alpha > 0$ and $\theta_1 \gg \theta_0$. When the arc is igniting or extinguishing, i is small and $\theta \approx \theta_1$. When i is large, $\theta \approx \theta_0$. The relationship between the arc length and the threshold arc voltage is given by

$$E_0 = A + B\ell, \tag{3.13}$$

where l is the arc length (in centimeters), A is a constant taking into account the sum of anode (electrode) and cathode (metallic charge) voltage drops and B represents the voltage drop per unit arc length [23].

3.2.2 The Electrical Supply System

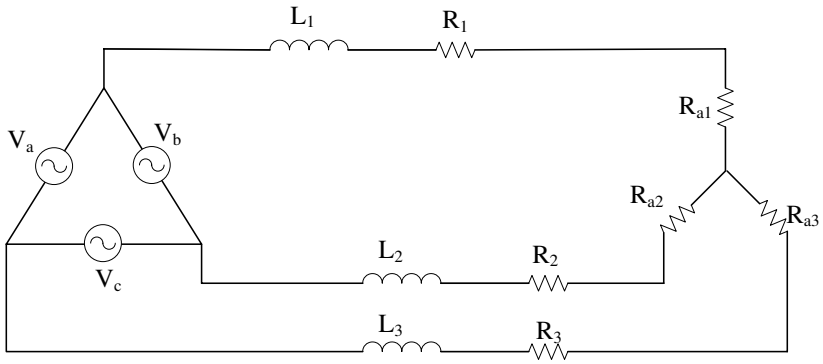

Figure 3.2: Simplified three-phase electrical circuit diagram used to model the supply system.

The electrical supply system, for the aim of this dissertation, is modelled as three-phase voltage supplies with finite source resistance and inductance which are connected in delta. Similar configurations have been used in the literature [59]. The modelling of submerged arc furnaces also use the same configuration for the three-phase load [48]. The utility supply and all other connections to the primary side of the furnace transformer are neglected as it falls outside the scope of this dissertation. This simplified configuration minimizes the introduction of noise and other quality aspects common in power system [60] and [61]. The electric arc model serves as the three-phase load and is connected in a star configuration to the delta supply to conclude the simplified electrical circuit of a three-phase electric arc furnace. The electric circuit used in this dissertation to model the electrical supply system is illustrated in figure 3.2. L_k and R_k represent source inductances and resistances, respectively. Ra_k represent the inverse of the arc conductances determined by 3.10 and 3.11. V_a, V_b and V_c are the voltages at the secondary side of the furnace transformer and i_k denote arc currents for each phase, respectively. Differential equations for the complete transmission system is determined with Kirchoff's law as follow:

$$V_a = i_1(R_1 + R_{a1}) + L(\frac{di_1}{dt} - \frac{di_2}{dt}) - i_2(R_2 + R_{a2}), \tag{3.14}$$

$$V_c = i_3(R_3 + R_{a3}) + L(\frac{di_3}{dt} - \frac{di_1}{dt}) - i_1(R_1 + R_{a1}) \tag{3.15}$$

and

$$i_1 = i_2 + i_3. \tag{3.16}$$

3.2.3 State Definitions and the Complete Electrical Model

The aim is to derive the nonlinear electrical model as first order differential equations. As mentioned earlier, this is a standard form of modelling for the purpose of linearization, which is necessary for controller design in chapter 6. First order differential equations

are best illustrated if state variables are defined for the model. The following states were defined to illustrate the three-phase electrical model for this dissertation:

- x_1 - Arc current in phase 1.
- x_2 - Arc current in phase 2.
- x_3 - Arc current in phase 3.
- x_4 - Arc conductance for phase 1.
- x_5 - Arc conductance for phase 2.
- x_6 - Arc conductance for phase 3.

The electric arc model in equations 3.10 to 3.13 together with the transmission system in equations 3.14 to 3.16 are combined and assigned with the state variables to formulate the complete electrical model for a three-phase electric arc furnace. The differential equations are illustrated in equations 3.17 to 3.22 below.

$$\dot{x}_1 = \frac{\frac{V_a - x_1(R_1+\frac{1}{x_4})+x_2(R_2+\frac{1}{x_5})}{L} - \frac{V_c - x_3(R_3+\frac{1}{x_6})+x_1(R_1+\frac{1}{x_4})}{L}}{3}. \tag{3.17}$$

$$\dot{x}_2 = \frac{-2(\frac{V_a - x_1(R_1+\frac{1}{x_4})+x_2(R_2+\frac{1}{x_5})}{L}) - \frac{V_c - x_3(R_3+\frac{1}{x_6})+x_1(R_1+\frac{1}{x_4})}{L}}{3}. \tag{3.18}$$

$$\dot{x}_3 = \dot{x}_1 - \dot{x}_2. \tag{3.19}$$

$$\dot{x_4} = \frac{x_4 - G_{min} - (1 - exp(-\frac{x_1^2}{I_0^2}))\frac{x_1^2}{x_2(A+B\ell)^2} - (exp(-\frac{x_1^2}{I_0^2}))\frac{x_1^2}{P_0}}{-\theta_0 - \theta_1 exp(-\alpha|x_1|)}. \tag{3.20}$$

$$\dot{x_5} = \frac{x_5 - G_{min} - (1 - exp(-\frac{x_2^2}{I_0^2}))\frac{x_2^2}{x_2(A+B\ell)^2} - (exp(-\frac{x_2^2}{I_0^2}))\frac{x_2^2}{P_0}}{-\theta_0 - \theta_1 exp(-\alpha|x_2|)}. \tag{3.21}$$

$$\dot{x_6} = \frac{x_6 - G_{min} - (1 - exp(-\frac{x_3^2}{I_0^2}))\frac{x_3^2}{x_3(A+B\ell)^2} - (exp(-\frac{x_3^2}{I_0^2}))\frac{x_3^2}{P_0}}{-\theta_0 - \theta_1 exp(-\alpha|x_3|)}. \tag{3.22}$$

These state differential equations for the electrical system, combined with three hydraulic actuators,which are modelled next, form the basic configuration for an electrode controlled system of a three-phase electric arc furnace. The modelling of the hydraulic actuators are discussed in the section to follow.

The differential equations, derived in this chapter, are in symbolic form and realistic values are necessary for simulation purposes. Choosing values for the model variables are very important to ensure accurate and meaningful results. Ideally, physical measurements and commissioning specifications, relating to an arc furnace process, are needed to make accurate decisions regarding values for the variables. This information is not always easy to come by and some variables are not measured in practice. For this reason, some values in the electrical model are obtained from literature and some from personal experience.

Source inductance and resistance vary with adjustments on the transformer's tap-changer [10]. Amplitudes of the supply voltages are also affected by the various settings on the transformer primary winding if the utility supply remains constant. In an industrial arc furnace process with an online tap-changer, predetermined programs are worked out before production and used to determine the necessary settings for the transformer. Each program is divided into various steps, each consisting of specified arc current, transformer secondary voltage and transformer tap. A typical worked out program (melting specifications) and the effect it has on certain variables are illustrated in table 3.1.

The remaining constants, not affected by the different tap settings, are related to the electric arc models in equations 3.6, 3.7 and 3.9. The selected values for these variables are summarized in table 3.2.

Table 3.1: Typical melting program and the constants affected by the various tap settings on the transformer windings (Obtained from industrial data documentation).

Step	**Tap**	**KA[1]**	**KA[2]**	**KA[3]**	**Voltage**	$R_k(m\Omega)$	$L_k(\mu H)$	**Period**
1	10	50	50	50	596	0.669	1.1733	Start
2	17	44	44	44	750	0.796	1.3675	Melting
3	17	44	44	44	750	0.796	1.3675	Melting
4	17	43	43	43	750	0.796	1.3675	Melting
5	17	44	44	44	750	0.796	1.3675	Melting
6	17	38.5	38.5	38.5	750	0.796	1.3675	Melting
7	17	38.5	38.5	38.5	750	0.796	1.3675	Melting
8	17	46	46	46	750	0.796	1.3675	Melting
9	17	43	43	43	750	0.796	1.3675	Melting
10	15	48	48	48	706	0.7775	1.336	Refining
11	14	50	50	50	684	0.764	1.3124	Refining
12	13	52	52	52	662	0.747	1.284	Refining
13	18	38.5	38.5	38.5	0	0	0	Refining
14	18	38.5	38.5	38.5	0	0	0	Refining
15	18	38.	38.5	38.5	0	0	0	Refining
16	18	38.	38.5	38.5	0	0	0	Refining

3.3 The Hydraulic Actuator

Three hydraulic actuators are used in the electric arc furnace process to move each graphite electrode in a vertical position to adjust the length of its electric arc [45]. Constant arc length implies constant arc current, which is the choice of control variable for this dissertation and also in many industrial furnace processes. The main objective is to maintain a constant RMS (root-mean-square) value for the electrical energy input. Measured arc current are compared with specified reference values an the generated error signals serve as inputs to intelligent controllers, which determine whether the electrodes should be raised or lowered and by how much.

Figure 3.3 shows a typical hydraulic actuator configuration used for the vertical move-

Table 3.2: Constants in the electric arc model. These are all constants not affected by the tap settings on the transformer windings.

Symbol	**Description**
A	$40V$
B	$10V/cm$
I_0	$1kA$
P_0	$50W$
θ_0	1
θ_1	100
α	0.01

ments of electrodes. HRR is a high response regulating valve, D is a hydraulic distributor and V is a high pressure vessel. P_1 and P_2 are pressure pumps and T is a tank which contains 90% water and 10% oil. This is mostly a safety precaution because water will prevent the hydraulic fluid from catching fire when operating in close range with the electric arc furnace. A simplified model for a single hydraulic actuator system ,such as illustrated in figure 3.3, can be described by six state variables. All three hydraulic actuators will thus be described by eighteen state variables.

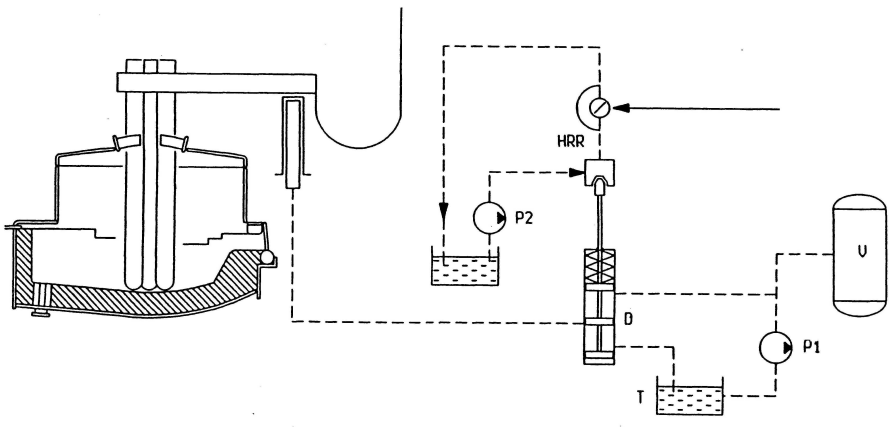

Figure 3.3: Hydraulic actuator system for electrode control (Constructed from various industrial data documents).

Some components in a hydraulic actuator, not included for the purpose of this disser-

tation, are:

- The hydraulic transmission line: In modern hydraulic systems the transmission line from the valve to the cylinder in kept as short as possible to eliminate unnecessary disturbances. In some instances the transmission line is eliminated by mounting the regulating valve output directly to the cylinder [12]. For these reasons the transmission line can be neglected.
- The hydraulic return line: The return line was also omitted because of the same reasons mentioned above for the transmission line.
- Position or pressure sensor: To prevent the hydraulic actuator model from becoming to complex, the dynamics of the sensor were modelled as a constant gain.

The interested reader is referred to [62] for more complex and complete models related to hydraulic actuators.

The input to the servo valve is a controlled electrical current which causes a rotation of an armature to which a flapper arm is rigidly connected ([43] and [44]). A summary of how the servo valve operates follows. The servo valve is used to operate the movement of a bigger HRR valve, shown in figure 3.3.

The first two state variables describe the dynamics of the HRR valve as follow:

- x_1 - spool position of the hydraulic distributor and
- x_2 - velocity of the spool.

The spool of the regulating valve controls the flow of hydraulic fluid that change the pressure in the cylinder chambers. This generates the up or down movements of the hydraulic piston. A more complete description for such a hydraulic actuator is given in [12]. The final four state variables describe the dynamics of the cylinder and piston configuration for the hydraulic actuator as follow:

- x_3 - position of the hydraulic piston,
- x_4 - velocity of the piston,

- x_5 - pressure in the chamber above the piston in the cylinder and
- x_6 - the pressure in the chamber below the piston.

The hydraulic model is derived as first order differential equations in (3.23) to (3.31) below.

$$\dot{x_1} = x_2. \tag{3.23}$$

$$\dot{x_2} = -2\zeta_v\omega_v x_2 - \omega_v^2 x_1 + \frac{\omega_v^2 x_{max} I_c}{I_0}. \tag{3.24}$$

$$\dot{x_3} = x_4. \tag{3.25}$$

$$\dot{x_4} = \frac{[A_p(x_6 - x_5) - F_s - \delta x_4 - F_{ext}]}{m}. \tag{3.26}$$

$$\dot{x_5} = \frac{-(x_1 C_1 \sqrt{dp} - C_2 x_4)}{V_0 - A_p x_3}. \tag{3.27}$$

$$\dot{x_6} = \frac{x_1 C_1 \sqrt{dp_1} - C_2 x_4}{V_0 + A_p x_3}. \tag{3.28}$$

where

$$\begin{aligned} F_s &= F_{sc}(1 - exp(-\gamma|x_4|))sgn(x_4), \\ C_1 &= BwC_d\sqrt{\tfrac{2}{\rho}}, \\ C_2 &= BA_p, \end{aligned} \tag{3.29}$$

and

$$dp = \begin{cases} x_5 - p_r \text{ if } x_1 \geq 0 \\ p_s - x_5 \text{ if } x_1 < 0 \end{cases} \tag{3.30}$$

and

$$dp_1 = \begin{cases} p_s - x_4 \text{ if } x_1 \geq 0 \\ x_6 - p_r \text{ if } x_1 < 0 \end{cases} \tag{3.31}$$

The constants and variables used in this model are described in table 3.3. The values for these variables are obtained from available industrial measurements and data, and from related literature.

Table 3.3: Constants and variables in the hydraulic model.

Symbol	**Description**	**Values**
ζ_v	valve damping ratio	1
ω_v	valve natural frequency	$2 \times \pi \times 21 rad/s$
x_{max}	maximum valve opening	$6 \times 10^{-}3m$
I_0	valve operating current	$150 \times 10^{-}3A$
I_c	input current to torque generator	$-150mA < I_c < 150mA$
A_p	piston surface area	$0.102m^2$
V_0	initial volume for the cylinder chambers	$0.47m^3$
m	external masses connected to the piston	$11700kg$
δ	damping coefficient of hydraulic fluid	$178700.4kg/s$
F_{sc}	friction force of cylinder seals	$1000N$
γ	seal friction coefficient	10000
β	bulk modulus of hydraulic fluid	$1.7232 \times 10^9 Pa$
ρ	density of hydraulic fluid	$200kg.s^2/m^4$
w	width of orifice opening	$0.0203124m$
Cd	fluid flow coefficient	0.6
p_s	supply pressure	$6 \times 10^6 Pa$
p_r	return pressure	$1 \times 10^4 Pa$

3.4 Conclusion

This chapter described the modelling of the two main sections in an electrode system for a three-phase electric arc furnace. These are the electrical system (the electric arc and the electrical supply) and the hydraulic actuators.

The electrical system model consisted of an electric arc, which serve as the electrical load, and the three-phase supply system. A three-phase electric arc furnace consist of three separate hydraulic actuator systems, one for each graphite electrode. However, only one hydraulic actuator was modelled in this chapter because the other two will be similar.

The models derived in this chapter will be used in the next chapter to obtain simulation results relating to a three-phase electric arc furnace.

Chapter 4

Model Simulation Results

4.1 Introduction

The electric arc furnace model, consisting of an electrical system and three hydraulic actuators, is simulated in this section without feedback control. The results in this chapter therefore do not illustrate the performance of a complete electrode controlled arc furnace process. Complete results will follow the controller design, discussed in chapter 6.

The open loop model in this chapter consists of a three-phase electrical model with a variable three-phase load, represented by the highly nonlinear electric arcs. Each of the electrical phases is separately connected in series with a hydraulic actuator model, with the main objective of changing the electrode tip displacements. Note that the electrode tip positions are assumed to be equal to the arc lengths with the assumption that electric arcs are present at all times. Disturbances on the length of the electric arcs are added externally. For example, when molten metal is present beneath the electrodes, the arc causes a depression to form in the metal (so increasing the arc length).

The electrical and hydraulic models for the three-phase electric arc furnace are initially simulated separately to illustrate the respective responses. The combined open loop model is illustrated in figure 4.1, which shows the connection between the three hydraulic actuators and the electrical model. sv_n denote the current inputs to the servo-valves for each of three hydraulic actuators. The three hydraulic actuators are denoted by H_n and the three electrical phases in the electrical model by P_n. The output arc currents for the

electrical model are denoted by Ia_n.

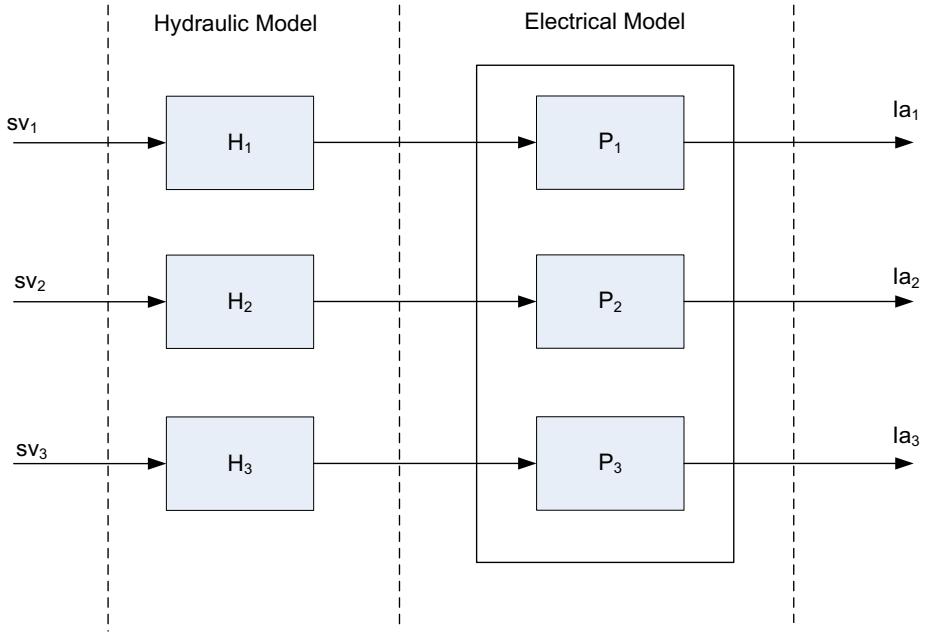

Figure 4.1: Connection between the hydraulic and electrical system in a three-phase electric arc furnace.

The remainder of the chapter gives separate simulation results for the electrical system, the hydraulic actuators and finally the combined model.

4.2 The Electrical System

The inputs to the electrical model in figure 4.1 are the electrode tip displacements or simply the arc lengths and also the constant supply voltages from the secondary side of the three-phase furnace transformer, which is assumed to be ideal.

Solutions to the differential equation models are obtained by using a Runga-Kutta approximation with appropriate initial conditions for all states and inputs. The simulation results relating to the electrical system are illustrated in the following order:

- Constant arc lengths,
- variable arc lengths on a single phase, and
- variable arc length on multiple phases.

4.2.1 Constant Arc Length

In this section, transient responses are illustrated for the electrical behaviour of the three-phase electrical arc furnace model if the distances between the electrode tips and the steel content in the furnace bath remain constant. The constant arc lengths, used for this simulation, are kept relatively short (realistic) to ensure that the electric arcs operate in a stable manner. The choice for arc lengths (inputs to the electrical model) for all three phases in this simulation are 1 cm. The amplitude for the three-phase supply voltage used to represent the secondary transformer voltage is 600 V, and is illustrated in figure 4.2. The 120° phase difference between the respective phases are typical for a balanced three-phase system. The operating frequency is 50 Hz as used in South Africa.

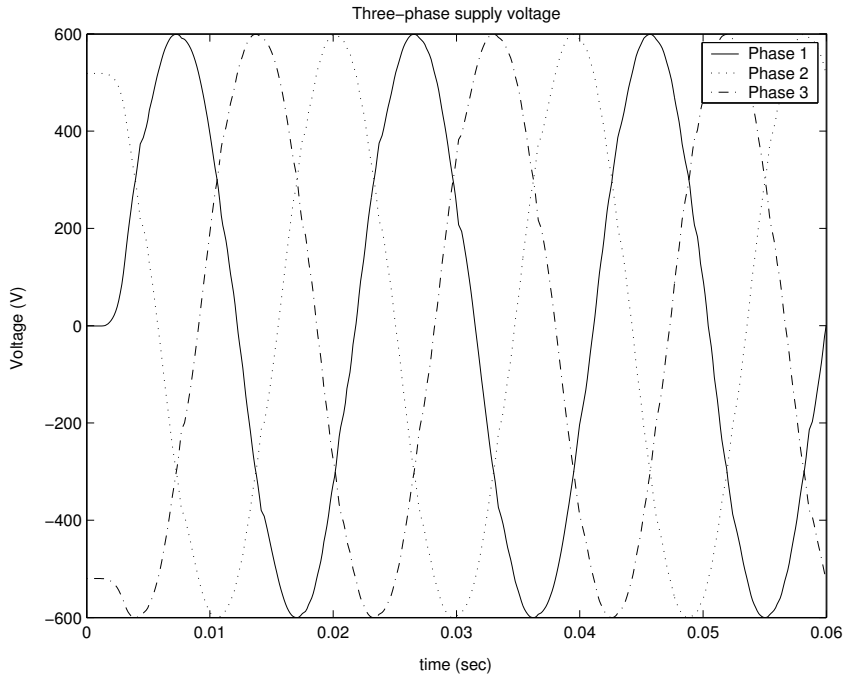

Figure 4.2: Supply voltages representing the secondary transformer voltage and also the electrical supply to the electrical system of the three-phase electric arc furnace.

The three interesting variables regarding the electrical behaviour of the electric arc furnace, specifically for this dissertation, are arc current (also called electrode current), arc voltage and arc resistance. These variables, simulated with the derived electrical model for 0.06 seconds are illustrated in figures 4.3, 4.4 and 4.6. The simulation time is chosen mainly because of the 50 Hz operating frequency. If the duration of the simulation is to long, some detail in waveforms will be difficult to see. The arc conductance (inverse of arc resistance) is given in figure 4.5. Arc conductances are included as state variables in the model. as the values for arc resistances are very small.

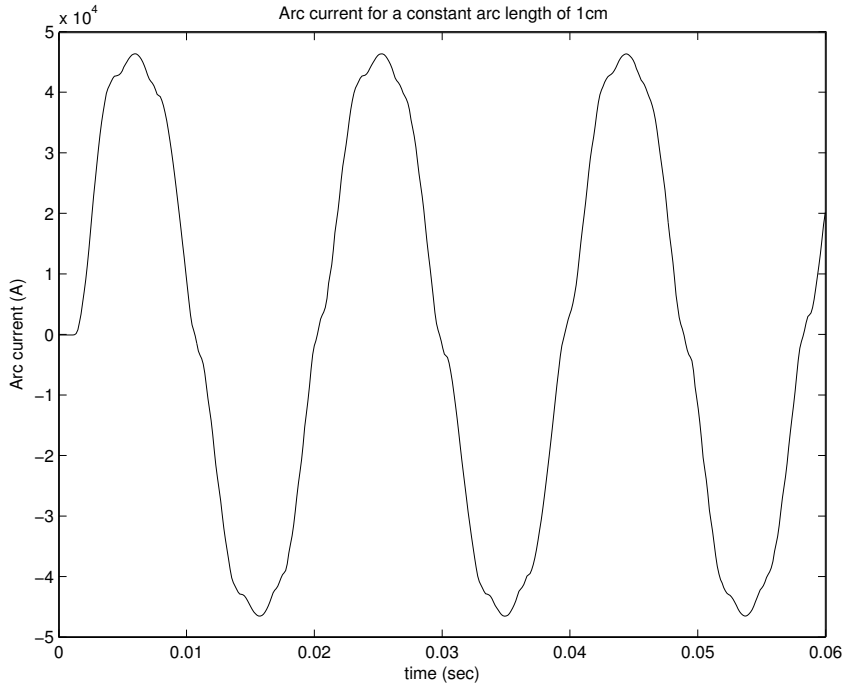

Figure 4.3: Simulated arc current on a single phase, obtained with the derived electrical model.

To recall, a three-phase electric arc vanishes every time the current crosses zero. To reignite the electric arc, the voltage across the electrode must be increased to a minimum value necessary to do so. The minimum voltage necessary to re-establish an electric arc is higher than its steady state value. This phenomenon is visible in figure 4.6. The higher value for arc voltage is visible at the beginning of every half wave. The re-ignition of the electric arc also has an effect on the waveforms for arc current and resistance as seen in figures 4.3 and 4.4. Arc current remains almost zero during the re-establishment of the arc.

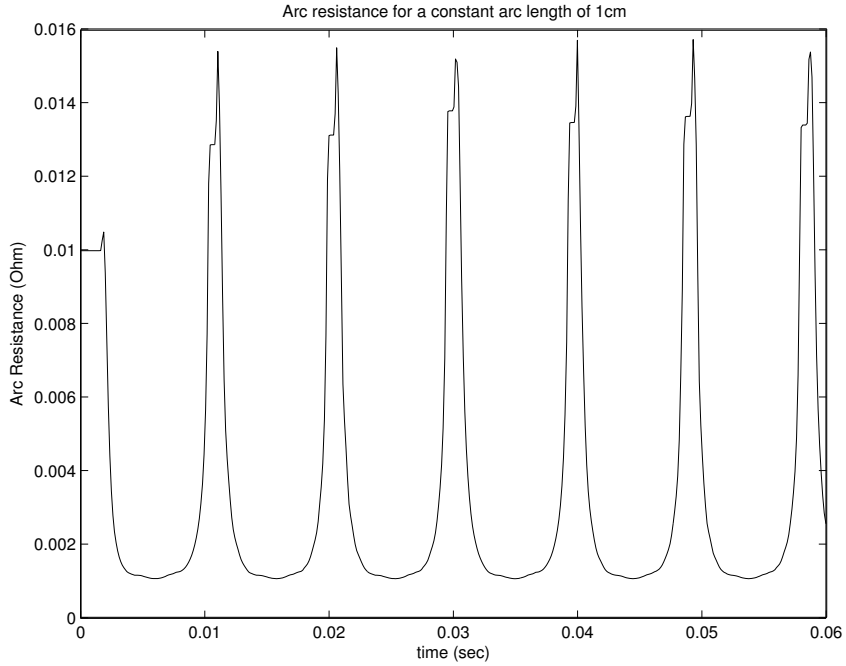

Figure 4.4: Simulated arc resistance (Ω) on a single phase, obtained with the derived electrical model.

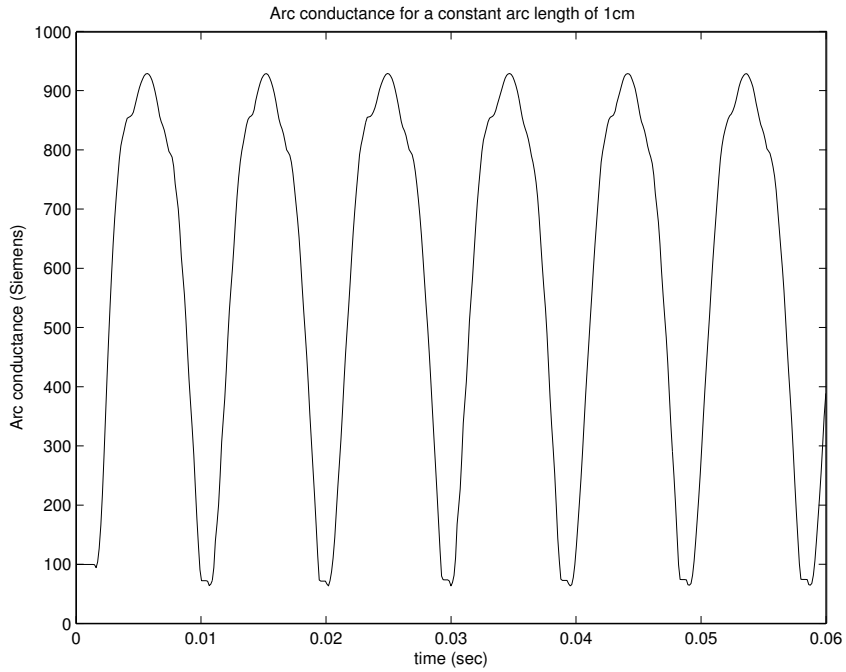

Figure 4.5: Simulated arc conductance on a single phase, obtained with the derived electrical model. Arc conductance is the inverse of arc resistance.

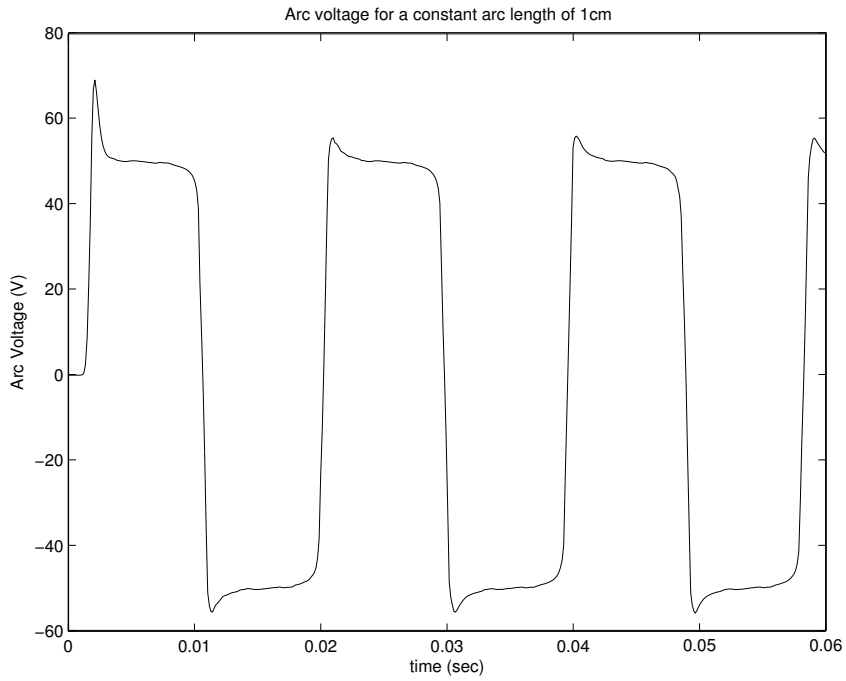

Figure 4.6: Simulated arc voltage on a single phase, obtained with the derived electrical model.

The voltage/current characteristic of an electric arc is a very common method used to illustrate the behavior of an electric arc. Such a characteristic for constant arc length is illustrated in figure 4.7. Note that there is very little variation in the characteristics for the various periods in this simulation. This should be very different during normal operation of an electric arc furnace because of the random movements (scrap cave-ins) of scrap metal, which causes the arc length to vary significantly. This might represent typical characteristics for flat bath conditions except for noise, which are not illustrated here.

The simulation results given so far illustrate only single phase properties when constant arc lengths are applied to all three inputs. Figure 4.2 illustrated a 120° phase difference between the supply voltages at the secondary transformer windings. Arc current is used to illustrate the presence of the 120° phase difference for all the electrical quantities, including the arc voltage and resistance. The arc current waveforms for the respective phases are illustrated in figure 4.8. The amplitudes for all three arc currents

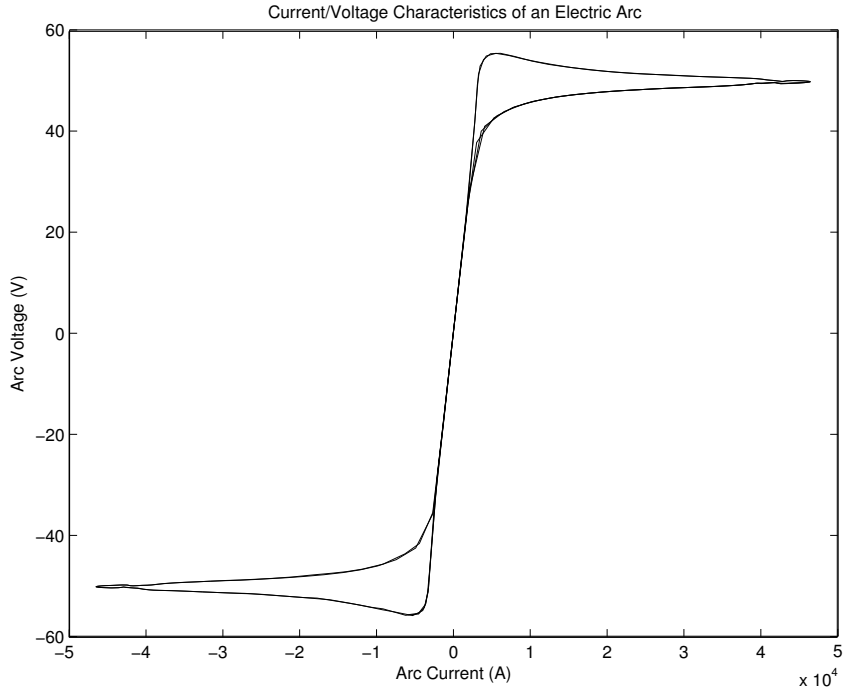

Figure 4.7: Arc Voltage vs. Arc Current for a constant arc length of 1cm.

are more or less the same. This is due to the chosen constant arc lengths on all three phases.

4.2.2 Variable Arc Length on a Single Phase

In an electric arc furnace process the distances between the electrode tips and the metallic charge is highly variable due to the random nature of the scrap. The electrical quantities are simulated in this section with variable arc lengths on the inputs of the electrical model. Note that these variations are completely random in practice and that the simulation in this section is only an illustrative example. Random inputs for a specific time duration have also been used in literature [63].

Arc current, arc impedance, arc conductance and arc voltage are again the interesting variables to illustrate the behavior of an electric arc furnace for variable arc lengths. For this specific simulation, the arc lengths of phase 1 and 2 are kept constant at 1cm. The arc length on phase 1 is varied for 0.1 seconds. The arc length applied to phase 1 for this simulation is illustrated in figure 4.9. Note that the arc lengths were not illustrated in

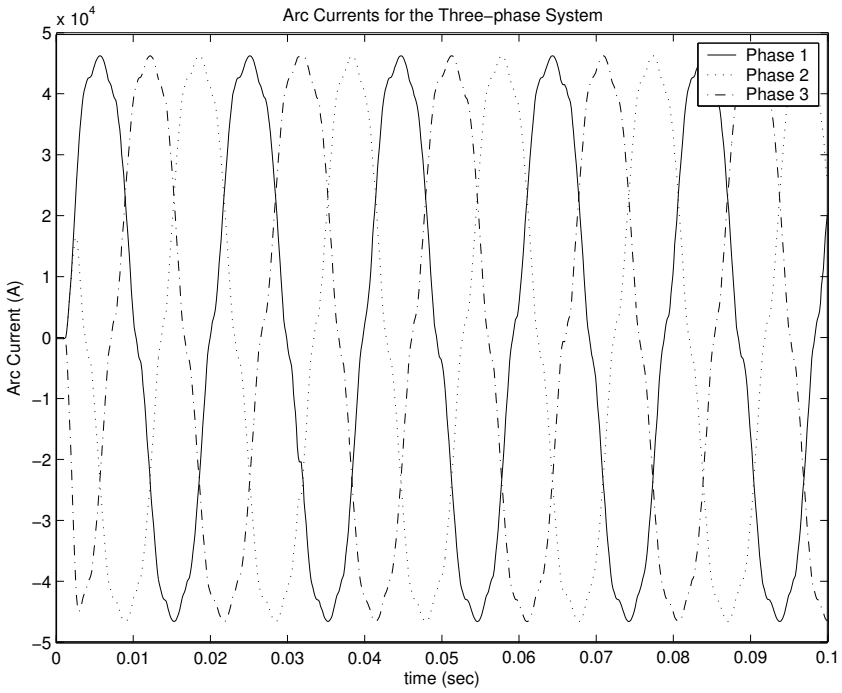

Figure 4.8: Three-phase arc currents for a balanced system if constant arc lengths are applied to all the phases. This simulation illustrates the 120° phase difference between the respective phases.

the previous simulation because it remained constant for the entire simulation time.

The same transformer secondary voltages are used for this simulation, i.e. 600 V. Arc current, arc resistance, arc conductance and arc voltage of phase 1 for the arc length described in figure 4.9 are illustrated in figures 4.10, 4.11, 4.12 and 4.13, respectively. Note time instances $0.03s$ and $0.065s$ when the arc length on phase 1 changes.

The waveforms obtained with variable arc length are very similar to that for constant arc length. The same discussion is also valid for these waveforms. The important thing to note here is the changes in amplitudes due to the arc length variation on phase 1. The arc current on phase 1 decreases almost with 1 kA (rms value) if the arc length is changed from 1 cm to 10 cm. The arc resistance, for the same step in arc length, increases from about 0.015 Ω to 0.05 Ω.

The voltage/current characteristic of the three-phase electric arc is different for re-

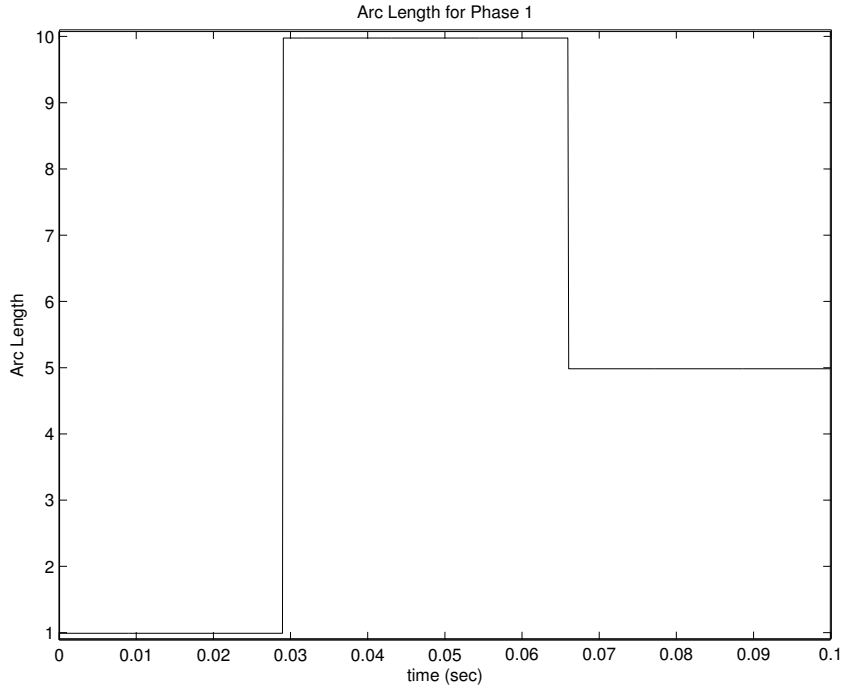

Figure 4.9: Variable arc length applied on phase 1. The arc lengths on phase 2 and 3 are constant at 1cm. The units for arc length above is also in cm.

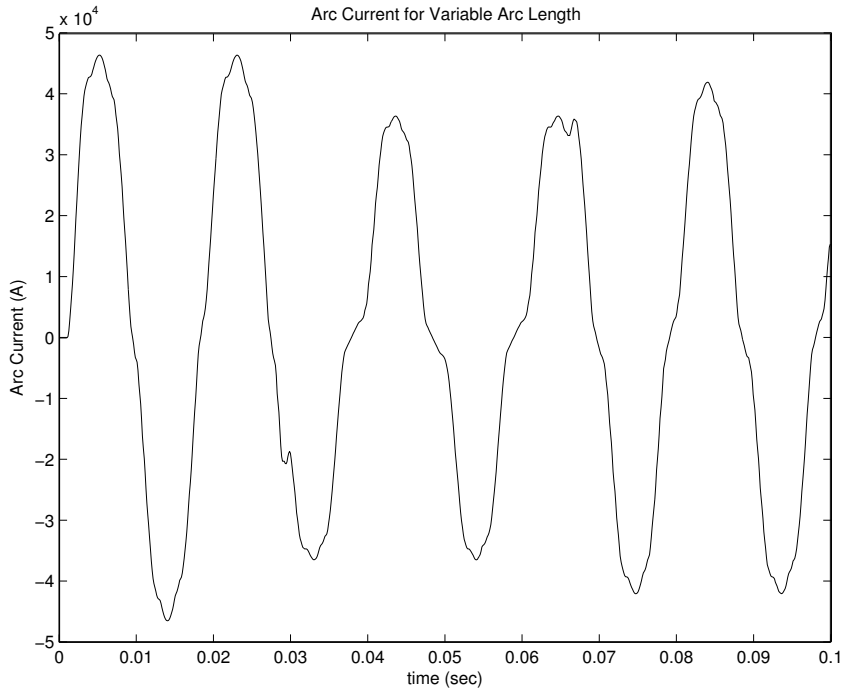

Figure 4.10: Simulated arc current obtained with the derived electrical model.

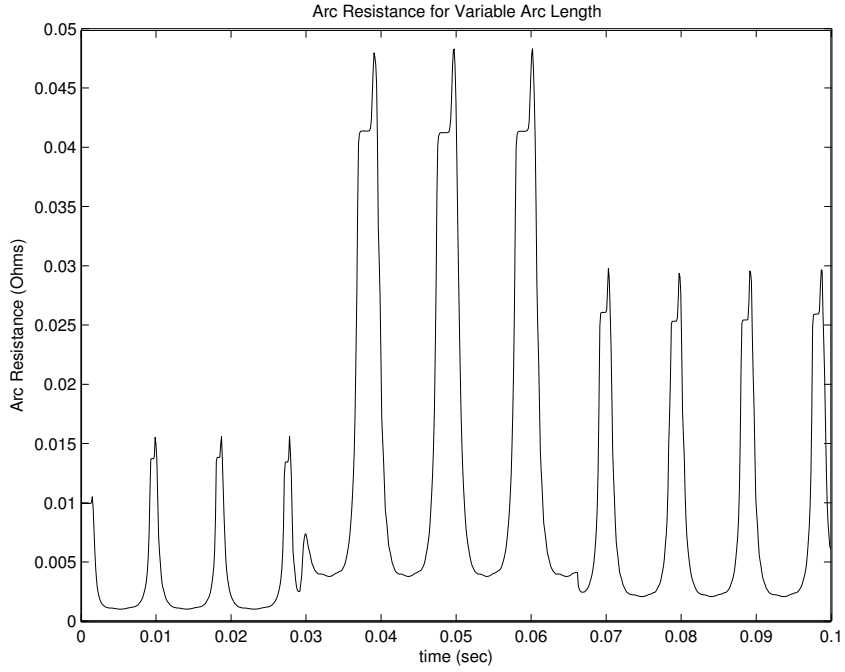

Figure 4.11: Simulated arc resistance (Ω) obtained with the derived electrical model.

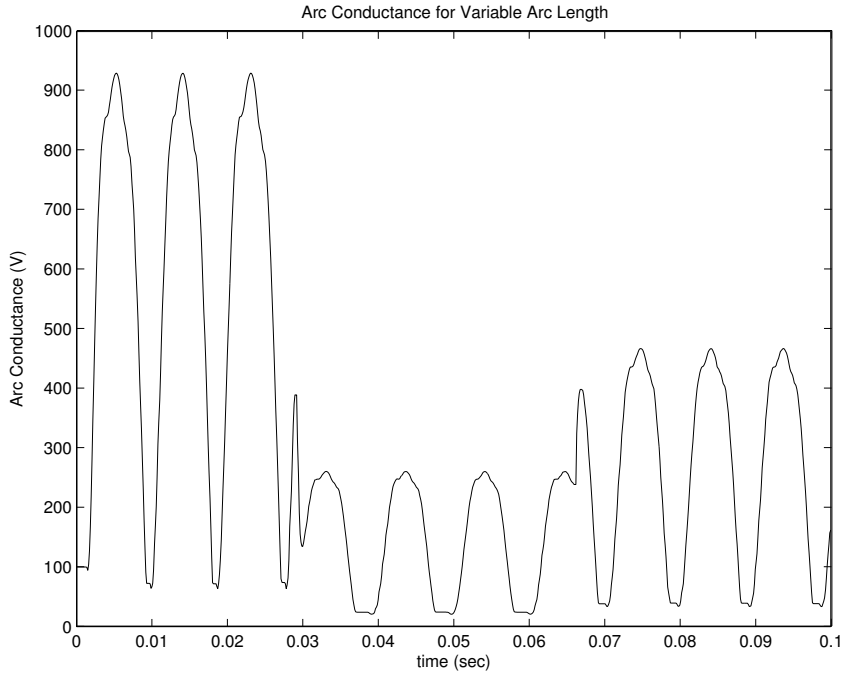

Figure 4.12: Simulated arc conductance obtained with the derived electrical model.

spective periods due to the variations in arc length on phase 1. This characteristic is illustrated in figure 4.14. The arc length in figure 4.9 has three different values which relate to three separate voltage/current characteristics in figure 4.14.

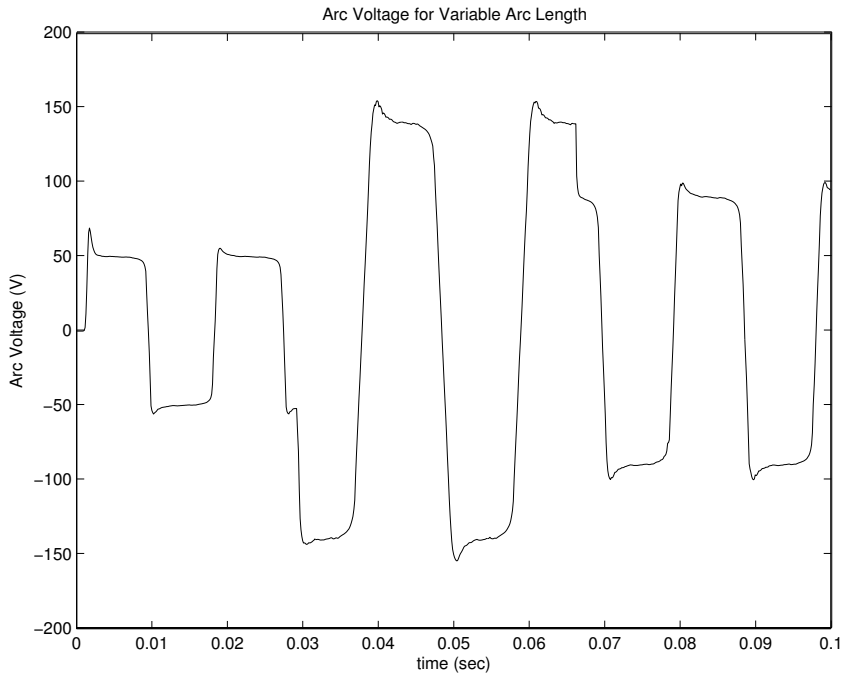

Figure 4.13: Simulated arc voltage obtained with the derived electrical model.

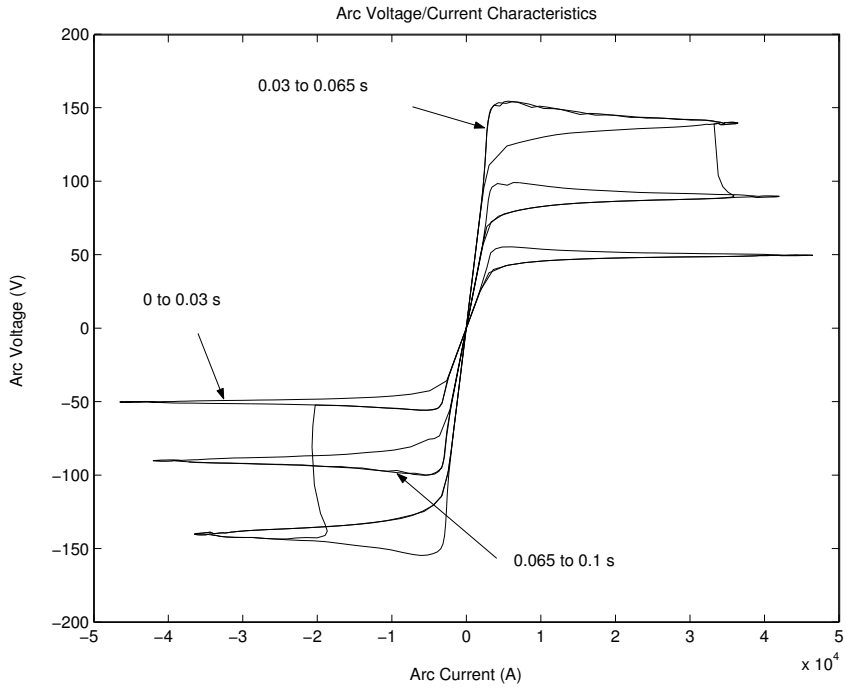

Figure 4.14: Arc voltage vs. arc current for variable arc length on phase 1.

4.2.3 Variable Arc Length on Multiple Phases

Another possibility in a three-phase electric arc furnace process is arc length variations on multiple phases. This section looks at the electrical properties when such variations occur in the electric arc furnace process.

The simulation is carried out for a duration of 0.1s, where the arc lengths on all three phases vary from 1 cm to 5 cm at 0.05 s. Figures 4.15, 4.16, 4.17 and 4.18 illustrate arc current, arc resistance, arc conductance and arc voltage on phase 1 with simultaneous steps in arc lengths.

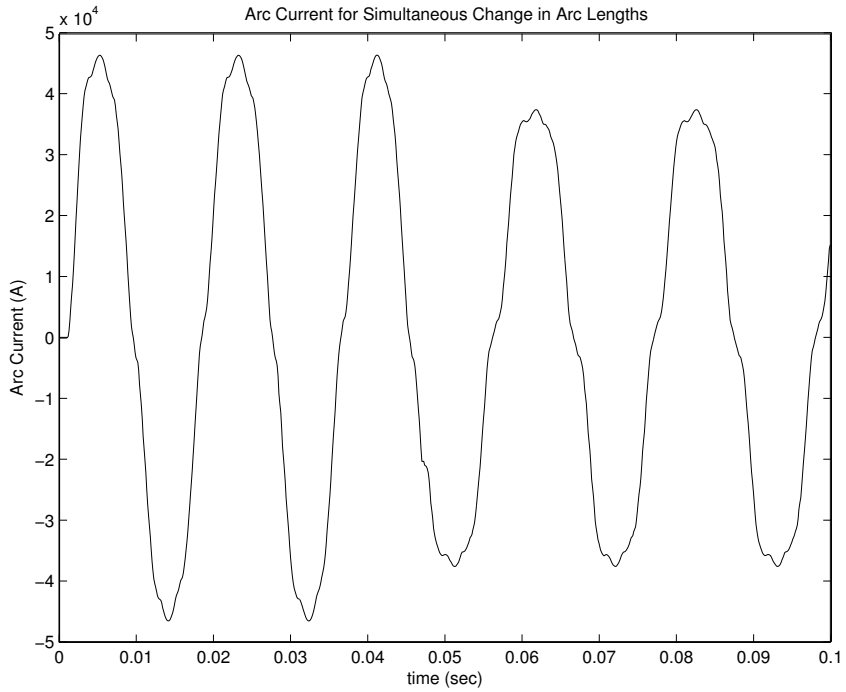

Figure 4.15: Simulated arc current on phase 1 with step changes on all 3 arc lengths.

From figure 4.15, the arc current on phase 1 decreases with about 1kA at 0.05s. In the previous section the arc current was decreased by the same amount. However, this was for a change in arc length from 1 cm to 10 cm on a single phase. This illustrates the significant interaction between the respective phases. Arc resistance on phase 1 increases from 0.015 Ω to 0.03 Ω. Also note that small variation in arc length doesn't affect the shape of the three-phase waveforms significantly except when it occurs during a half wave that is not yet completed.

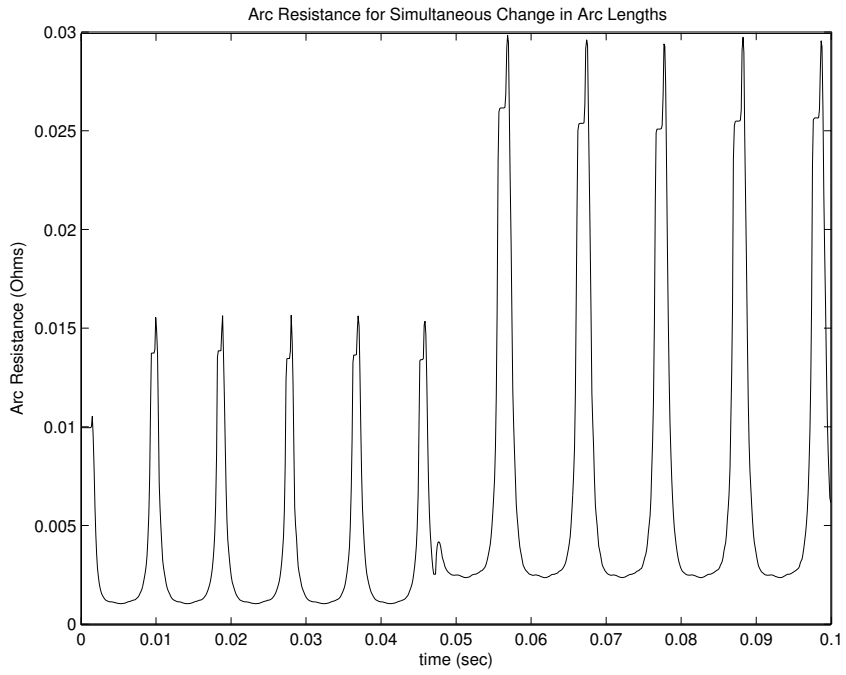

Figure 4.16: Simulated arc resistance on phase 1 with step changes on all 3 arc lengths.

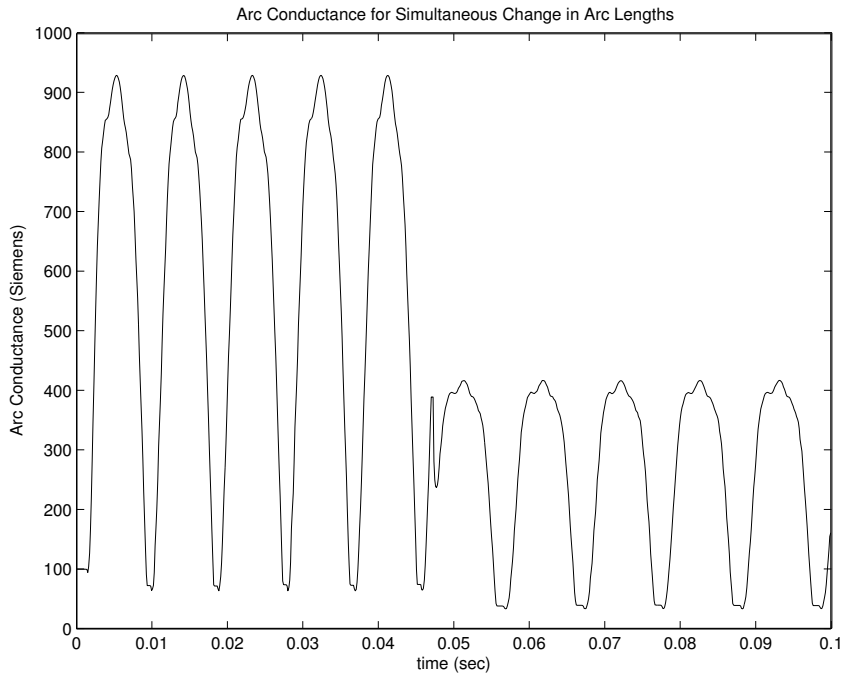

Figure 4.17: Simulated arc conductance on phase 1 with step changes on all 3 arc lengths.

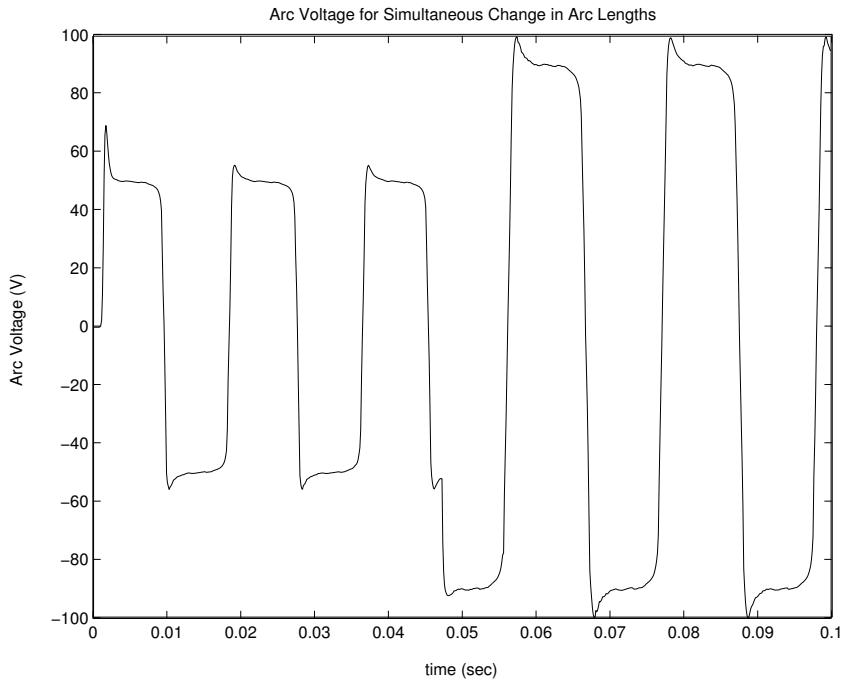

Figure 4.18: Simulated arc voltage on phase 1 with step changes on all 3 arc lengths.

4.3 The Hydraulic Actuator

The current input to the servo-valve of the particular hydraulic actuator under study ranges from -150mA to 150mA. In practice these inputs are either maximum or minimum depending whether the hydraulic piston needs to move up or down. The hydraulic piston will move up at maximum speed if the input current applied to the servo-valve is 150 mA and down if it is -150 mA.

The simulation in this section is done for a duration of 3 s. The input current for the first 1.5 s is 150 mA and -150 mA for the final 1.5 s. To recall from chapter 3, the hydraulic actuator model consists of six state variables which are:

- hydraulic distributor, spool position,
- hydraulic distributor, spool velocity,
- hydraulic piston position,
- hydraulic piston velocity,
- pressure in cylinder above the piston, and

- pressure in cylinder below the piston.

The important state variable is the hydraulic piston position, which is converted to the electrode tip displacement and serves as the input to the electrical model. The six states are simulated for the described input and the results are illustrated in figures 4.19 to 4.24.

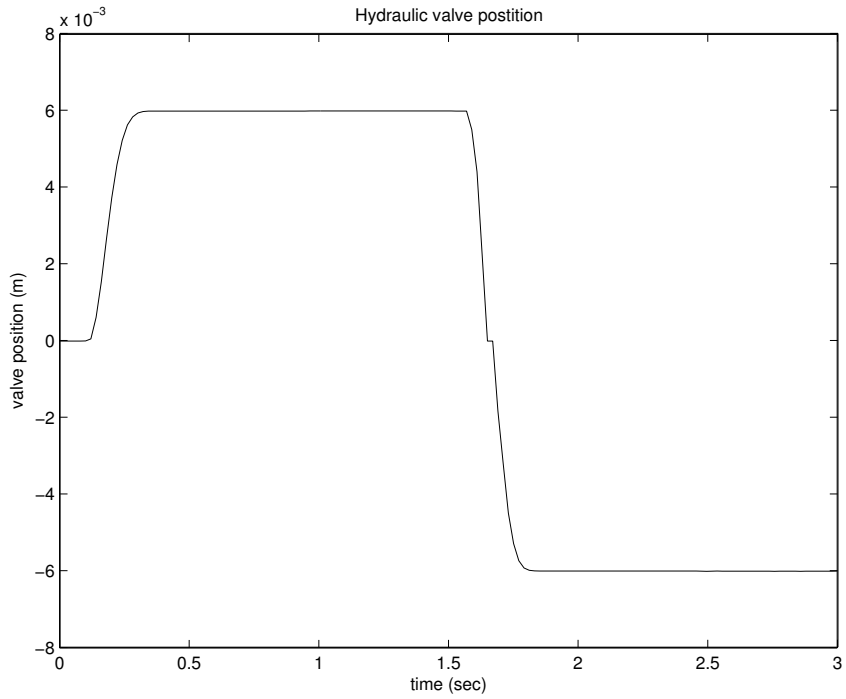

Figure 4.19: Hydraulic distributor valve position for a servo-valve input of 150 mA for the first 1.5 s and -150 mA for the final 1.5 s.

The hydraulic distributor valve in figure 4.19 is either completely open or closed, depending on the servo-valve input. This results in the valve velocity being zero whenever the servo-valve input current is constant, figure 4.20. In figure 4.21, the hydraulic piston is moving up for a servo-valve input of 150 mA and down for an input of -150 mA. Note that there is a time delay of about 0.25 s before the piston responds to a new servo-valve current. The velocity of the piston is about 0.1 m/s, which corresponds to typical speeds achieved in industry.

The pressure in the main cylinder is not used often in industry, but is used however

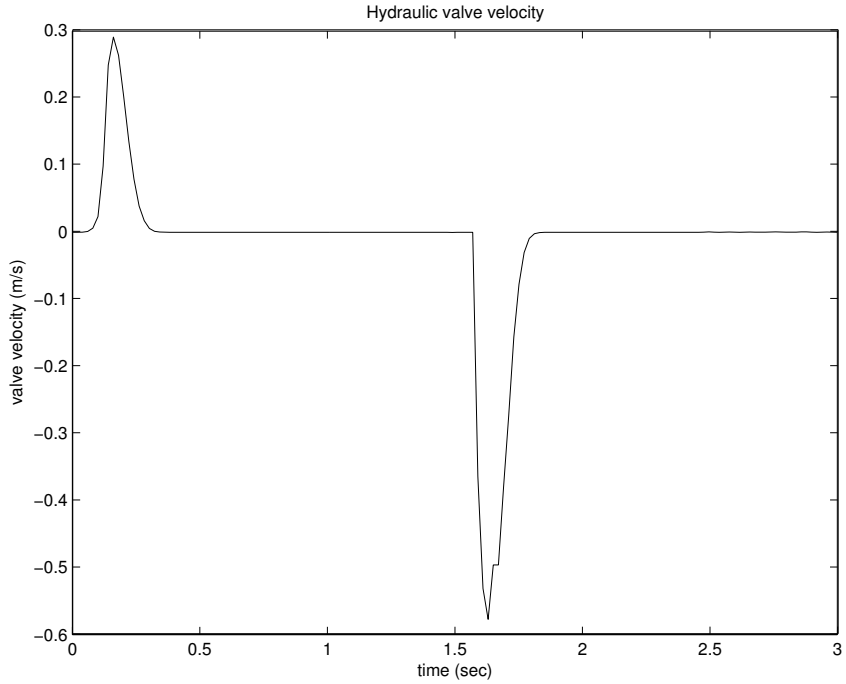

Figure 4.20: Hydraulic distributor valve velocity for the servo-valve input of 150 mA for the first 1.5 s and -150 mA for the final 1.5 s.

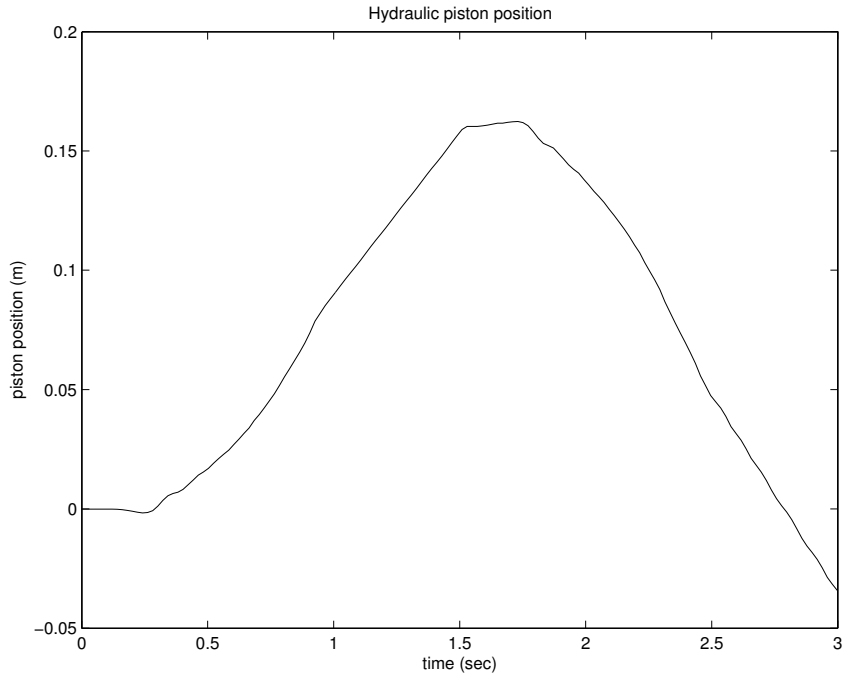

Figure 4.21: Hydraulic piston position for the servo-valve input of 150 mA for the first 1.5 s and -150 mA for the final 1.5 s.

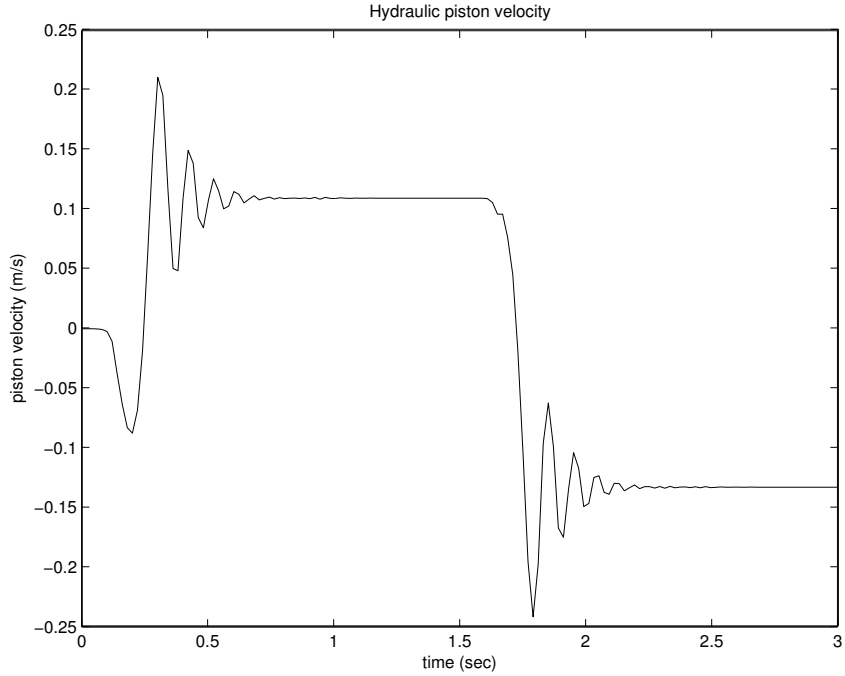

Figure 4.22: Piston velocity for the servo-valve input of 150 mA for the first 1.5 s and -150 mA for the final 1.5 s.

to detect collisions between the electrodes and raw materials.

4.4 Electric and Hydraulic Models Connected Together

In a three-phase electric arc furnace process, three hydraulic actuators are connected to each of three graphite electrodes, figure 4.1. For a complete electrode system, the connected hydraulic and electrical models have to be controlled. This section illustrates the complete open loop electrode system without feedback control. The controller design and implementation is carried out in chapter 6.

With the two models connected together, the overall inputs are the servo-valve input currents and the outputs the arc currents on the three respective phases. This simulation will illustrates the transient responses of arc currents when changes occur on the servo-valve input currents. Note that in practice, some of the inputs, outputs or state variables

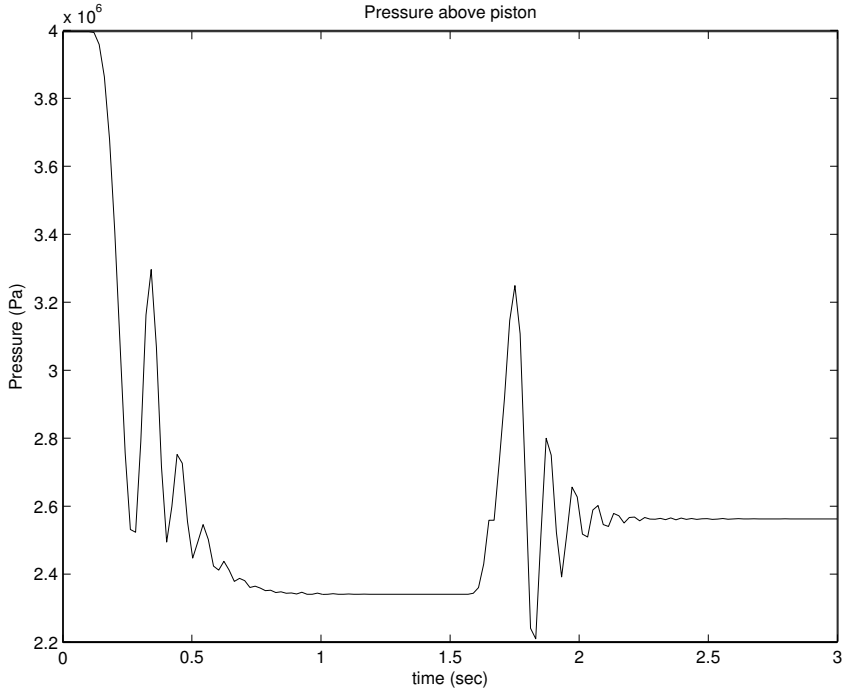

Figure 4.23: Pressure in chamber 1 for the servo-valve input of 150 mA for the first 1.5 s and -150 mA for the final 1.5 s.

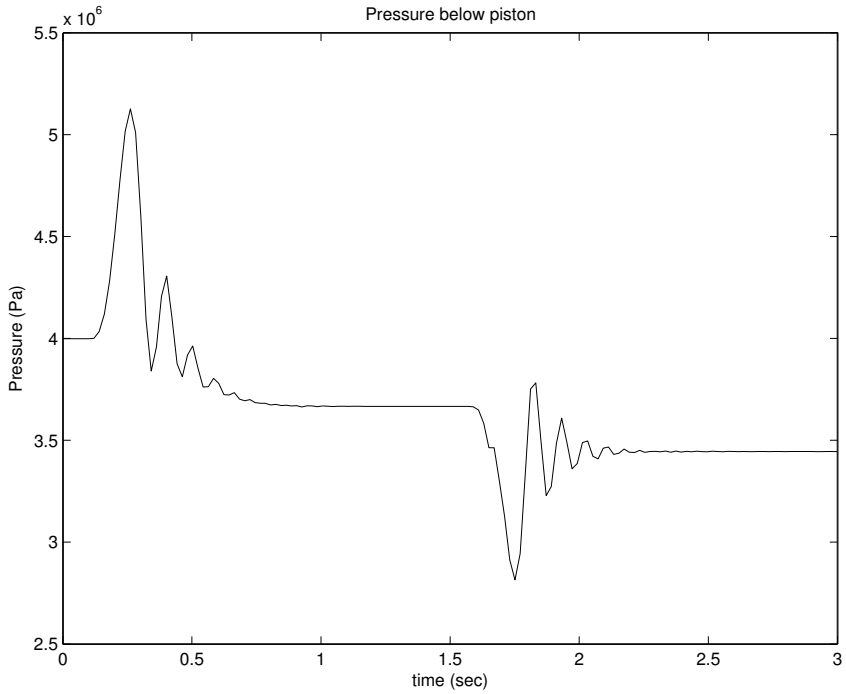

Figure 4.24: Pressure in chamber 2 for the servo-valve the input of 150 mA for the first 1.5 s and -150 mA for the final 1.5 s.

may saturate, but this is not yet included in the simulation.

The duration of the simulation in this section is 0.5 s. The servo-valve inputs are zero for the first 0.25 s and then stepped to 150 mA for the remainder of the simulation,as shown in figure 4.25. For clarity purposes the results in this section are given in rms-values rather than the complete waveforms. The simulation results on all three phases look similar and the results of only one phase is illustrated and discussed here. Note that the piston position in figure 4.26 is multiplied by 100 to convert the output to centimeters, which is needed for the electric model input. The remaining state variables, such as pressures in the cylinder, are not given here because such results will not be relevant to the simulation of the combined model.

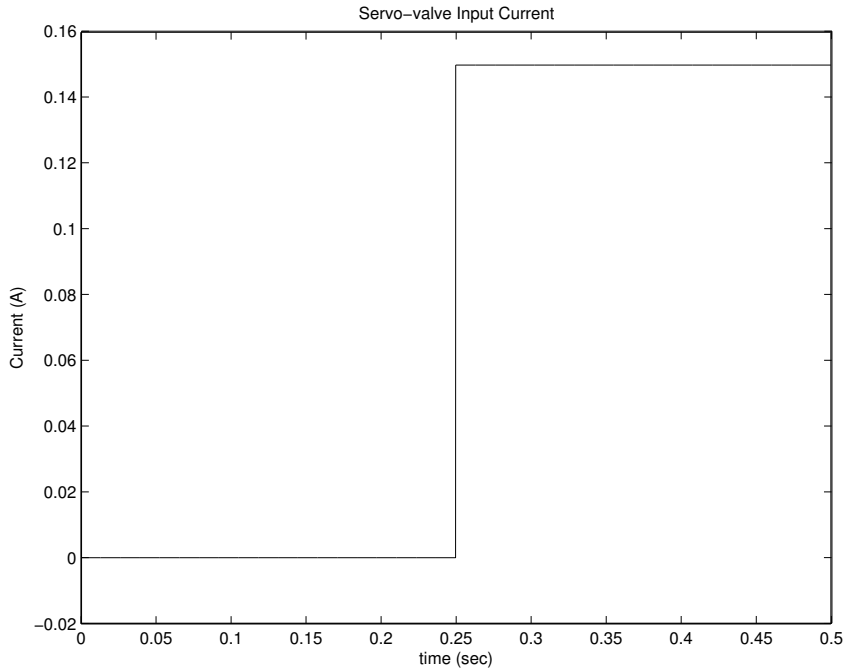

Figure 4.25: Servo-valve input current to one of the hydraulic actuators. The inputs to the other two actuators are constant for this simulation.

Arc current, arc voltage and arc resistance are all relatively constant if the hydraulic piston remains constant, see figures 4.27 to 4.29. When the pistons start to raise because of the step input at time instant 0.25 s, the arc currents as well as the arc conductances decrease and the arc voltages increase.

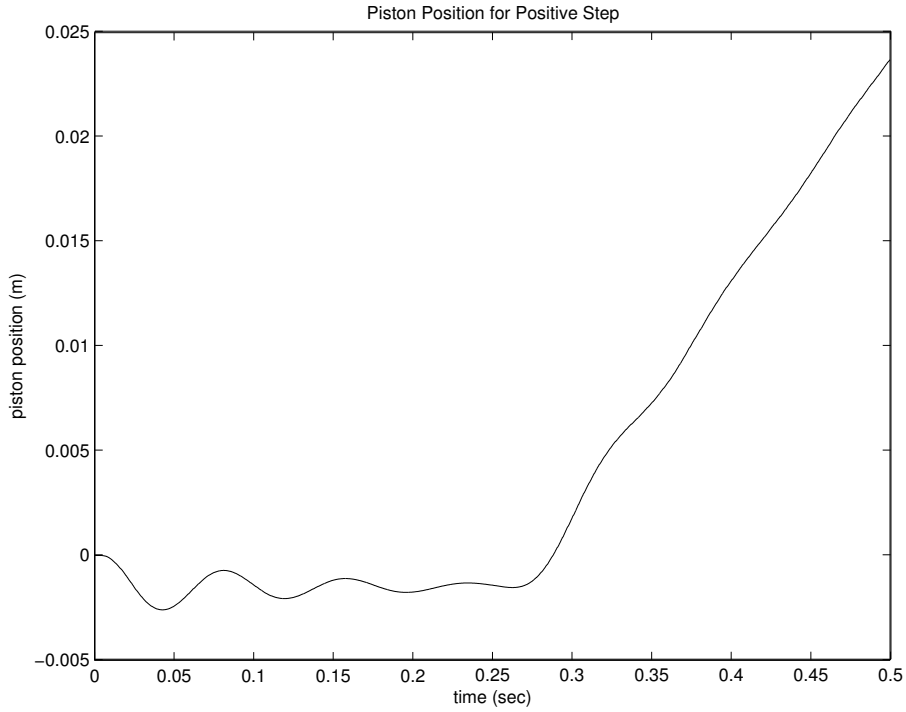

Figure 4.26: Piston position for the servo-valve input in figure 4.25.

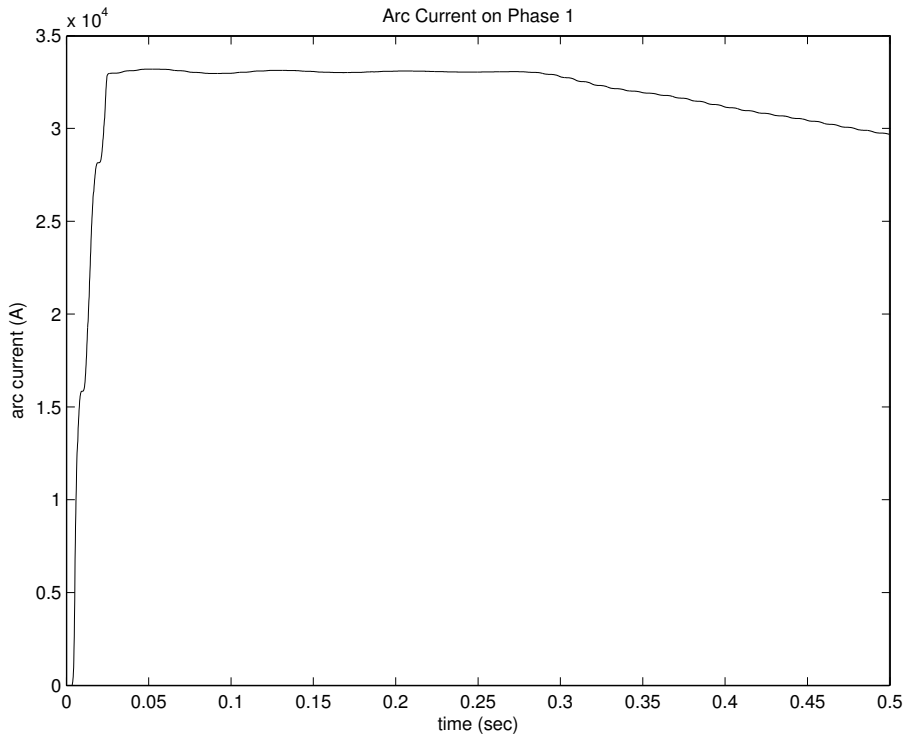

Figure 4.27: Arc Current with the electrode position as in figure 4.26.

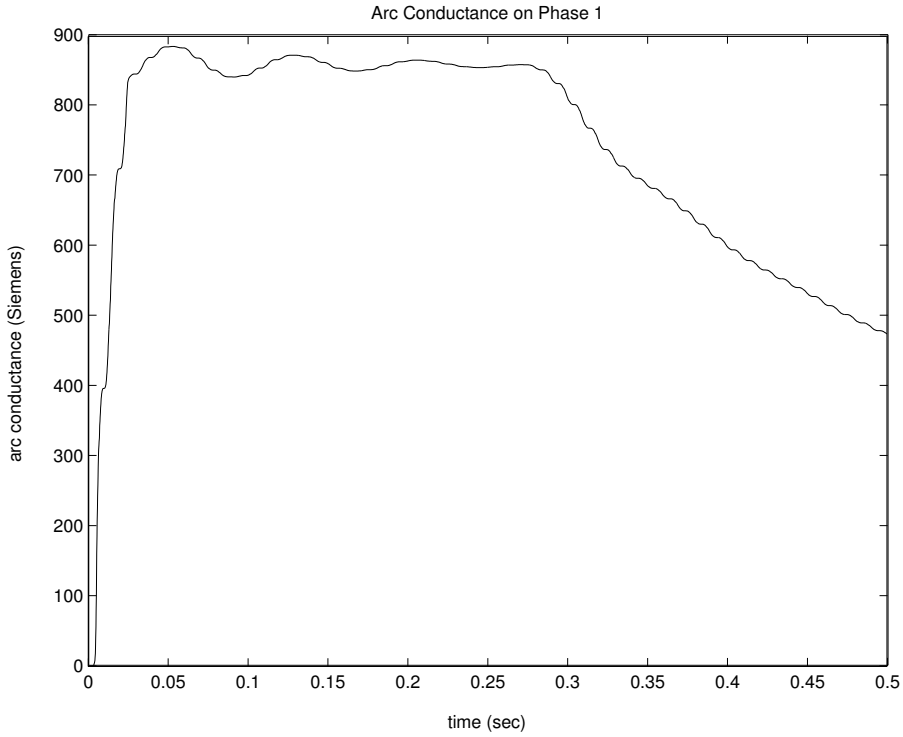

Figure 4.28: Arc conductance with the electrode position as in figure 4.26.

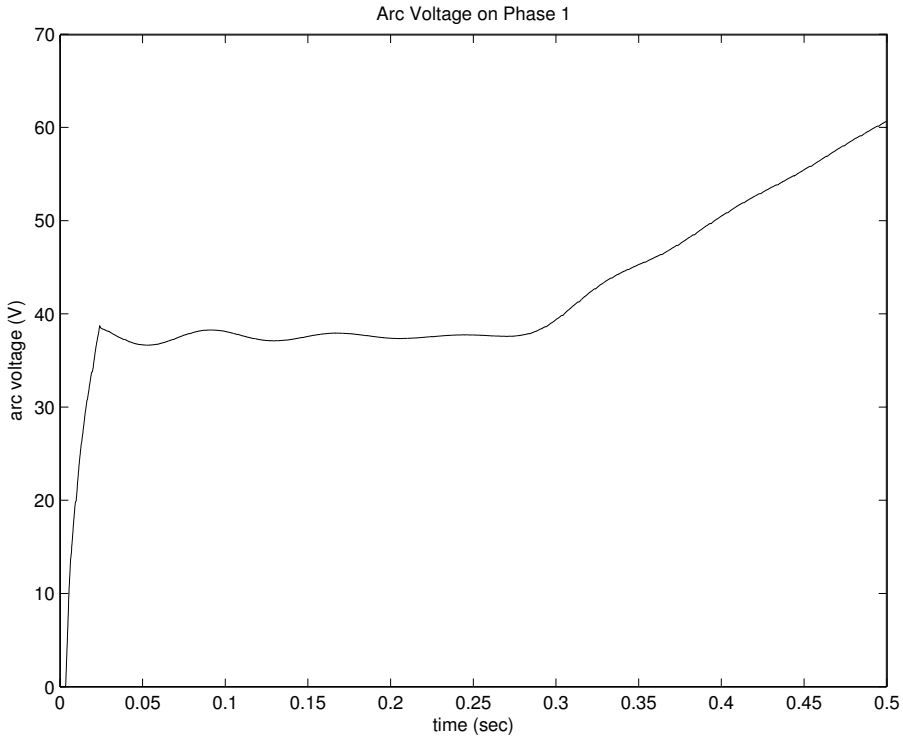

Figure 4.29: Arc voltage with the electrode position in figure 4.26.

Clearly from these results, an arc furnace can not operate without automatic control implemented, specially if the main objective is to maintain constant electrical power input. The chapters to follow deal with the linearization, controller design, and implementation on the electrode system.

4.5 Conclusion

The models derived in chapter 3 for the electrical system and the hydraulic actuators in an electrode system for a three-phase electric arc furnace were simulated separately as well as combined in this chapter.

The models are not yet controlled in this chapter and the simulation results illustrate only the dynamic behaviour of the open loop systems. The responses obtained in this chapter proved significant to use for linearization purposes in the chapter to follow.

Chapter 5

Linear Model Derivation

5.1 Introduction

The electric arc furnace model derived in chapter 3, consisting of an electrical system and three hydraulic actuators, is highly nonlinear. In this dissertation, model based controller design methods are used which requires a linear plant model [64]. The nonlinear open loop electrode system is used in this chapter to build a linear approximation for the model.

Such a linear approximation is done in the neighborhood of a chosen set of operating points. The linear model will typically perform fairly accurately in this region of operation. The best choice of operating regions is usually nominal steady state conditions.

Large changes in operating conditions for a nonlinear process cannot be approximated satisfactorily by linear expressions. Most of the variables relating to a three-phase electric arc furnace model are sinusoidal type signals, which mean that no nominal steady state conditions exist. The solution to this phenomenon is to re-model the nonlinear electrical model in terms of amplitudes or rms-values. This re-modelling is carried out in section 5.3.

In section 5.2 the method of linearisation used in this dissertation is discussed. In section 5.3, some adjustments are made to the hydraulic model as well to facilitate linearisation.

5.2 The General Linearisation Problem

The linearisation approach, used in this dissertation, is not particular to control system analysis, synthesis, and design but is also a key modelling tool in other fields, for example in analog electronics [65]. The linearisation strategy discussed here can also be applied equally well to models incorporating continuous or discrete time models.

5.2.1 State Space Models

The convenient method in linear control system design is to write the derived model in a well known form, called the state space description.

The general form of the state space presentation for linear differential equation models are given as follow:

$$\frac{d\mathbf{x}(t)}{dt} = \mathbf{A}\mathbf{x}(t) + \mathbf{B}\mathbf{u}(t), \tag{5.1}$$

$$\mathbf{y}(t) = \mathbf{C}\mathbf{x}(t) + \mathbf{D}\mathbf{u}(t), \tag{5.2}$$

where $\mathbf{A}$, $\mathbf{B}$, $\mathbf{C}$ and $\mathbf{D}$ are constant matrices of appropriate dimensions. $\mathbf{x}(t)$ represent the state variable matrix, $\mathbf{y}(t)$ the system output matrix and $\mathbf{u}(t)$ the input matrix.

With these equations in mind the objective is to obtain $\mathbf{A}$, $\mathbf{B}$, $\mathbf{C}$, and $\mathbf{D}$ which yield a linear time-invariant system.

5.2.2 Obtaining the Linear Model

Before starting with the linearisation procedure, the nonlinear model needs to be in first order differential equation format, as achieved in chapter 3. The model in the form:

$$\dot{\mathbf{x}}(t) = f(\mathbf{x}(t), \mathbf{u}(t)), \tag{5.3}$$

$$\mathbf{y}(t) = g(\mathbf{x}(t), \mathbf{u}(t)). \tag{5.4}$$

These equations are next approximated by a first-order Taylor series expansion to represent the linear model. Before applying the Taylor series to the differential equation model, equilibrium points are needed around which the linear model will be valid. These are normally found as the nominal steady state values of the nonlinear model and are represented by x_Q, u_Q and y_Q. The Taylor series expansion are then applied as follow:

$$\dot{x}(t) \approx f(x_Q, u_Q) + \frac{df}{dx}|_{x=x_Q;u=u_Q}(x(t) - x_Q) + \frac{df}{du}|_{x=x_Q;u=u_Q}(u(t) - u_Q), \tag{5.5}$$

$$y(t) \approx g(x_Q, u_Q) + \frac{dg}{dx}|_{x=x_Q;u=u_Q}(x(t) - x_Q) + \frac{dg}{du}|_{x=x_Q;u=u_Q}(u(t) - u_Q). \tag{5.6}$$

The important thing to note from these equations is that the derivative matrices will be constant. The derivation of the matrices, **A**, **B**, **C**, and **D** in equations 5.1 and 5.2 can be represented in a more general form. First denote the differential equation model of order n as follow:

$$\dot{x}_n = f_n(x(t), u(t)), \tag{5.7}$$

$$y_n(t) = g(x(t), u(t)), \tag{5.8}$$

where $x(t)$ and $u(t)$ are vectors of corresponding lengths. Each entry for **A**, **B**, **C** and **D** can then be derived by using the following equations:

$$\mathbf{A}(n, m) = \frac{df_n}{dx_m}|_{x=x_Q;u=u_Q}, \tag{5.9}$$

$$\mathbf{B}(n,m) = \frac{df_n}{du_m}|_{x=x_Q;u=u_Q}, \tag{5.10}$$

$$\mathbf{C}(n,m) = \frac{dg_n}{dx_m}|_{x=x_Q;u=u_Q}, \tag{5.11}$$

$$\mathbf{D}(n,m) = \frac{dg_n}{du_m}|_{x=x_Q;u=u_Q}. \tag{5.12}$$

The state variable in the three-phase electric arc furnace model consists mostly of sinusoidal signals. To choose nominal steady state values from such signals are impossible. However, with some adjustments, the model derived earlier can be expressed such that all the variables are represented by amplitude values. The next section will deal with the re-modelling of the electrical model.

5.3 Re-modelling and Adjustments on the Electrical Model

The model derived in chapter three is simulated with the variables represented as sinusoidal three-phase signals. The objective of re-modelling the nonlinear model is to ensure that all inputs and states are represented as steady state values. This can be achieved by applying the input voltages from the secondary side of the furnace transformer as imaginary phasors rather than sine waves.

To recall, the arc furnace supply system is modelled as constant voltage sources with finite source impedances and inductances and are connected in delta to represent the secondary side of the furnace transformer. The three-phase load is represented by the nonlinear electric arcs which are connected in a star configuration. Refer to figure 3.2 for the electrical supply configuration.

The voltage sources are represented by sine waves with constant and finite amplitudes. The phase difference between each phase is 120° and the three-phase supply voltages are

represented as follow:

$$V_a = V_m \sin(\omega t), \tag{5.13}$$

$$V_b = V_m \sin(\omega t + 120°), \tag{5.14}$$

$$V_c = V_m \sin(\omega t - 120°). \tag{5.15}$$

To represent the system in terms of amplitudes, these voltage sources are represented by phasors as follow:

$$V_a = V_m(1 + j0), \tag{5.16}$$

$$V_b = V_m(-\frac{1}{2} + j\frac{\sqrt{(3)}}{2}), \tag{5.17}$$

$$V_c = V_m(-\frac{1}{2} - j\frac{\sqrt{(3)}}{2}). \tag{5.18}$$

The reactance for each phase is approximated with zero inductance as this has no significant effect on the simulation results with a large reduction in complexity. The total phase impedances are then represented by the summation between the source and arc resistances as follow:

$$Z_n = R_n + R_{an}, \tag{5.19}$$

where R_n and R_{an} represent source and arc resistance respectively for each phase. The voltage and current equations are next constructed by using Kirchoff's law in the same manner as in section 3. The electrical equations are then given in 5.20 to 5.22 below.

$$-V_m + I_1 Z_1 - I_2 Z_2 = 0, \tag{5.20}$$

$$-V_m h' + I_3 Z_3 - I_1 Z_1 = 0, \tag{5.21}$$

$$I_1 + I_2 + I_3 = 0. \tag{5.22}$$

A three-phase operator, $h = -\frac{1}{2} + j\frac{\sqrt{(3)}}{2}$, is used to represent the phase difference between the supply voltages. I_1, I_2 and I_3 represent the arc currents for each phase, respectively. The objective is to derive equation for the arc currents in terms of their amplitudes. This is done by breaking the equations up into real and imaginary sections which is very easy to convert to amplitudes. The equations were derived as follow:

$$I_1 = [\frac{V_m Z_3}{k_1} + \frac{0.5 V_m Z_2}{k_1}] + j[\frac{\sqrt{(3)} V_m Z_2}{2k_1}], \tag{5.23}$$

$$I_2 = [\frac{-0.5 V_m Z_1 - V_m Z_3}{k_1}] + j[\frac{\sqrt{(3)} V_m Z_1}{2k_1}] \tag{5.24}$$

and

$$I_3 = [-Re(I_1) - Re(I_2)] + j[-Im(I_1) - Im(I_2)], \tag{5.25}$$

where

$$k_1 = Z_2 Z_3 + Z_3 Z_1 + Z_1 Z_2. \tag{5.26}$$

The arc impedance model derived in section 3 together with constant source resistances are used to represent the phase impedances in equations 5.23 to 5.26. Before approximating this model with a linear representation, it needs to be compared with the electric model in section 3.

5.3.1 Validation of Adjusted Electric Model

Similar simulations as in section 4 were done for the amplitude models derived in this section. The results are then compared with those in section 4 to validate the adjusted electrical model before using it for linearisation purposes.

5.3.1.1 Constant Arc Length

Constant arc length (see chapter 4, section 4.2.1) on all three phases were used here to simulate the arc current and conductance amplitudes. A detail description of all the values used for certain variables are discussed in chapter 4. The simulation results in terms of amplitudes are compared to the three-phase waveforms obtained in chapter 4.

The amplitude for the arc current signal (each phase) obtained in chapter 4 for constant arc lengths was 4.7kA. The arc current illustrated in figure 5.2 was obtained with the amplitude model and has an amplitude of 4.9kA. The reason for this small deviation is the source inductance that was neglected for the model derived in this chapter. The arc conductance amplitude obtained with the simulation in chapter 4 was 930 Siemens. The arc conductance amplitude obtained in this chapter is 990 Siemens. For controller design purposes, these deviations are insignificant and the amplitude model with negleced source inductance appear suitable for controller design.

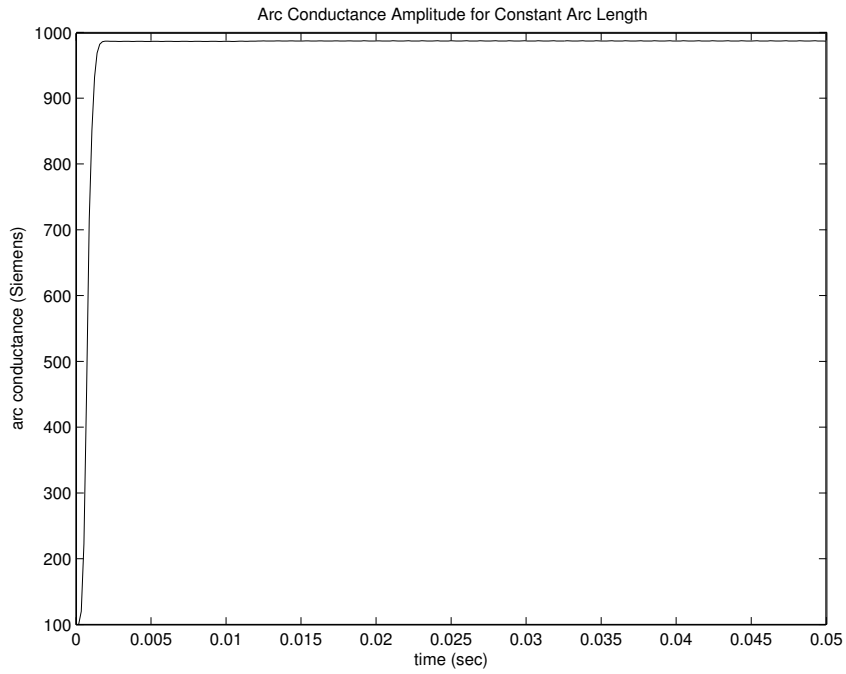

Figure 5.1: Arc conductance as simulated with the electrical amplitude model.

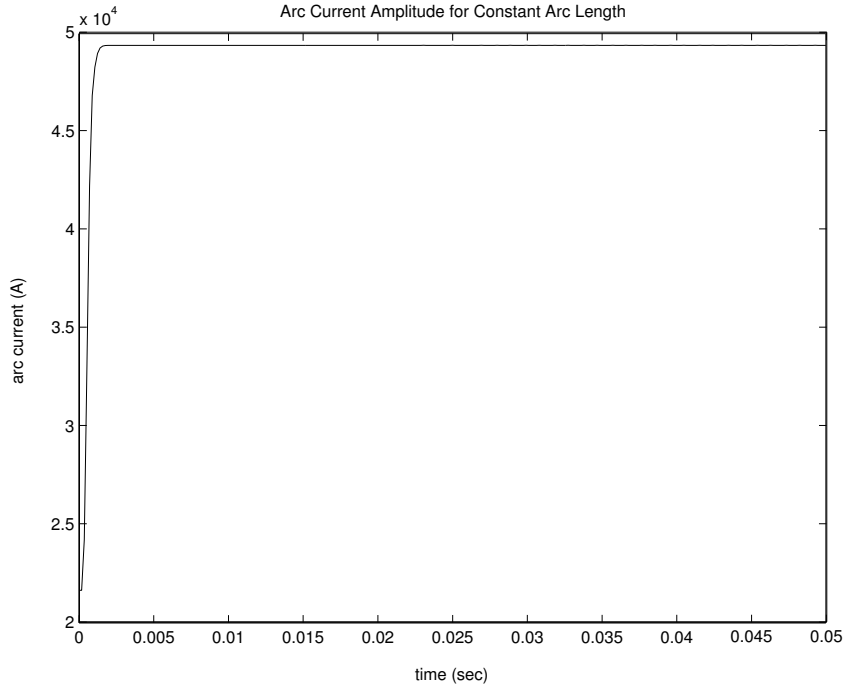

Figure 5.2: Arc current as simulated with the electrical amplitude model.

5.3.1.2 Variable Arc Length on a Single Phase

The following simulation in chapter 4, section 4.2.2, was with a step on the arc length of one of the electrical phases while the others remain constant. The reader is once again referred to chapter 4 for the various parameter values used for this simulation.

Figure 4.9 illustrates the variable arc length that was applied on phase 1 while the other two remain constant. Figures 5.3 and 5.4 below are compared with figures 4.10 and 4.12 in chapter 4. The deviations in arc current are between 0.2 kA and 0.3 kA. The arc conductance deviated with 60 Siemens or 6.4%. These deviations are once again acceptable for the purpose of controller design.

5.3.1.3 Variable Arc Length on Multiple Phases

The final simulation on the individual electrical model in chapter 4 was to vary the arc lengths on all three the phases. Figure 5.5 and 5.6 illustrates the arc conductance and current amplitudes for variable arc lengths when simulated with the electrical amplitude

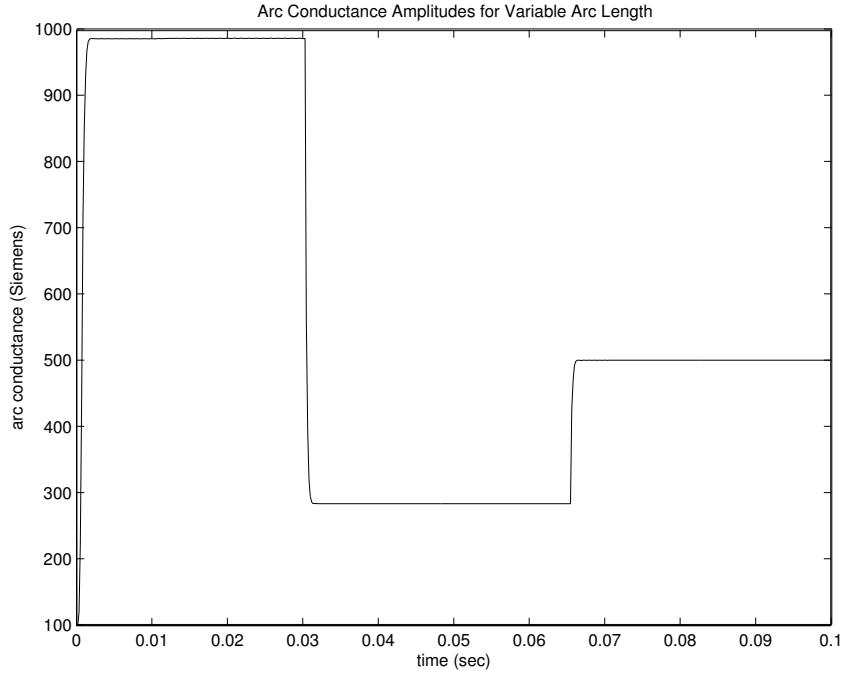

Figure 5.3: Arc conductance simulated with the electrical amplitude model with variable arc length applied to a single phase.

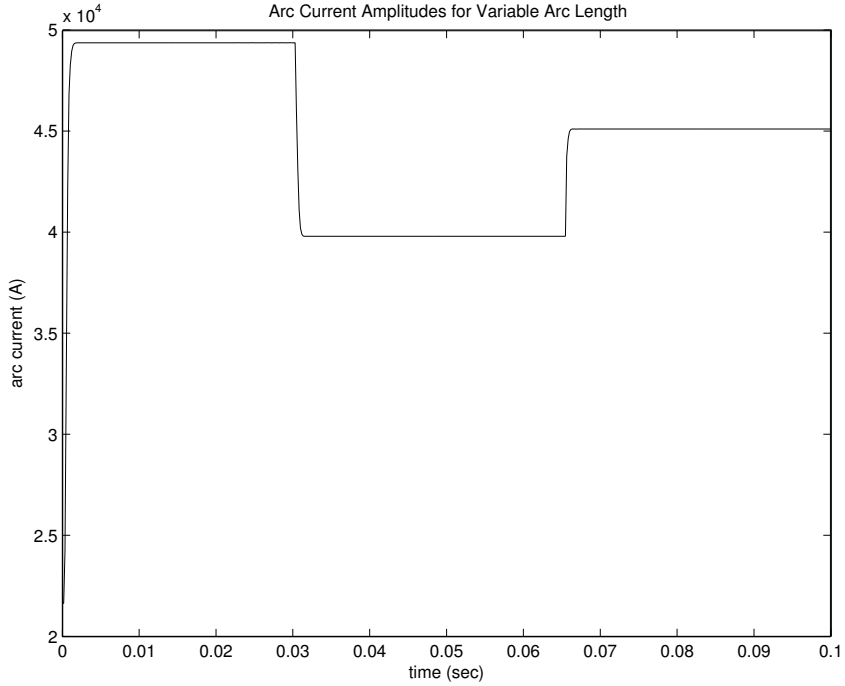

Figure 5.4: Arc current simulated with the electrical amplitude model when a variable arc length is applied on a single phase.

model.

Figure 4.15 and 4.17 illustrated the three-phase waveforms for arc current and arc conductance obtained in chapter 4. The deviations from the results obtained with the amplitude model are similar than in the previous sections. To conclude, the amplitude model, derived in this section together with the necessary approximations, is acceptable to use for linearisation of the arc furnace model.

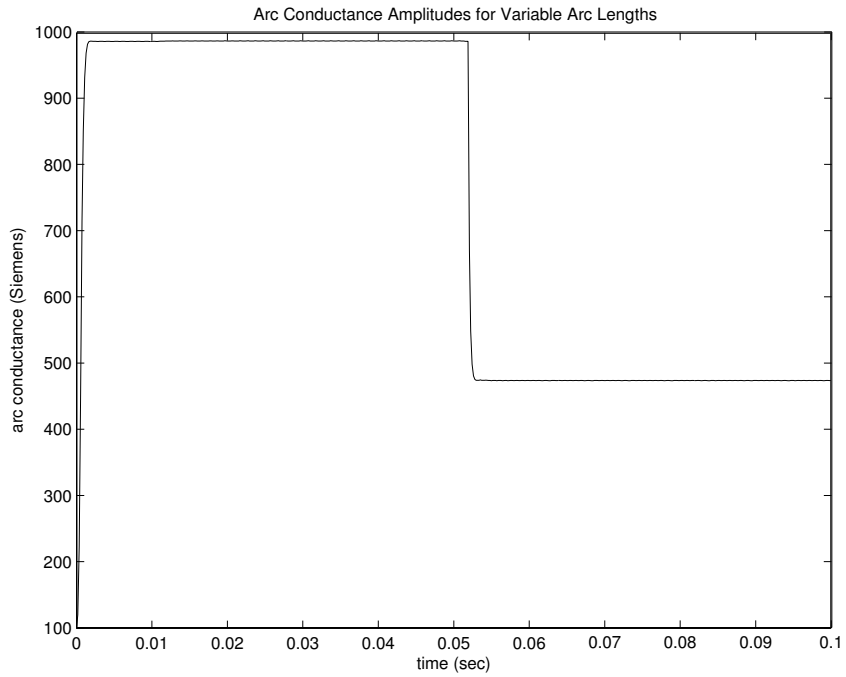

Figure 5.5: Arc conductance simulated with the electrical amplitude model when variable arc lengths are applied on all three phases.

5.4 Re-modelling the Hydraulic Model

The hydraulic actuator model derived earlier contains signum functions which are not differentiable, which is critical when a Runga-Kutta approximation is used. To approximate a linear model for the hydraulic actuator, a new differentiable model is thus needed that will yield similar results as the existing one.

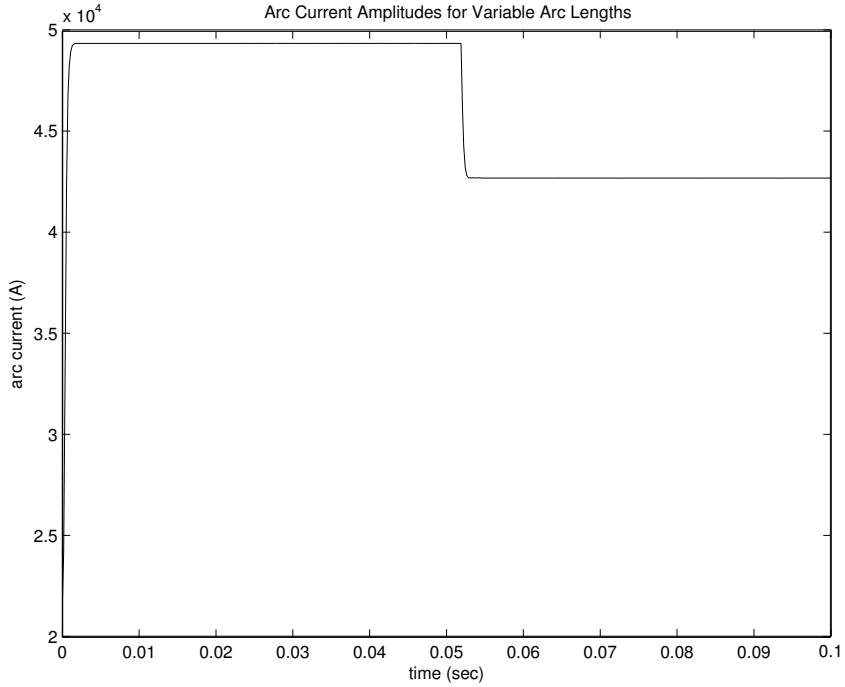

Figure 5.6: Arc current simulated with the electrical amplitude model when variable arc lengths are applied on all three phases.

The hydraulic piston position is the main output of the hydraulic actuator and has almost linear up or down movements. The dynamics in figure 4.21 can easily be approximated with a linear differential equation.

The following differential equation is used to approximate the nonlinear piston position obtained in chapter 4:

$$\dot{x} = 0.6666\dot{u}. \tag{5.27}$$

The input, u, to equation 5.27 is the servo-valve current which ranges between -150 mA and 150 mA and correspond to vertical speeds of 0.1m/s. The simulated piston position for this simple model is illustrated in figure 5.7. This result compare good enough to the piston position obtained in chapter 4.

The new electrical and hydraulic models will next be used to obtain a linear approximation for the complete open loop electrode system. The linear model will then be used

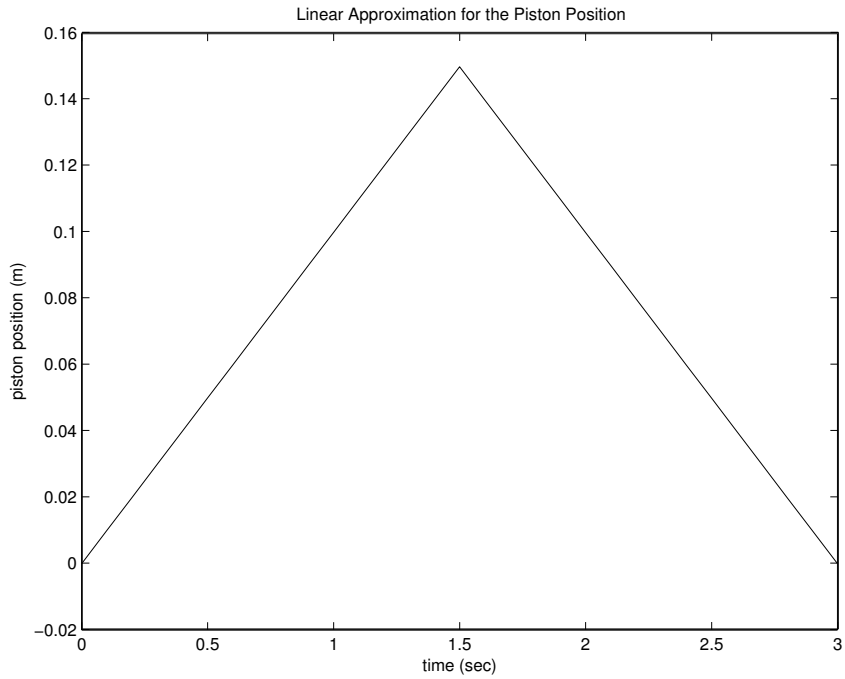

Figure 5.7: Linear approximation for hydraulic piston position.

for the design of feedback controllers, which are required for maintaining constant arc lengths.

5.5 The Linear Arc Furnace Model

Connecting the electrical and hydraulic models from this section, the complete model to be linearised consists of six state variables, three inputs and three outputs. These are defined as follow:
States:

- x_1 - Arc conductance in phase 1
- x_2 - Arc conductance in phase 2
- x_3 - Arc conductance in phase 3
- x_4 - Piston position for hydraulic actuator 1
- x_5 - Piston position for hydraulic actuator 2

- x_6 - Piston position for hydraulic actuator 3

Inputs:

- u_1 - Servo-valve input for hydraulic actuator 1
- u_2 - Servo-valve input for hydraulic actuator 2
- u_3 - Servo-valve input for hydraulic actuator 3

Outputs:

- y_1 - Arc current on phase 1
- y_2 - Arc current on phase 2
- y_3 - Arc current on phase 3

One of the main steps for linearisation purposes is the choice of operating conditions for the state variables as well as the inputs. The following operating conditions were chosen for the electric arc furnace model:

- Arc conductances - 1240 Siemens,
- Servo-valve inputs - 150mA, and
- Piston positions - 0.1m.

5.5.1 Simulation Results and Validation of the Linear Model

The Taylor series described earlier together with the choice of operating conditions were next used to linearise the arc furnace model. The constant matrices for the linear model are:

$$\mathbf{A} = 1 \times 10^6 \begin{bmatrix} -0.018 & 0.00038 & 0.00038 & -5.64 & 0 & 0 \\ 0.00038 & -0.018 & 0.00038 & 0 & -5.64 & 0 \\ 0.00038 & 0.00038 & -0.018 & 0 & 0 & -5.64 \\ 0 & 0 & 0 & 0 & 0 & 0 \\ 0 & 0 & 0 & 0 & 0 & 0 \\ 0 & 0 & 0 & 0 & 0 & 0 \end{bmatrix}, \tag{5.28}$$

$$\mathbf{B} = \begin{bmatrix} 0 & 0 & 0 \\ 0 & 0 & 0 \\ 0 & 0 & 0 \\ 66.7 & 0 & 0 \\ 0 & 66.7 & 0 \\ 0 & 0 & 66.7 \end{bmatrix}, \tag{5.29}$$

$$\mathbf{C} = \begin{bmatrix} 3.24 & 0.811 & 0.811 & 0 & 0 & 0 \\ 0.811 & 3.24 & 0.811 & 0 & 0 & 0 \\ 0.811 & 0.811 & 3.24 & 0 & 0 & 0 \end{bmatrix}, \tag{5.30}$$

and

$$\mathbf{D} = \begin{bmatrix} 0 & 0 & 0 \\ 0 & 0 & 0 \\ 0 & 0 & 0 \end{bmatrix}. \tag{5.31}$$

The simulation results for linear models are normally the deviations from the operating conditions. Thus, the nonlinear simulation results need to be adjusted to compare with those obtained from the linear model. The results given in figure 5.8 to 5.10, illustrate that the hydraulic piston position and electric arc current compare very well. Inaccuracies were found with the comparison of arc conductance. This is mostly due to the high nonlinearity in the equation for arc conductance compared with that of arc current and piston position. This is not critical because arc conductance is not used as a control variable. This concludes the approximation of the nonlinear model with that of a linear one. This linear model will be used in the following chapter to design appropriate feedback controllers for the electric arc furnace process as modelled in this dissertation. The controller will be tested on the full nonlinear model of chapter 3.

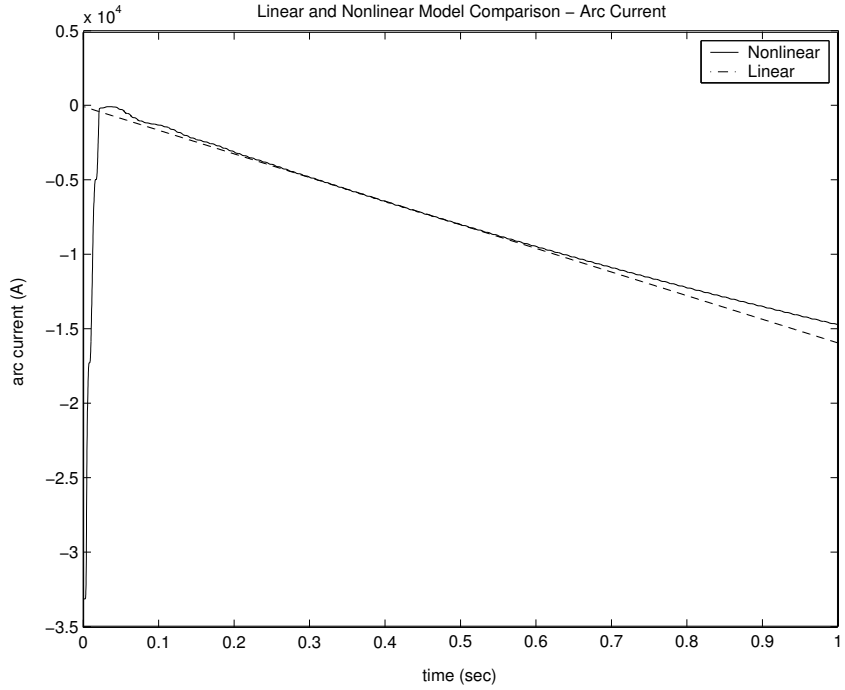

Figure 5.8: Arc current comparison between the linear and nonlinear model. The accuracy of this comparison is critical, because arc current is the control variable used to maintain constant arc length. Note that this is only a deviation from the operating value.

5.6 Conclusion

The re-modelling of the previous derived models proved sufficient enough to use for the derivation of a linear time invariant model for the purpose of linearisation.

With these new derived models, all of the variables are measured as amplitudes and not sinusoidal signals where it is impossible to derive the equilibrium points from. A complex three-phase operator were used to represent the phase difference between the respective phases which prove to work sufficient enough.

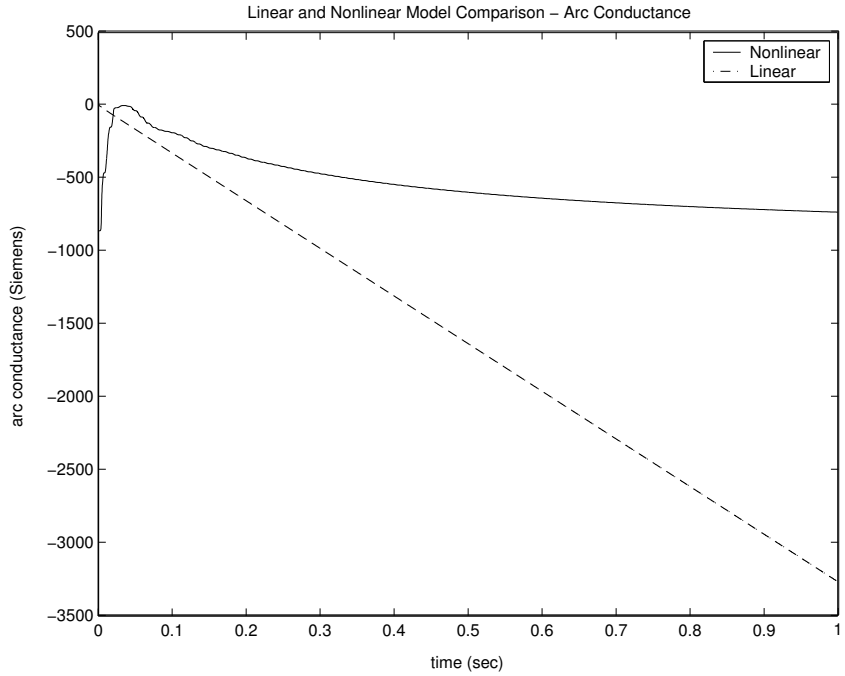

Figure 5.9: Arc conductance comparison between the linear and nonlinear model. The accuracy of this variable is not as critical as that of the arc current.

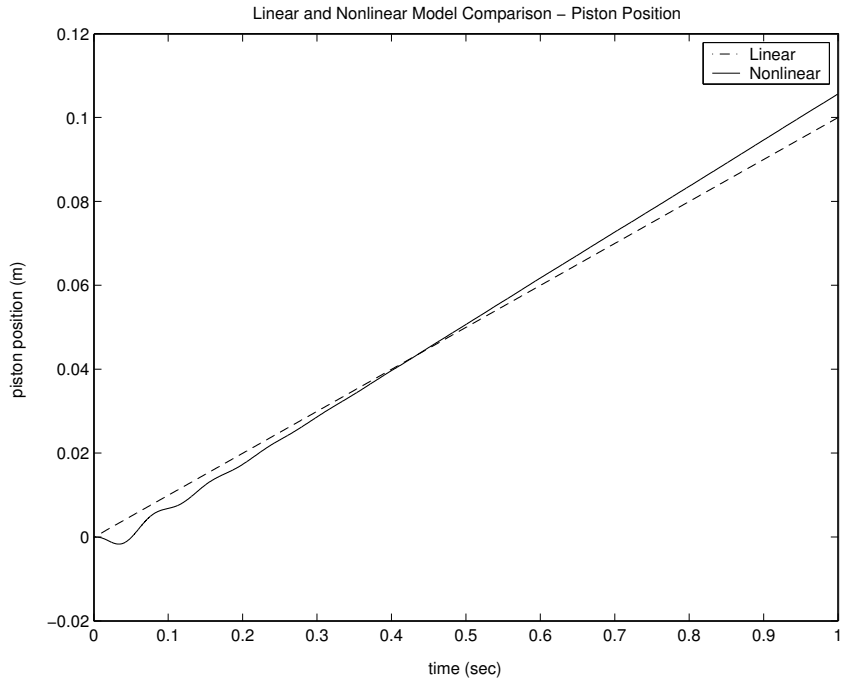

Figure 5.10: Piston position comparison between the linear and nonlinear model.

Chapter 6

Controller Design

6.1 Introduction

Hydraulic actuators are used to move three graphite electrodes vertically to adjust the lengths of the electric arcs and hence, maintaining a constants electrical power input. Most industrial furnaces use arc current as the main control variable to ensure that the arc lengths are maintained at constant preset values. Arc current is also the control variable used in this dissertation.

Most industrial arc furnaces use PID (Proportional Integral and Derivative) Control to maintain constant and efficient energy input to the process. Approximately 95% of all industrial process can be controlled satisfactorily with PID control strategies [66]. However, this control strategy is mostly known for its performance relating to SISO (Single-input-single-output) systems. The electric arc furnace is a multi-variable process, also called a MIMO (Multi-input-multi-output) system [67]. The electric arc furnace model, derived in chapter 3, consists of three manipulated inputs and three outputs. Various control strategies have been proposed for systems with multi interacting variables. The most common multi-variable control strategy used in industry, especially for systems with input and output constraints, is MPC (model predictive control). Another control strategy that has been investigated for the control of electric arc furnaces is radial basis function networks [68] and [18], which is not discussed in this dissertation.

In this section, PID and model predictive control are applied separately to the full

nonlinear electric arc furnace model. These strategies are then compared to illustrate whether multi variable control is justified for the control of an electric arc furnace.

6.2 PID Control

The PID control strategy is first investigated. The linear arc furnace model derived in the previous chapter will be used for the design of the PID controllers on the nonlinear arc furnace model. The linear plant model, represented in state space format, can be represented by transfer functions as follow:

$$\mathbf{G}(s) = \mathbf{Y}(s)\mathbf{U}(s)^{-1} = \begin{bmatrix} G_{11}(s) & G_{12}(s) & G_{13}(s) \\ G_{21}(s) & G_{22}(s) & G_{23}(s) \\ G_{31}(s) & G_{32}(s) & G_{33}(s) \end{bmatrix}. \tag{6.1}$$

For this linear model, the inputs and outputs are presented as follow:

$$\mathbf{U}(s) = \begin{bmatrix} U_1(s) \\ U_2(s) \\ U_3(s) \end{bmatrix}, \tag{6.2}$$

where $U_k(s)$ represents the respective servo-valve inputs to the hydraulic actuators.

$$\mathbf{Y}(s) = \begin{bmatrix} Y_1(s) \\ Y_2(s) \\ Y_3(s) \end{bmatrix}, \tag{6.3}$$

where $Y_k(s)$ represents the respective arc currents for each electrical phase. For this specific linear model,

$$G_{11}(s) = G_{22}(s) = G_{33}(s) \tag{6.4}$$

and

$$G_{12}(s) = G_{13}(s) = G_{21}(s) = G_{23}(s) = G_{31}(s) = G_{32}(s). \tag{6.5}$$

The system is diagonally dominant. For example, the output, $Y_1(s)$ is dependant on the first row in 6.1 which is dominated by $G_{11}(s)$. The step responses for G_{11} and G_{12} or G_{13} are given in figure 6.1 to illustrate the dominance of the diagonal components. Note the larger negative slope or bigger gain of the step response for G_{11}. Given the dominant diagonal components for the multi-variable plant in equation 6.1, the configuration for the PID control strategy is approximated as in figure 6.2.

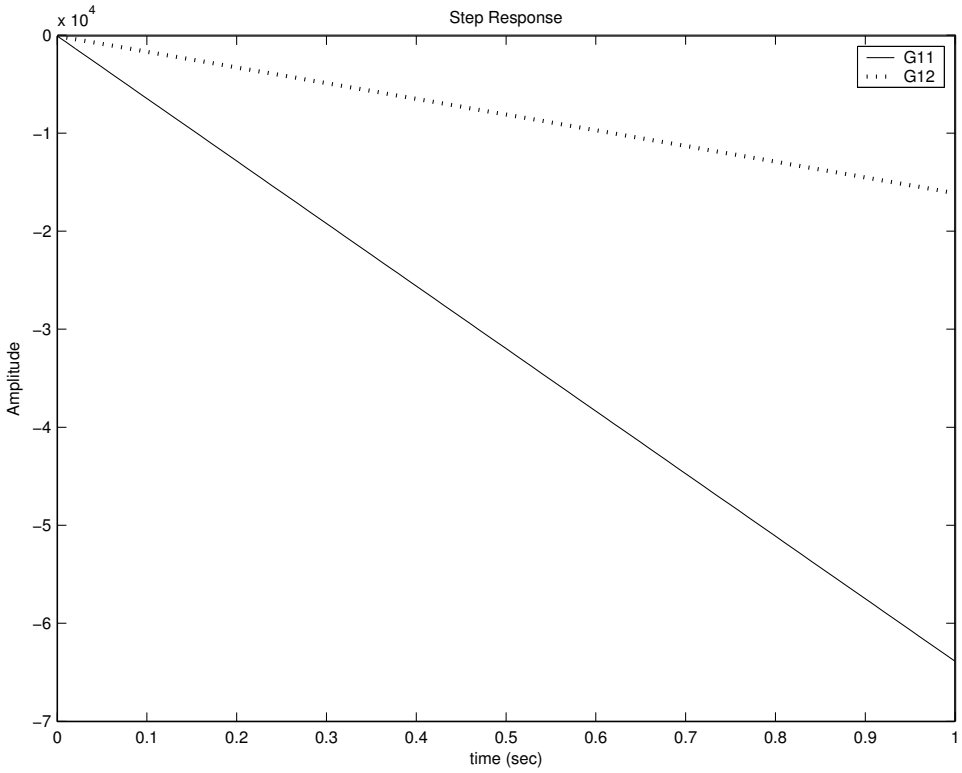

Figure 6.1: Step responses for G_{11} and G_{12}.

With the configuration in figure 6.2, the PID controllers are represented as follow:

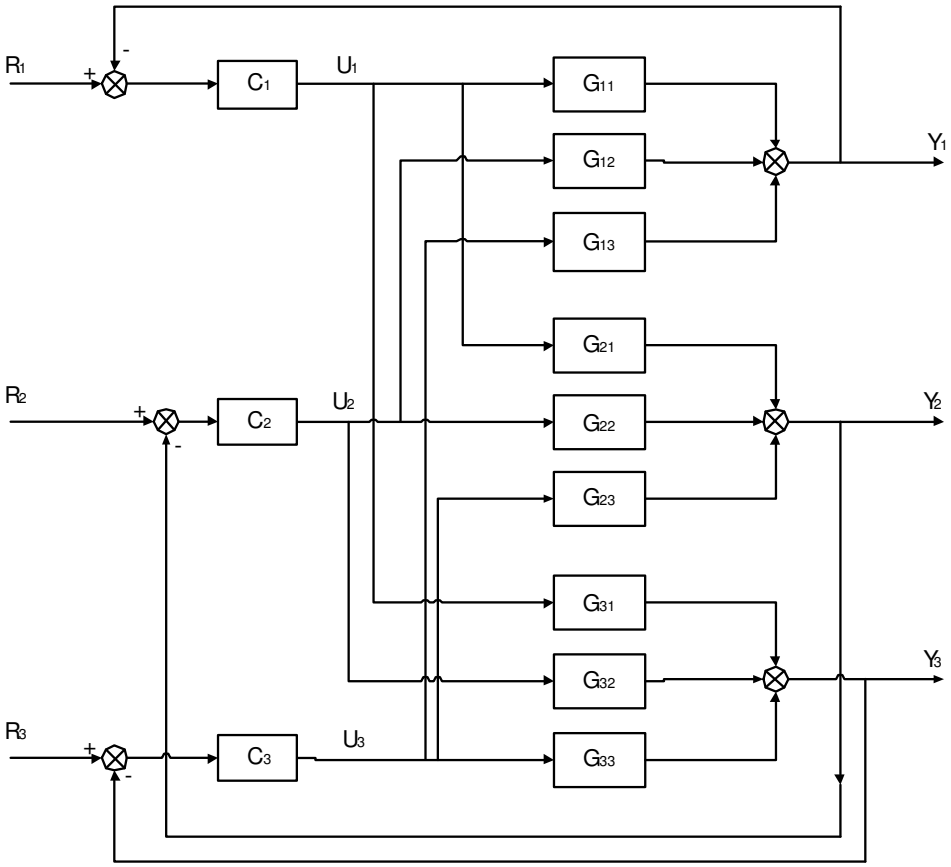

Figure 6.2: PID Control configuration for the linear arc furnace model.

$$\mathbf{C}(s) = \begin{bmatrix} C_1(s) & 0 & 0 \\ 0 & C_2(s) & 0 \\ 0 & 0 & C_3(s) \end{bmatrix}. \tag{6.6}$$

With this strategy it is assumed that the off-diagonal transfer functions in 6.1 can be neglected. With this assumption, SISO controller design strategies are used for the design of the PID controllers. The MIMO closed loop transfer function matrix are then derived as follow:

$$\mathbf{T}(s) = \mathbf{C}(s)\mathbf{G}(s)(\mathbf{I} + \mathbf{C}(s)\mathbf{G}(s))^{-1} \tag{6.7}$$

where $\mathbf{I}$ is an identity matrix od appropriate order.

6.2.1 PID Synthesis by Using Pole Assignment

The PID control structure used in this chapter has become almost universally accepted for simple industrial control problems. PID controllers are proven to be robust in the control of many important industrial applications. However, these controllers have a limited range of industrial processes that can be controlled satisfactorily. This is because of the simplicity proposed by this specific control structure and the complex dependency of variables in typical MIMO systems.

The simple SISO control loop used for the implementation of PID control systems is illustrated in figure 6.3. $C(s)$ is the controller transfer function and the relating error serving as the input to the controller is $E(s) = R(s) - Y(s)$. $R(s)$ is the reference input, $Y(s)$ the measured output of the plant and $U(s)$ is the controller output or plant input.

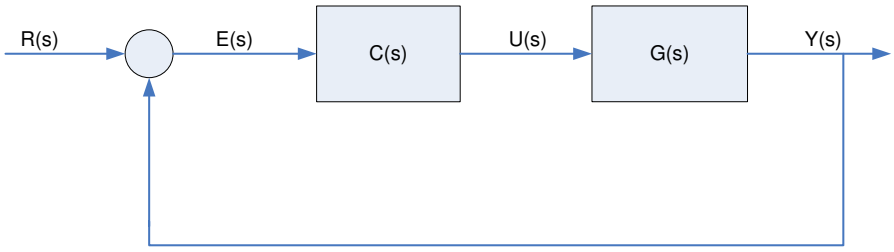

Figure 6.3: Basic SISO feedback control loop.

The traditional expression for a PID controller is given by

$$C_{PID}(s) = K_p + \frac{K_p}{T_r s} + \frac{K_p T_d s}{\tau_D s + 1}. \tag{6.8}$$

T_r and T_d are known as the integral time (reset time) and derivative time, respectively. K_p is known as the controller gain or simply the proportional gain.

6.8 can also be expressed in the following form:

$$C_{PID}(s) = K_p + \frac{K_I}{s} + \frac{K_D s}{\tau_D s + 1}. \tag{6.9}$$

Various existing methods exist for the design of PID controllers for SISO plants. Some well known methods are:

- Ziegler-Nichols Oscillation Method,
- Ziegler-Nichols Reaction Curve Method,
- Cohen-Coon Oscillation Method,
- Cohen-Coon Reaction Curve Method, and
- Close Loop Pole Placement.

Pole placement is used in this dissertation for the model based design of PID controllers for the three-phase electric arc furnace. The basic principle behind this method is to choose the desired close loop poles such that the controlled system is operating accurately according to some specifications. For this design, consider the following alternative PID controller expression [64]:

$$C(s) = \frac{n_2 s^2 + n_1 s + n_0}{d_2 s^2 + d_1 s}, \tag{6.10}$$

where

$$K_p = \frac{n_1 d_1 - n_0 d_2}{d_1^2}, \tag{6.11}$$

$$K_I = \frac{n_0}{d_1}, \tag{6.12}$$

$$K_D = \frac{n_2 d_1^2 - n_1 d_1 d_2 + n_0 d_2^2}{d_1^3} \tag{6.13}$$

and

$$\tau_D = \frac{d_2}{d_1}. \tag{6.14}$$

The closed loop expression for a SISO process relating to its desired controller is given by the nominal complementary sensitivity function as follow:

$$T_0(s) = \frac{G(s)C(s)}{1 + G(s)C(s)} = \frac{B_0(s)P(s)}{A_0(s)L(s) + B_0(s)P(s)}, \tag{6.15}$$

where

$$G(s) = \frac{B_0(s)}{A_0(s)} \tag{6.16}$$

and

$$C(s) = \frac{P(s)}{L(s)}. \tag{6.17}$$

From the step responses given in figure 6.1, the plant model for $G_{11}(s)$ can be approximated by an integrator response with the following form:

$$G_a(s) = \frac{-K}{s}, \tag{6.18}$$

where K is equal to 65469. The next step is to choose desired close loop poles, characterized by the roots of the nominal closed-loop characteristic polynomial, which is the denominator polynomial in 6.15. The following are typical specifications to consider when choosing closed loop poles:

- Stability,
- Transient Response,
- Steady state error,
- Noise Rejection,
- Disturbance Rejection, and

- Robustness

For the close loop system to be stable the poles need to be located in the left-half s-plane. A standard requirement is that, in steady state, the nominal control loop should yield zero error on the output. For this to be achieved, a necessary condition is that the nominal loop be internally stable and that the controller have at least one pole located at the origin. This is automatically achieved by using the PID controller in 6.9. With this controller and the plant approximation in 6.18, the closed-loop system consists of four poles.

Noise is normally associated with sensor measurement. Measurement noise is typically dominated by high frequencies, which can be filtered out if the bandwidth of the close loop system is taken into account. This is possible with the pole placement strategy used in this section. The same conclusion holds for the rejection of input and output disturbances, depending on the specific frequency. These specifications were considered to choose close loop poles for the electric arc furnace model.

The poles of the open loop plant, $G_{11}(s)$, are located at

$$s = 0, \quad 0, \quad 0, \quad -10258, \quad -10258, \quad and \quad -10224. \tag{6.19}$$

All the open loop poles are on or left of the origin, which conclude that the open loop system is already marginally stable. Initially the aim was to choose the close loop poles as close to the origin as possible for disturbance rejection. However, due to the high system gain, acting as in integrator, this is difficult to achieve. The open loop poles are also located far to the left of the origin. After various simulations and different choices of closed loop poles, the following values were chosen:

$$s = 0, \quad -6500, \quad -20000, \quad -30000 \tag{6.20}$$

Note that the pole located on the origin is cancelled out by a zero also on the origin. With these poles, the following parameters were obtained for the PID controller in 6.10:

$$n_0 = 0 \qquad n_1 = -3000 \qquad and \qquad n_2 = -0.25 \tag{6.21}$$

and

$$d_1 = 20000 \qquad and \qquad d_2 = 1. \tag{6.22}$$

Equations 6.11 to 6.14 are used next to compute the PID parameters in 6.9. The following values were obtained:

$$K_p = -0.15, \tag{6.23}$$

$$K_I = 0, \tag{6.24}$$

$$K_D = -0.000005, \tag{6.25}$$

and

$$\tau_D = 5 \times 10^{-5}. \tag{6.26}$$

6.2.2 Controller Implementation on the Linear Model

The PID controller designed via the pole placement strategy are implemented next on the linear arc furnace model. A step response is given in figure 6.4, to illustrate the close loop response, $T_0(s)$, with the controller implemented on the diagonal component $G_{11}(s)$. The reference input in this simulation was chosen to be 1000 for illustration purposes. In this response no limits were placed on the controller output, which is the servo-valve input to the electrode system. However, this is not the case in a typical arc furnace process where the servo-valve input ranges between $-0.15A$ and $0.15A$. The respective frequency response is given in figure 6.5.

Figure 6.6 illustrates the closed loop step response with an upper limit of 0.15A and a lower limit of -0.15A on the controller output. The reference used in this simulation was

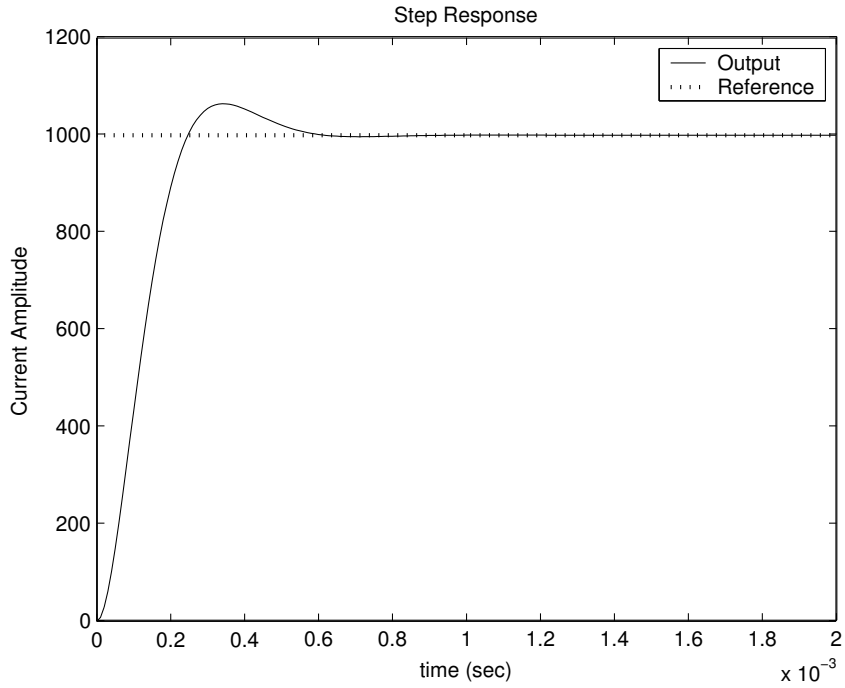

Figure 6.4: Step responses for the SISO close loop system. G_{11} is used as the plant for this simulation. The interactions of other phases are not included here.

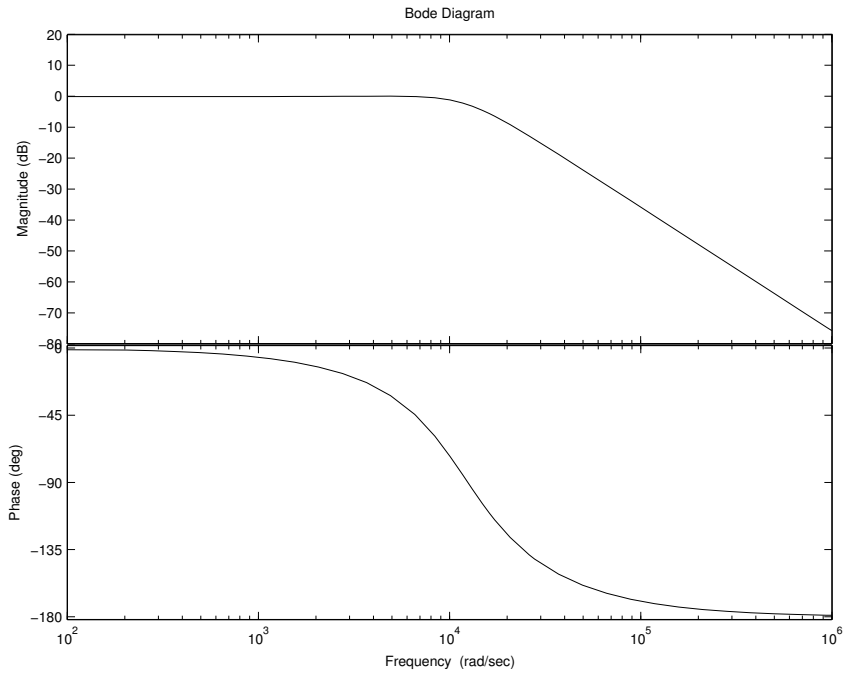

Figure 6.5: Frequency responses for the SISO closed loop system. G_{11} is used as the plant for this simulation. The interactions of other phases are not included here.

again equal to 1000. The step response in figure 6.4 takes approximately 1ms to settle with zero steady error. In contrast, the step response in figure 6.6 takes approximately 100 ms to reach similar results. This illustrates the significance of the limits on the output of the controller. The close loop response without any limits on the controller output in not realistic and all the responses to follow contain appropriate controller output limits. Also note that the overshoot in figure 6.4, is not present in figure 6.6. This is mainly due to the very slow response of the hydraulic actuator when the inputs are limited.

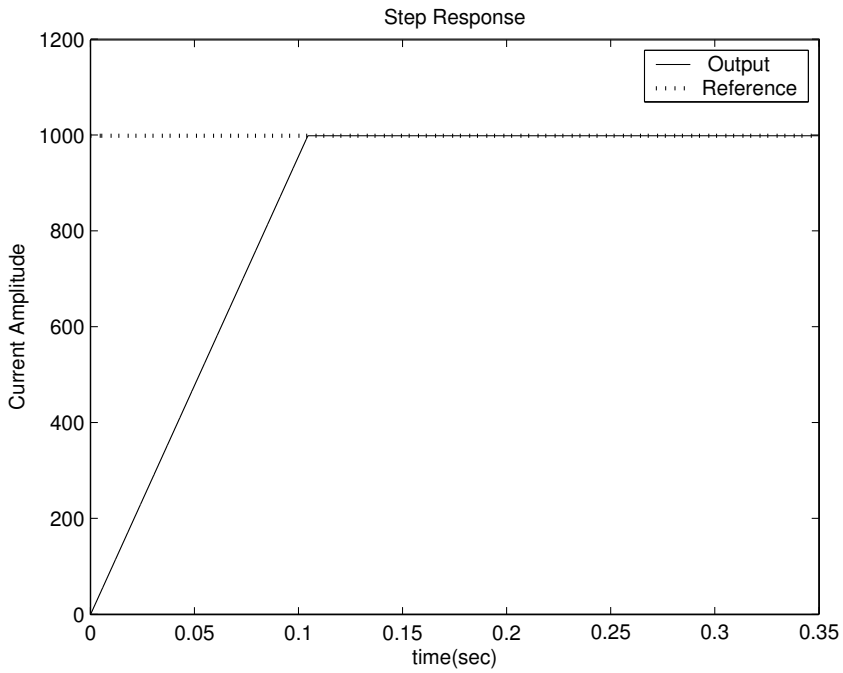

Figure 6.6: Close loop step response for the SISO system with limits placed on the controller output. G_{11} is again used as the plant model. The sharp change in the step response is due to the very high open loop gain.

The three-phase electric arc furnace is a multi-variable process and the next step was to implement the PID control strategy on the complete model as illustrated in figure 6.2. The controllers were applied and tested on the complete linear model as given in 6.1. A reference of 1000 was used on all three phases. The simulation results for the close loop linear system are illustrated in figures 6.7 to 6.9. Note that the rise time for the three phases differs from the single phase simulation in figure 6.6. This is mainly due to interactions between the respective phases, which were not taken into account earlier. All

three phases reach the desired reference values in approximately 100ms and this conclude that the designed PID controllers are acceptable when implemented on the linear electric arc furnace model.

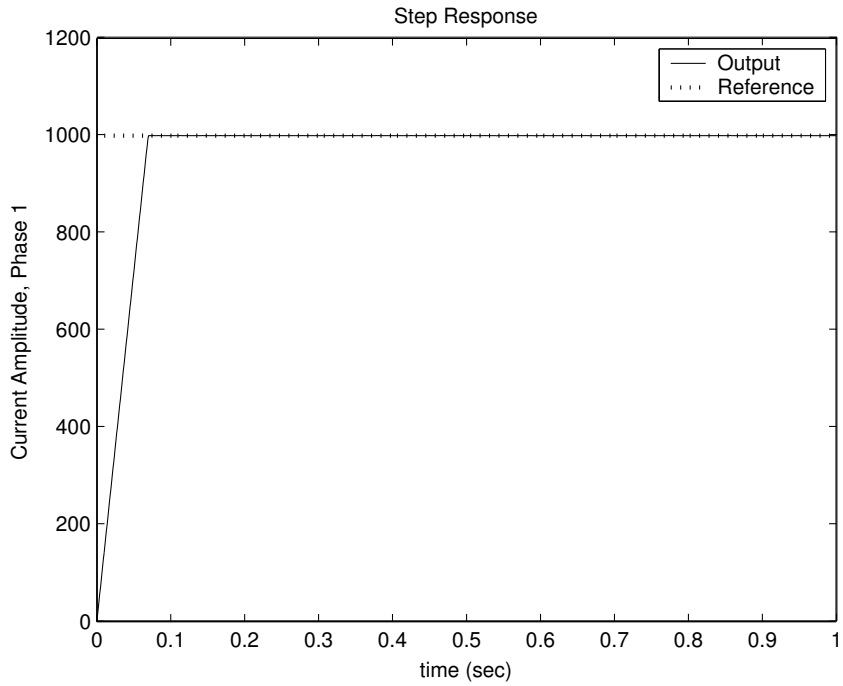

Figure 6.7: Step response on phase 1 of the linear model. All three phases are stepped simultaneously. This is to illustrate the functioning of the controllers with the interactions of all three phases taken into account.

6.2.3 PID Controller Implementation on the Nonlinear Model

6.2.3.1 Initial Controller Implementation

The main objective is to implement the designed controller strategy on the nonlinear arc furnace model. For this strategy, three different steps are applied to the respective electrical phases and the inputs and outputs are all measured in rms-values.

The set-points applied to the three electrical phases are illustrated together with the simulated outputs to show the accuracy of the controlled responses. The simulation results, obtained with the nonlinear model, are given in figures 6.10 to 6.12. The designed

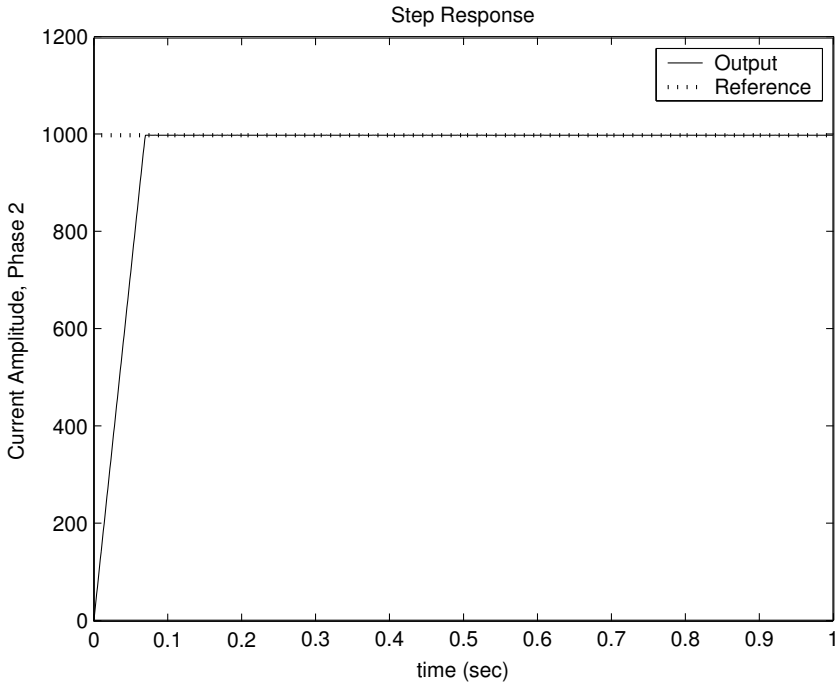

Figure 6.8: Step response on phase 2 with the linear model.

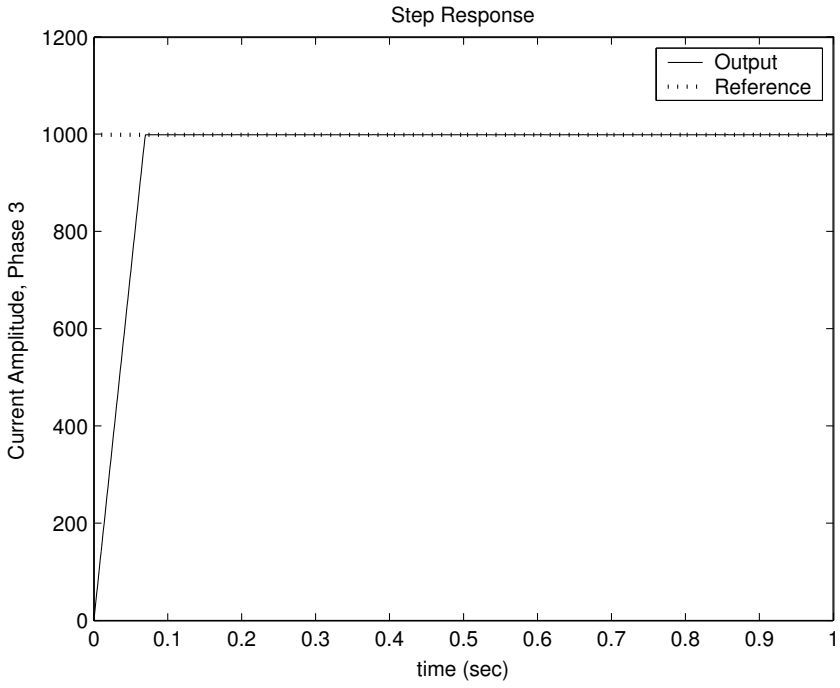

Figure 6.9: Step response on phase 3 with the linear model.

PID controllers used in the previous sections are used here. After some tuning it was decided that the results obtained with the initial PID controllers are most effective.

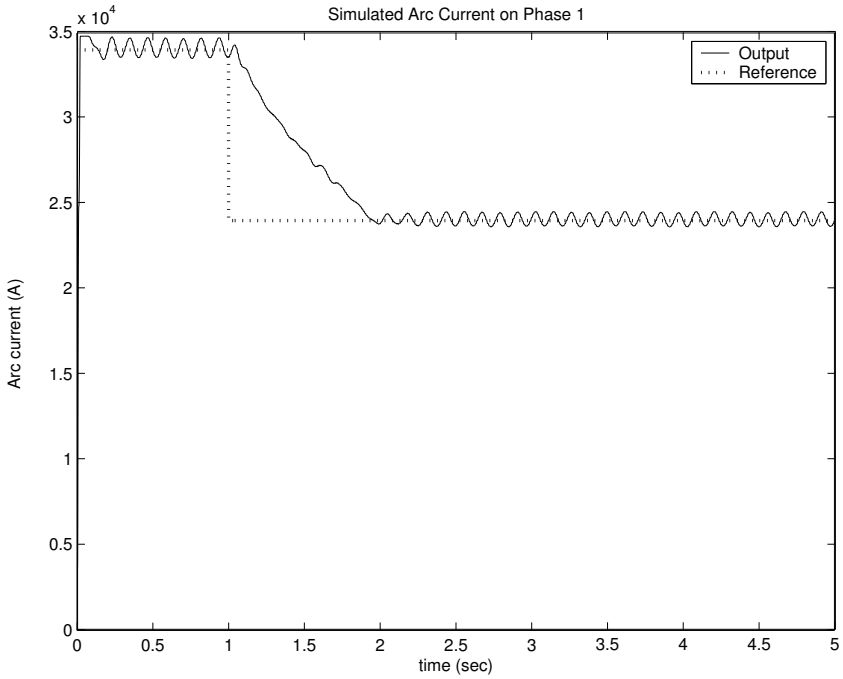

Figure 6.10: Phase 1, simulated arc current obtained with the nonlinear arc furnace model. The oscillations is due a time delay of approximately 0.25s.

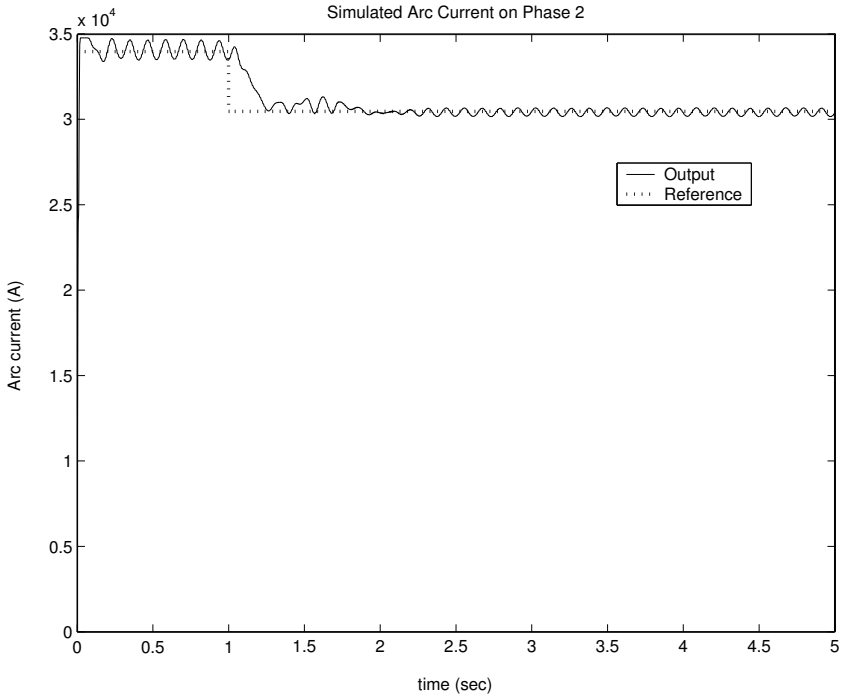

Figure 6.11: Phase 2, simulated arc current obtained with the nonlinear arc furnace model.

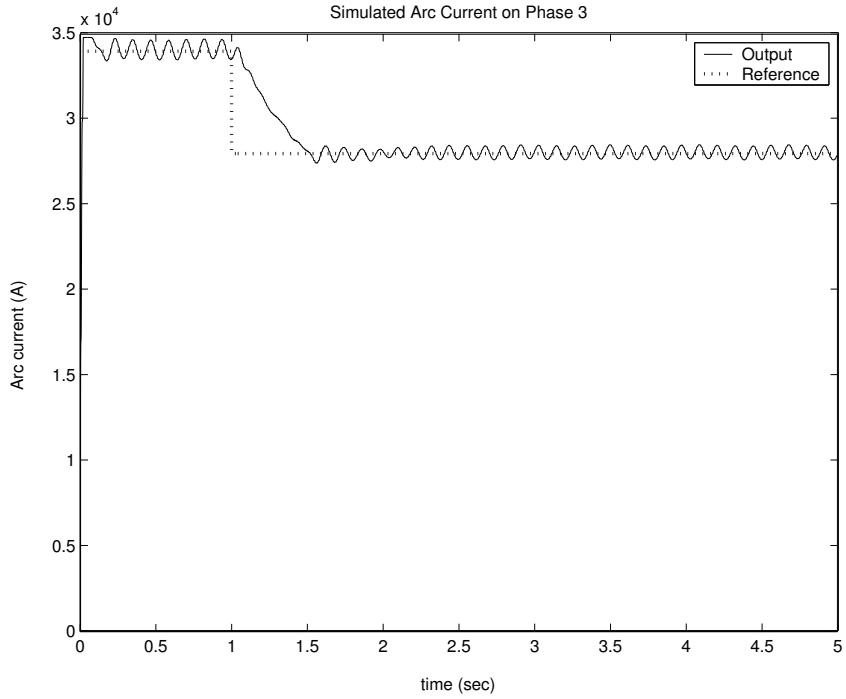

Figure 6.12: Phase 3, simulated arc current obtained with the nonlinear arc furnace model.

The simulated arc currents in figure 6.10, 6.11 and 6.12 are oscillating around its respective set-points with frequencies of about 8Hz. These oscillations are mainly due to dead times of approximately 0.25s on the hydraulic piston positions when step inputs are applied to the model. These dead times were not originally taken into account during the controller design phase. The controllers are thus reacting on non-zero error signals while the hydraulic actuators only react positively after about 0.25s. The respective controller outputs, obtained from this simulation, are illustrated in figures A.1 to A.3. Note that the controller outputs are either on or off (minimum or maximum). In this simulation, the controller outputs are 150mA if arc current need to be decreased and -150mA if arc current needs to be increased.

The amplitudes of the oscillations are fairly small compared to the value of the reference inputs and can be neglected. However, with some controller tuning these oscillations can be reduced, which result in more effective responses.

6.2.3.2 PID Controller Tuning

The controlled arc currents oscillate with amplitudes of approximately 700A, which result in steady state errors up to 1.5%. As mentioned earlier, this is acceptable results but the small additional electrical power consumption has a direct effect on the plant efficiency. Two methods can be used to compensate for the oscillations on the controlled electrical arc currents. These are frequency domain analysis or simply by including an approximation of the dead time in the linear transfer functions before controller design. Both these methods are used to design appropriate controllers which will reject the oscillations present in figures 6.10, 6.11 and 6.12. The frequency domain analysis method is not included in this chapter. This method is illustrated in Appendix A. The reason for this is because this method will not really be used in the industry. The engineers should be able to adjust the controller parameters in such a way that the dead times are taken into account.

6.2.3.2.1 Frequency Domain Analysis See Appendix A.

6.2.3.2.2 Direct Inclusion of the Time Delay The second method used to reject the oscillations on the controlled arc currents is to include a first order pade approximation for the 0.25s time delay in the linear model.
A first order pade approximation for the 0.25s time delay is given in transfer function format as follow:

$$TD(s) = \frac{-s+8}{s+8}. \tag{6.27}$$

With TD(s) included into the linear model, PID controller parameters are designed in similar fashion as in section 6.2.1.

After some trial and error tuning, the following parameters were used for controlling the non-linear electric arc furnace model:

$$K_p = -0.00005, \tag{6.28}$$

$$K_I = -0.000001, \tag{6.29}$$

$$K_D = -0.00000005 \tag{6.30}$$

and

$$\tau_D = 5 \times 10^{-5}. \tag{6.31}$$

The implementation of this strategy on the linear model is not included here. The controlled arc currents are given in figures 6.13, 6.14 and 6.15.

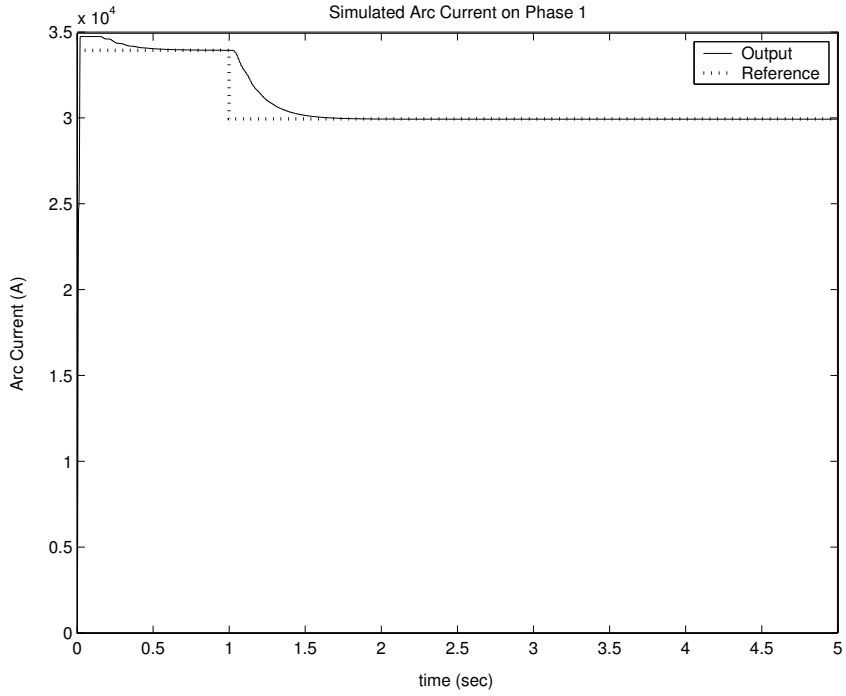

Figure 6.13: Controlled arc current, phase 1, for the close loop system in figure A.6.

The controller inputs and outputs are given in figures A.10 to A.15. From these results we can conclude that the oscillations are removed successfully by both tuning methods. However, with the inclusion of the time delay in the linear model less strain are applied to the actuator inputs via the controller outputs. This is a big advantage over the first method where band rejection was used to remove the oscillations on the arc currents. Both tuning methods reacted with similar speeds to steps in the arc current set points.

The next section looks at model predictive control (mpc) implemented on the electric arc furnace model. Model predictive control is a very effective multi-variable control strategy for systems with input and output constraint.

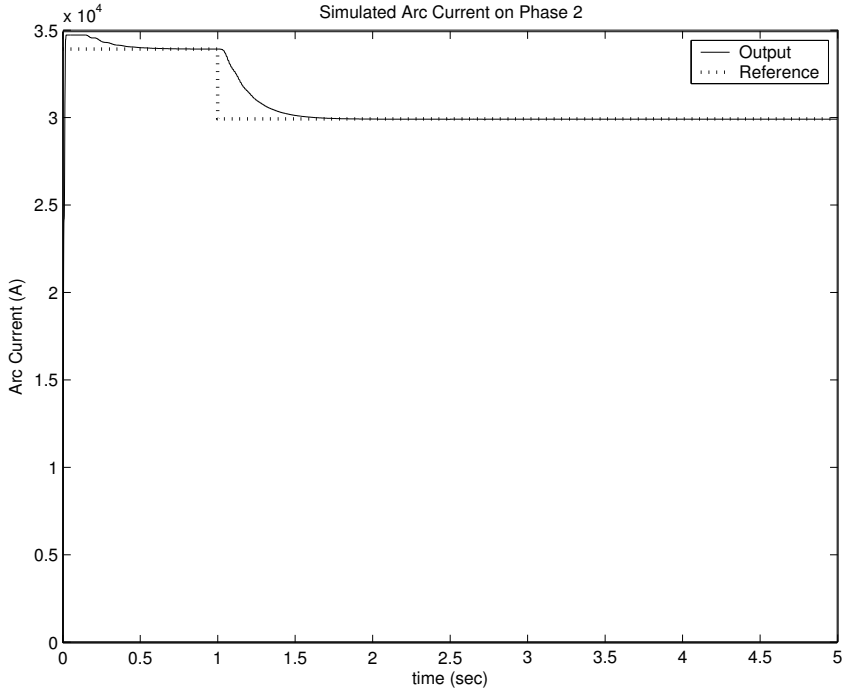

Figure 6.14: Controlled arc current, phase 2, for the close loop system in figure A.6.

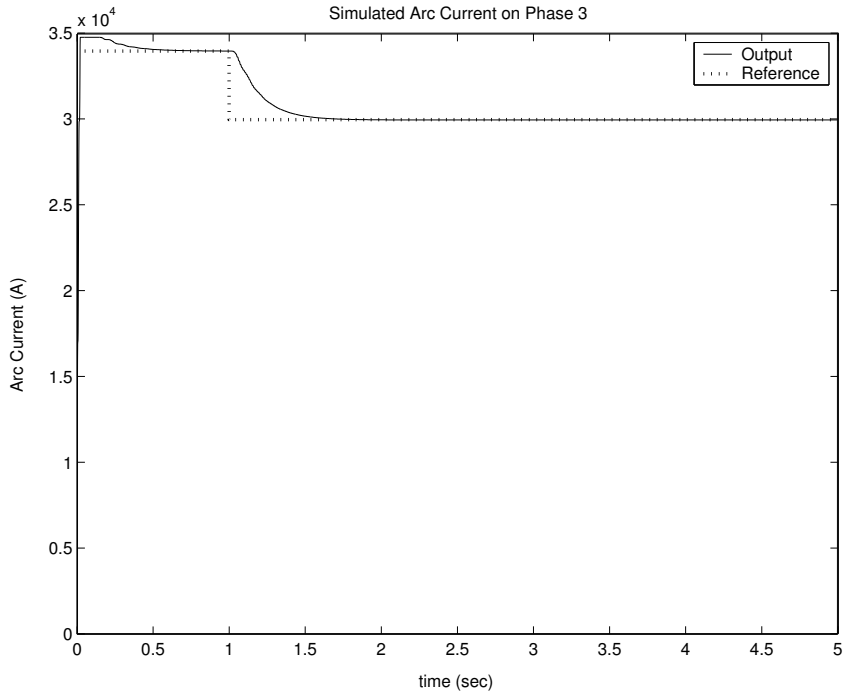

Figure 6.15: Controlled arc current, phase 3, for the close loop system in figure A.6.

6.3 Model Predictive Control

PID control is a well known control strategy for SISO systems and proved sufficient for the control of the three-phase electric arc furnace. The outputs of the arc furnace model are dominated by its respective inputs as illustrated in figure 6.1. This leads to an approximation that the linear model is diagonal, which means that the outputs of the respective phases are only dependant on its respective input.

A more general and accurate approach will be to design controllers while taking the effects of the other phases into consideration. This can easily be accomplish by using a multi-variable control strategy to design the electric arc furnace controller instead of the SISO technique from the previous section. Apart from Mintek, not a lot of research has been done where MIMO control strategies have been applied for electrode control. A well known multi-variable control strategy for dealing with input and output constraints are the so-called model predictive control algorithm. The essential idea in this method is to formulate the controller design as an on-line receding-horizon optimization problem that is solved subject to given constraints.

6.3.1 Background on Model Predictive Control

Consider the block diagram of a model predictive control system in figure 6.16. In simulation the process is represented by the nonlinear plant model and a linear approximated model is used to predict the current values of the output variables. The residuals are the differences between the actual and predicted outputs and serves as the feedback signal to the prediction block. These predictions are then used for set-point calculations and control calculations. Inequality constraints can then be placed on the inputs and outputs for both of these calculations.

The set points for the control calculations are often determined by an economic optimization routine. The optimum values of set points are changed frequently due to varying process conditions and changes in the inequality constraints. In MPC the set-points are calculated each time control calculations are performed.

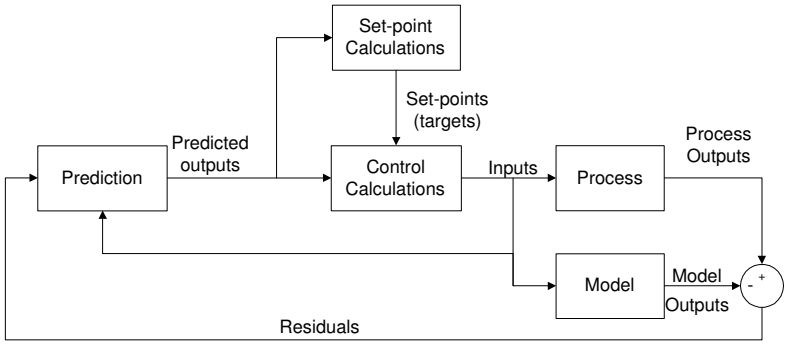

Figure 6.16: Block diagram for model predictive control [64].

The control calculations are based on current measurements and predictions of the future values of the outputs. The objective of the MPC control calculation is to determine a sequence of control moves so that the predicted response moves to the set point in an optimal manner. At sampling interval, k, the MPC strategy calculates a set of M values for the input. The set consists of the current input $u(k)$ and $M-1$ future inputs. The input is held constant after the M control moves. The inputs are calculated so that a set of P predicted outputs reaches the set point in an optimal manner. The control calculations are based on optimizing an objective function. The number of predictions P is referred to as the prediction horizon while the number of control moves M is called the control horizon.

Although a sequence of M control moves is calculated at each sampling instant, only the first move is actually implemented. A new sequence is then calculated at the next sampling instant. This procedure, referred to as the receding horizon approach, is repeated at each sampling instant.

6.3.2 Applying Model Predictive Control to the Three-phase Electric Arc Furnace Model

The first step in MPC design is to select the controlled, manipulated, and measured disturbance variables. The next step is to select the MPC design parameters, which include

the sampling period, weighting factors and the control and prediction horizon. These parameters are then, after testing, adjusted until satisfactory results are obtained.

A general rule is that the sampling period $\triangle t$ and the model horizon N should be chosen such that $N\triangle t = t_s$ where t_s is the settling time for the open-loop response [69].

Some typical rules of thumb are $5 \leq M \leq 20$ and $N/3 < M < N/2$. A different value of M can be specified for each input. The prediction horizon P can be selected to be $P = N + M$ such that the full effect of the last input move is taken into account.

The output weighting matrix allows the output variables to be weighted according to their relative importance. In similar fashion, the input weighting matrix allows the input variables to be weighted according to their relative importance.

The initial simulation carried out on the electric arc furnace model with MPC implemented used the following values for the parameters as described above:

Table 6.1: Variables used for the implementation of MPC on the electric arc furnace.

Symbol	**Description**	**Value**
P	Prediction Horizon	10
M	Control Horizon	5
ywt	Output Weighting	[1 1 1]
uwt	Input Weighting	[1 1 1]
$\triangle t$	Sampling Period	$0.02s$
ny	Number of Control Variables	3

The respective set-points are illustrated together in the simulated arc currents. These simulations are illustrated in figures 6.17, 6.18 and 6.19. The oscillations obtained with initial PID control are also present in the simulations where MPC is used to control the arc currents. The same conclusion holds. The respective controller outputs are illustrated in figures A.22, A.23 and A.24.

The MPC design tool in MATLAB allows for disturbance rejection factors on both,

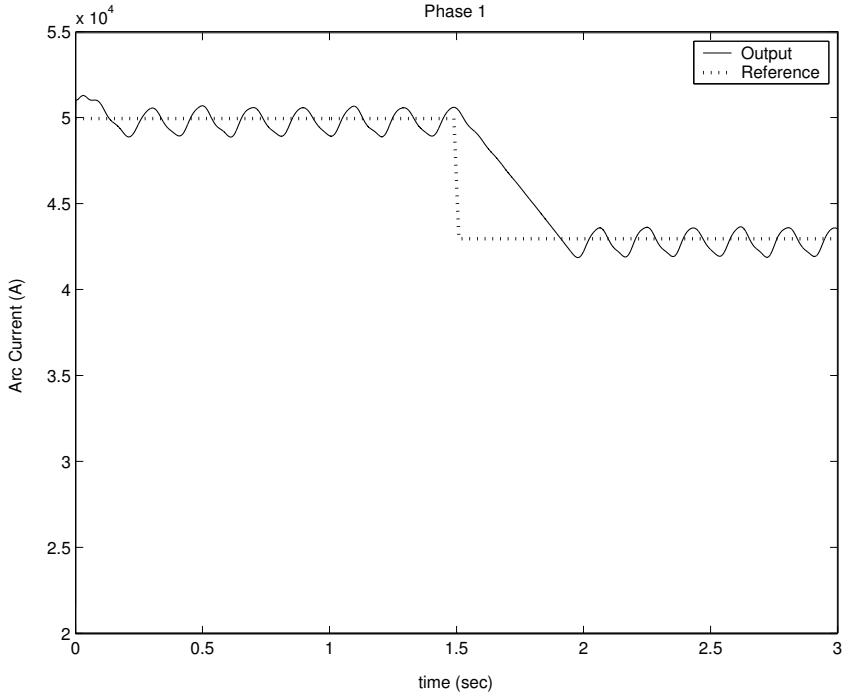

Figure 6.17: Simulated arc current on phase 1 with MPC.

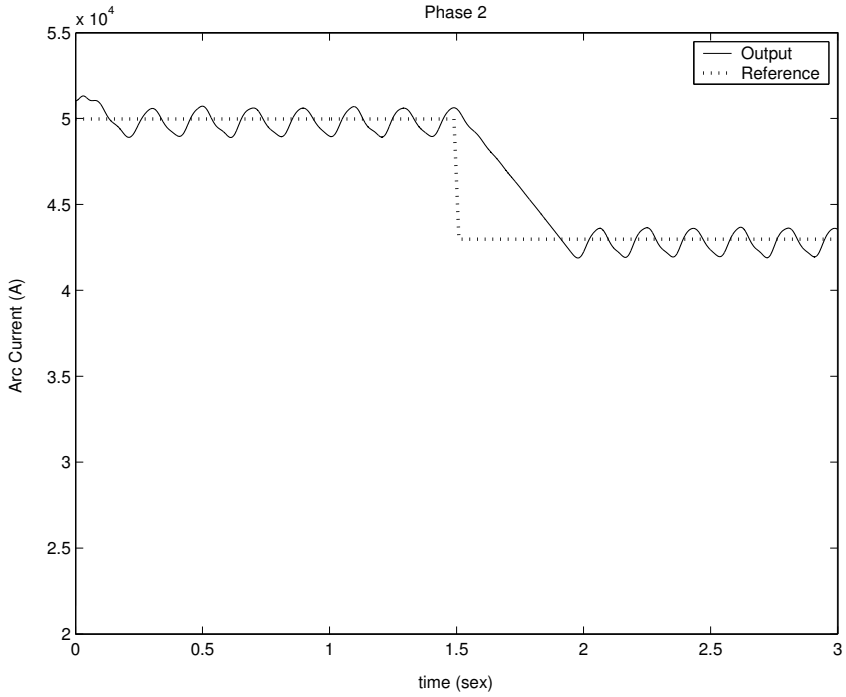

Figure 6.18: Simulated arc current on phase 2 with MPC.

input and output, which makes this a fast and effective method to reject the 8Hz oscillations. For this reason, the design where the time delay is included in the linear model

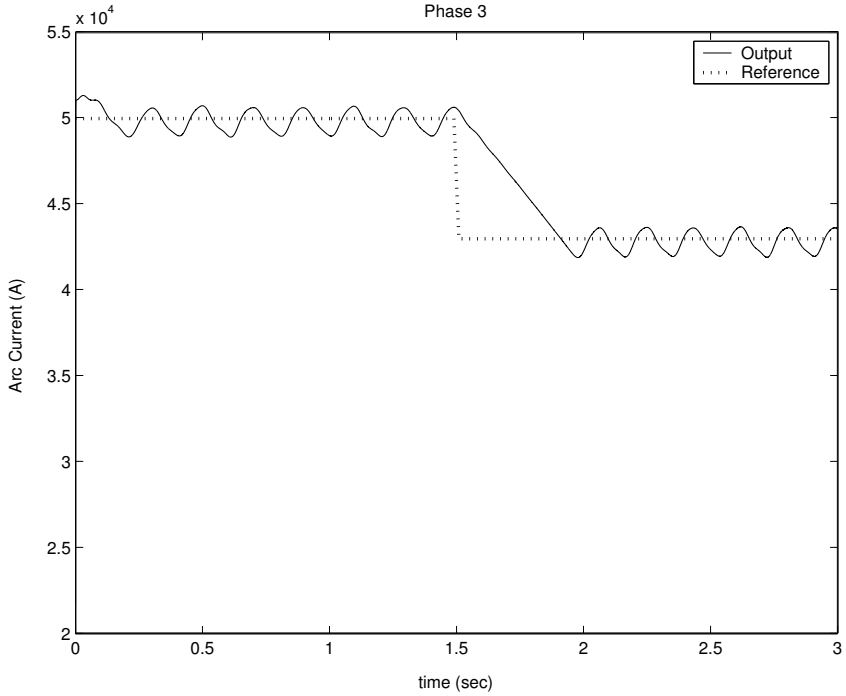

Figure 6.19: Simulated arc current on phase 3 with MPC.

is not included for MPC control. The simulation results together with the respective references are illustrated in figures 6.20, 6.21 and 6.22. The respective controller outputs are illustrated in figures A.25, A.26 and A.27.

6.4 Conclusion

In this chapter, PID Control as well as Model Predictive Control were implemented on the nonlinear electric arc furnace model to control the arc currents of the respective phases.

Both these strategies achieved similar results in terms of reference tracking, response time and disturbance rejection. PID control is however much more simple to implement and tune, which makes it the primary choice for electrode control in the industry.

Although the simulated arc currents are acceptable without the inclusion of the band rejections around 8Hz, the controller outputs will vary continuously which might not be acceptable to the hydraulic actuator inputs. The concludes the need to reject the oscillations due to variable dead times on the hydraulic actuator outputs.

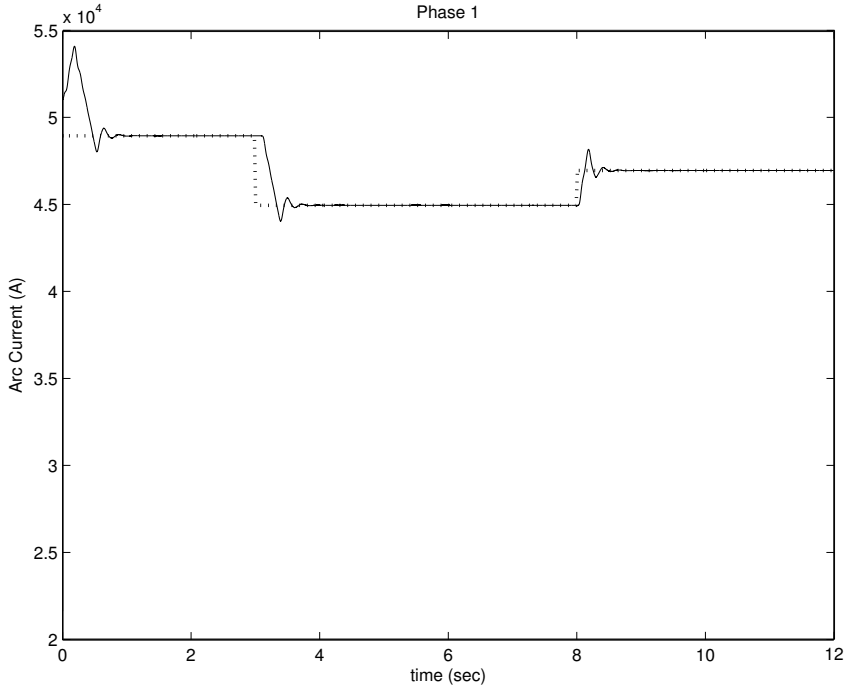

Figure 6.20: Simulated arc current on phase 1 with MPC together with disturbance rejection filters.

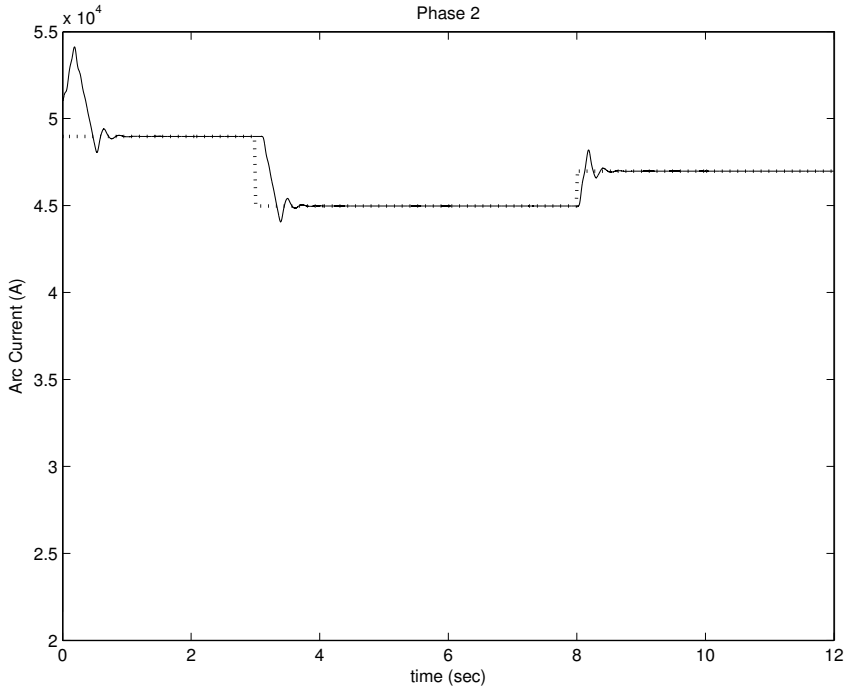

Figure 6.21: Simulated arc current on phase 2 with MPC together with disturbance rejection filters.

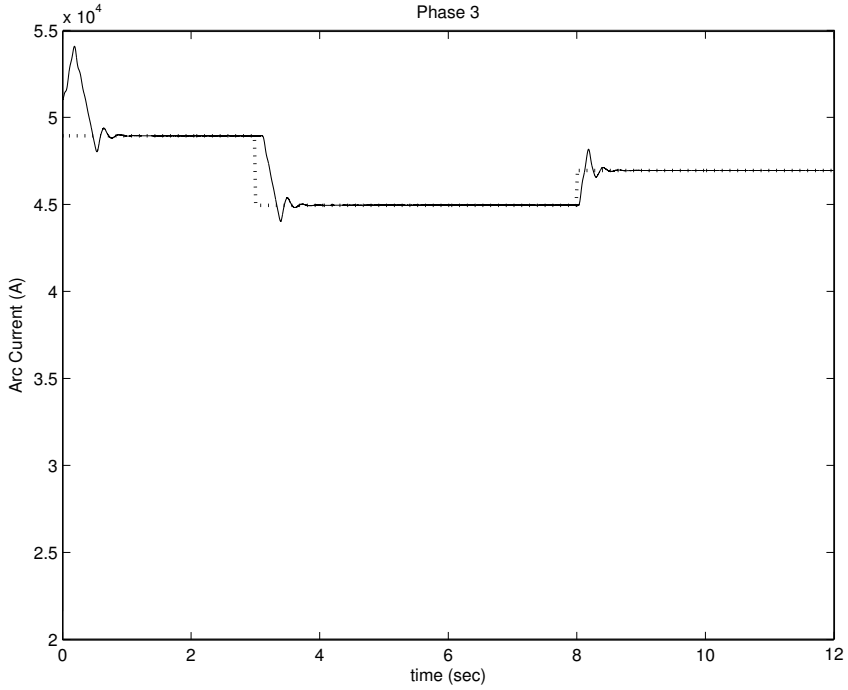

Figure 6.22: Simulated arc current on phase 3 with MPC together with disturbance rejection filters.

Chapter 7

Industrial Measurements and Comparisons

7.1 Introduction

The disturbances on the electric arc lengths in a furnace process occur randomly and are impossible to simulate accurately. Disturbances and some other quality aspects from the electrical transmission system are not included in the derived model. These neglected factors make it difficult to validate the derived model for the electrode system accurately.

Measurements from an electrode control point of view are very limited in literature and not good enough for testing the performance of the derived model. The standard measurements taken in an arc furnace during production might be acceptable for validation but is most certainly not ideal.

A brisk experiment during the refining stage of a specific arc furnace process,[22], was carried out to obtain acceptable measurements for model validation. The tap changes on the furnace transformer were not varied for this experiment. The aim was to step each of the respective phases individually, while the inputs to the remaining phases remain constant. This is the reason for choosing the refining stage to apply the validation procedure.

7.2 The Industrial Experiment

Various revisions of the validation procedure were carried out. After several plant visits and discussions with personnel on site, a final decision was made for the exact procedures that will be followed.

The main objective, as mentioned earlier, is to change the arc length of a single phase while the remaining two phases remain constant. This will allow for investigation of the response due to disturbances on each of the respective phases. Another key factor is to ensure that production is not affected by the validation experiment, which means that the duration has to be limited. The refining period was used to carry out the validation experiment because fewer disturbances take place during this period. The bath consists of liquid metal alone, which means that the arc length can not vary because of scrap cave-ins.

The rate at which measurements are taken in a typical arc furnace production will be too slow for model validation, especially for simulations being almost continuous. An increased measurement rate is therefor required for the duration of the validation experiment. The maximum obtainable sampling rate for this application is about 0.135s which is fast enough for validation. This is almost 15 times faster than normal measurement rates.

The duration of the entire validation experiment is about 500s, which will not have a significant effect on the production. The important measurement is the electric arc current, also referred to as the electrode current in industry. The inputs to the open loop model are the servo-valve currents to the three hydraulic actuators. These are the variables used to validate the performance of the derived model for an electrode system for a three-phase electric arc furnace.

Another factor that complicates the validation of the derived model is that the controllers used in the industry is regarded as black boxes by the personell. The reason for this is due to fact that external companies are used for the installation of the arc furnace controllers. This together with the absence of arc length and disturbance measurements,

makes is almost impossible to validate a derived arc furnace model is detail.

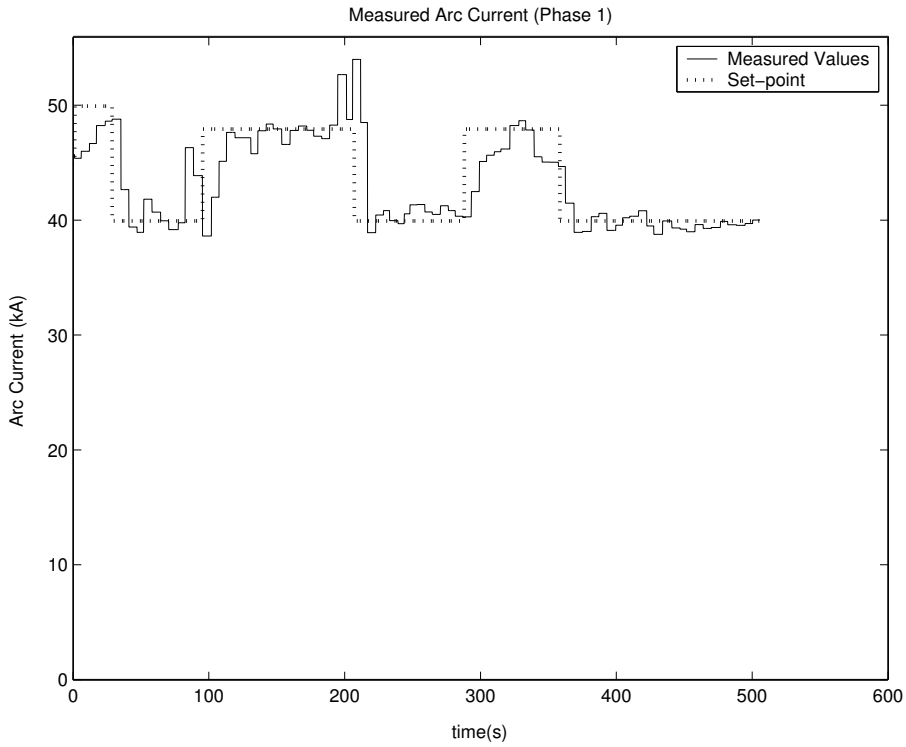

Figure 7.1: Arc current as measured on phase 1 together with the desired set-point.

The measured arc currents obtained from the validation experiment are illustrated in figures 7.1, 7.2 and 7.3. During the refining stage, the transformer operates on tap position 1, which is relatively low power operation. The control system is implemented digitally with a relative slow sampling rate, which is visible from the measured results. This complicates the task of validation even more as all simulations on the derived model are almost continuous with much faster sampling rates. Also visible from the measured results are significant disturbances as one would expect in arc furnace industries. During the validation experiment, between the duration of 100s to 270s, the set-points on phases 2 and three are constant at 48kA when phase 1 is stepped from 48kA to 40kA at 200s. This data is sufficient enough to use for validation purposes.

The respective servo-valve inputs (controller outputs) obtained during validation are illustrated in figures 7.4, 7.5 and 7.6. The aim of the hydraulic piston, when placed under electrode control, is to remain at a constant desired position which correlates to the arc

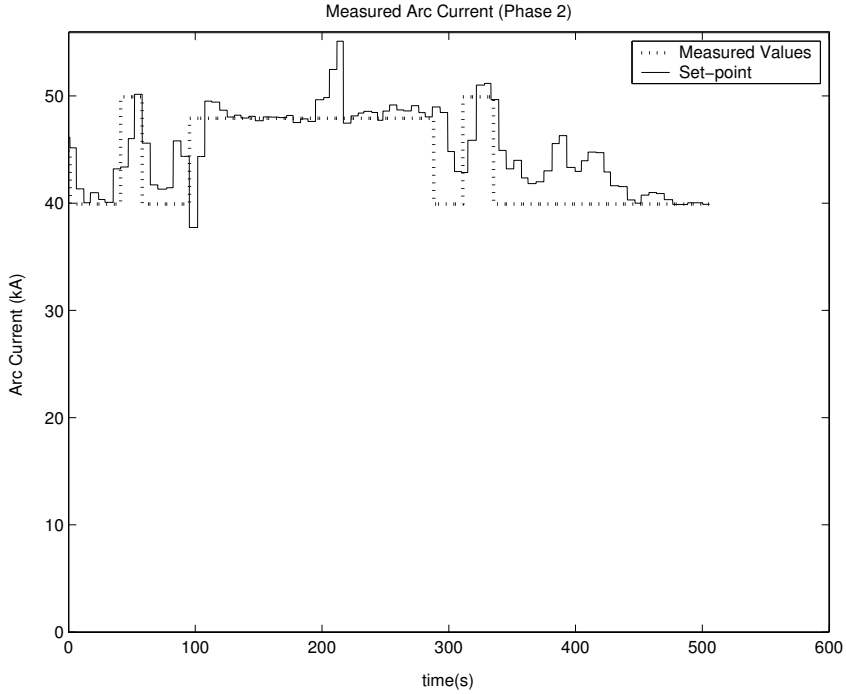

Figure 7.2: Arc current as measured on phase 2 together with the desired set-point.

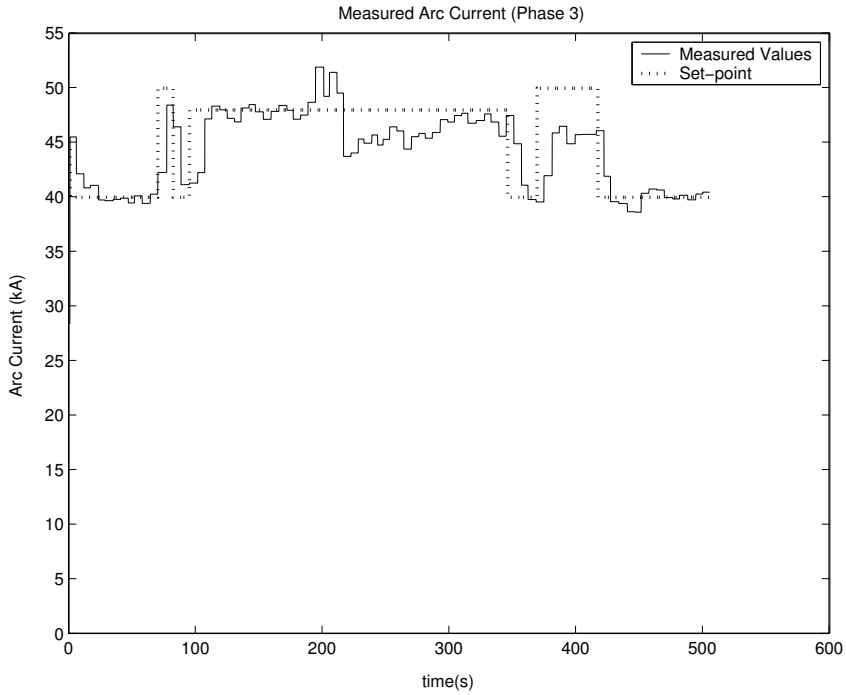

Figure 7.3: Arc current as measured on phase 3 together with the desired set-point.

current set-point. This is achieved with a servo-valve input of 0mA. This is why the measured results oscillate around 0mA for most of the experiment.

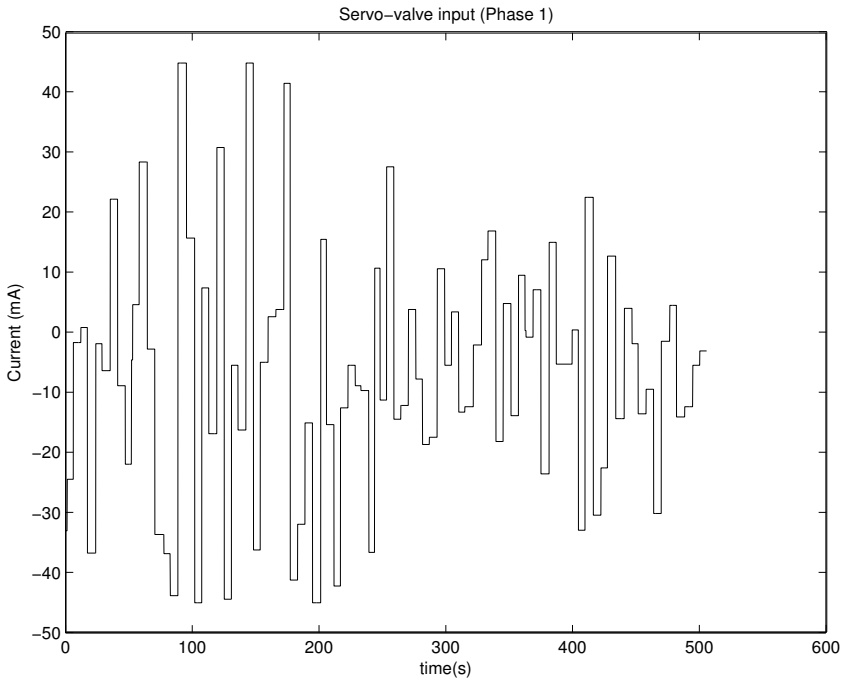

Figure 7.4: Measured servo-valve input for phase 1 obtained with the arc current set-point in figure 7.1

7.3 Simulations

In chapter 6, four different controllers were implemented on the derived arc furnace model. The most effective results were obtained with the model predictive control strategy with disturbance rejection implemented. This control strategy will also be used to test the performance of the derived model against the industrial measurements.

With no disturbances on the lengths of the electric arcs, the simulated responses does not correlate with the measured results. See figures 7.4, 7.5 and 7.6 for the measured servo-valve inputs. The rejection of disturbances on phase 2 and 3, due to step input on phase 1, is fast because of no applied external disturbances. These results are illustrated in figures 7.7, 7.8 and 7.9 together with the respective measured results. The simulated servo-valve inputs are illustrated in figures 7.10, 7.11 and 7.12. The simulated servo-valve inputs are extremely stable because of the disturbances not present on the electric arc

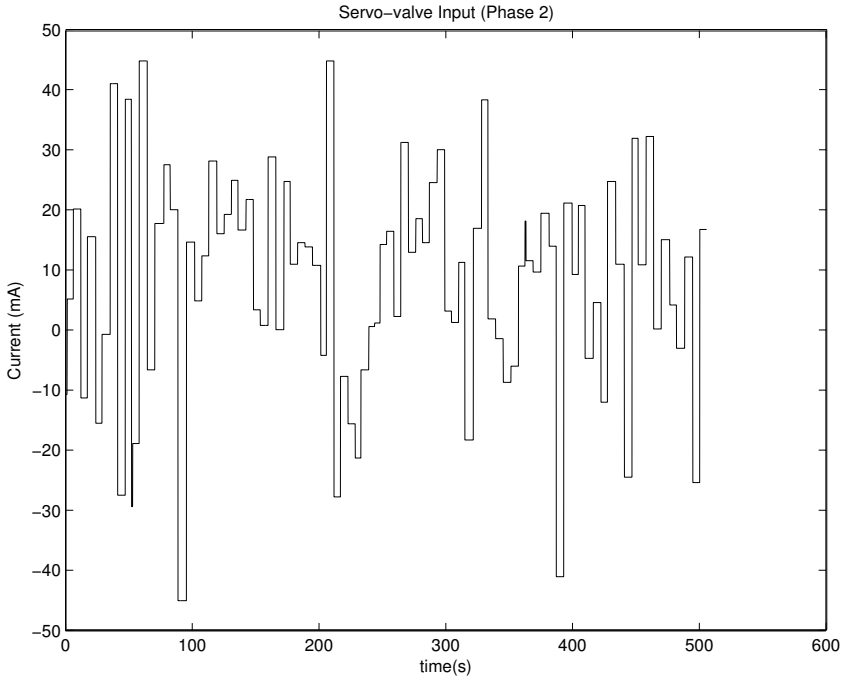

Figure 7.5: Measured servo-valve input for phase 2 obtained with the arc current set-point in figure 7.2

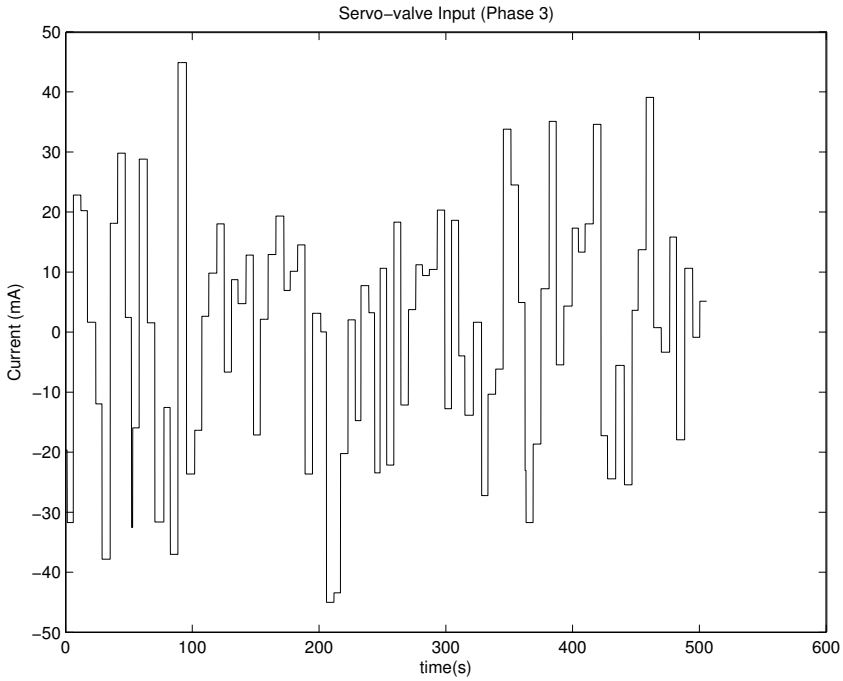

Figure 7.6: Measured servo-valve input for phase 3 obtained with the arc current set-point in figure 7.3

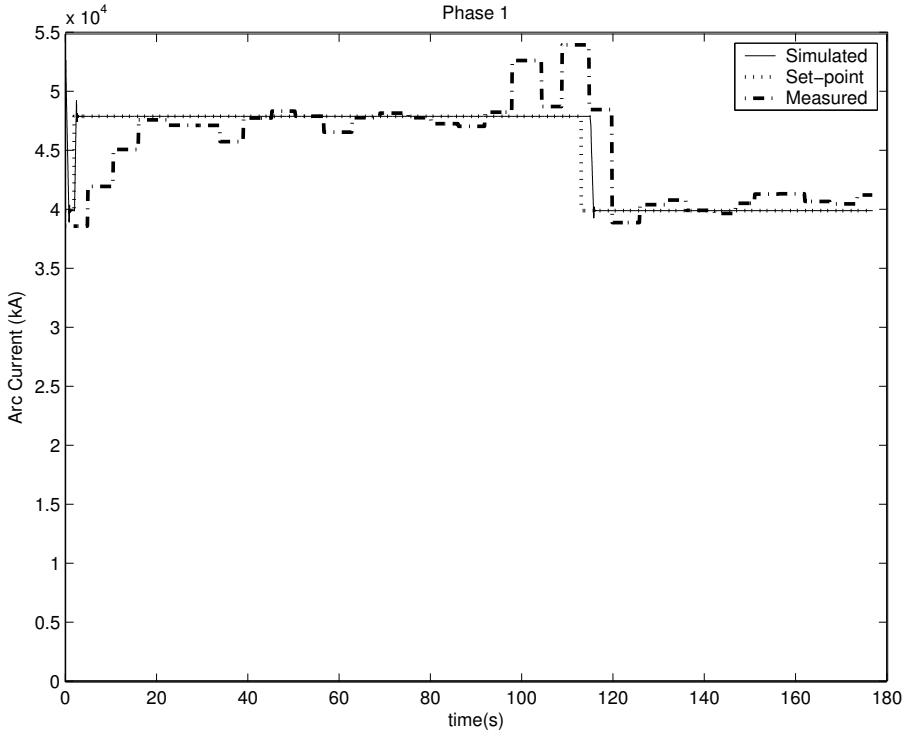

Figure 7.7: Simulated and measured arc currents on phase 1

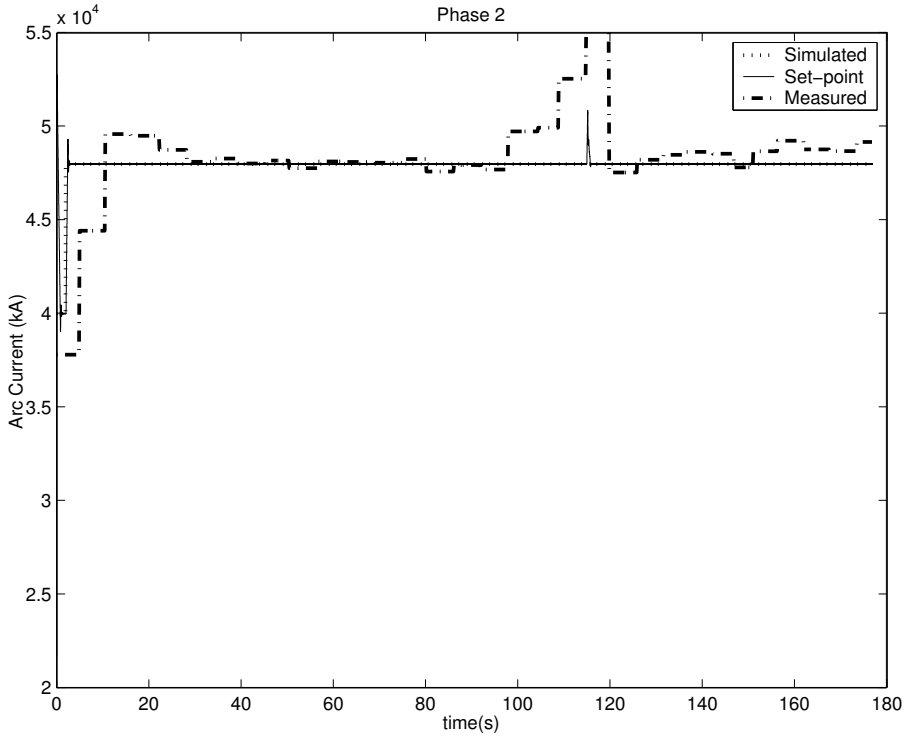

Figure 7.8: Simulated and measured arc currents on phase 2

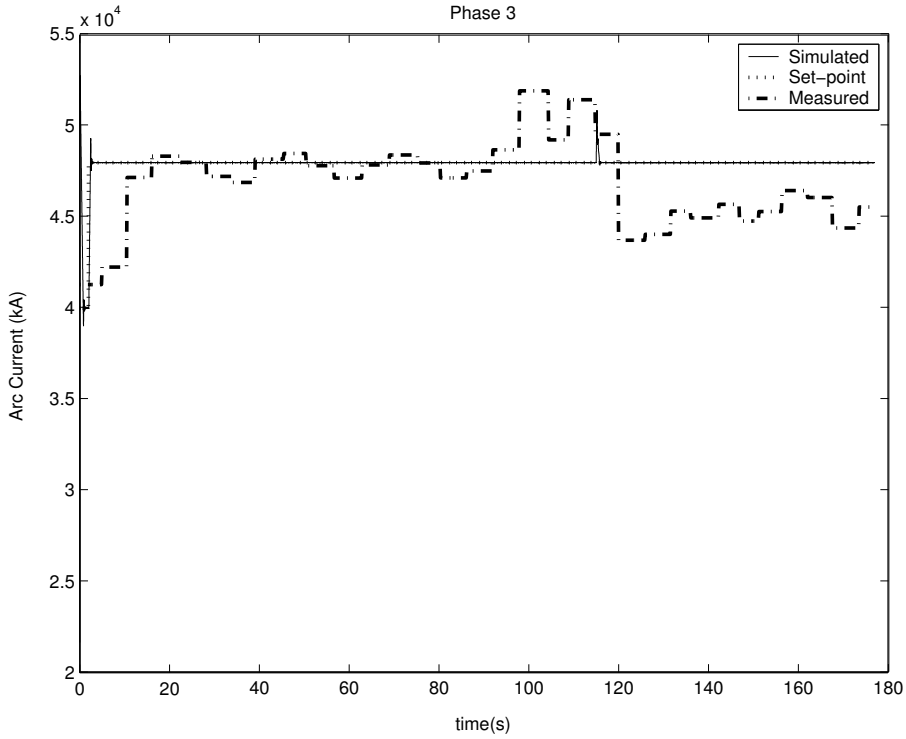

Figure 7.9: Simulated and measured arc currents on phase 3

lengths.

The validation with no disturbances on the electric arc lengths is not very accurate as can be seen in the illustrated results. A more realistic simulation will be to place random disturbances on the lengths of the electric arcs. The amplitudes of the disturbances, chosen through trial and error, are limited between 5kA and -5kA to mimic the disturbances of the refining stage as closely as possible. The sampling rate of the applied random disturbances is 0.25s. Continuous white noise was used for the random arc length disturbances. These disturbances resulted in the arc currents being more noisy and much more realistic to the measured results. Because of the random nature of the disturbances, it is difficult to relate the simulated responses to that of the measured results. This is illustrated in figures 7.13, 7.14 and 7.15. These results, however illustrates the significant effect that disturbances have on the transient response of the electric arc current.

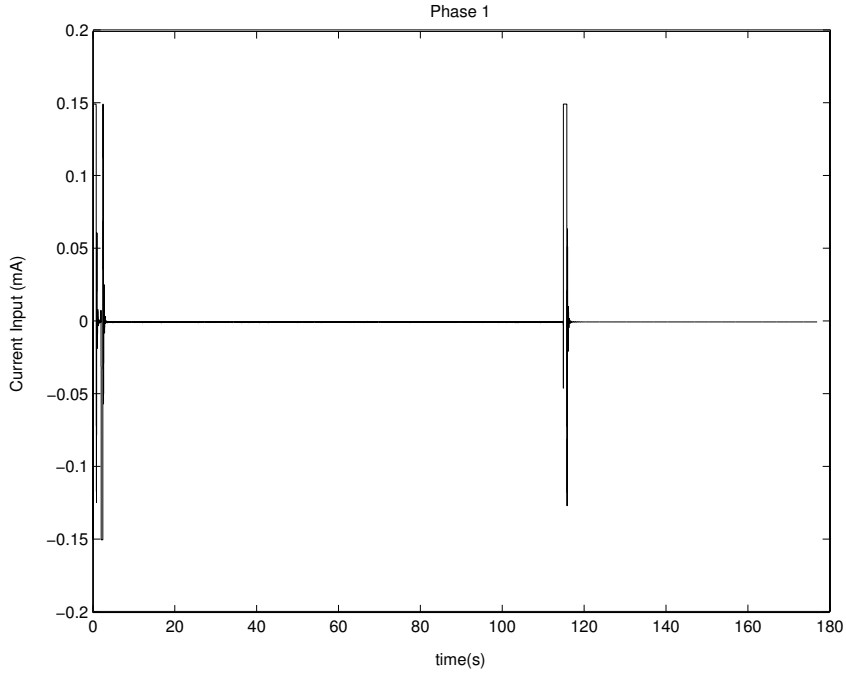

Figure 7.10: Simulated servo-valve input on phase 1, for the arc current set-point in figure 7.7

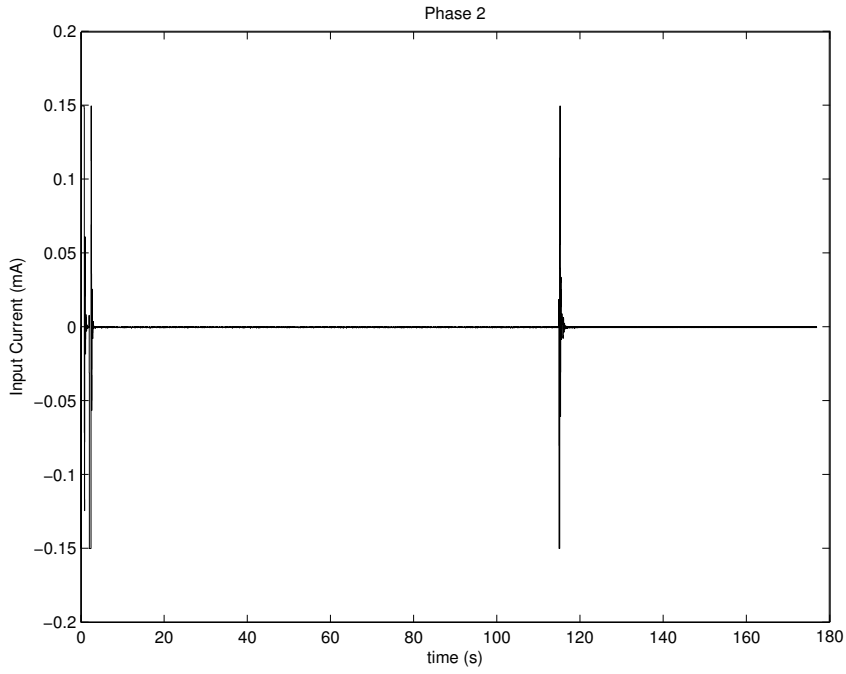

Figure 7.11: Simulated servo-valve input on phase 2, for the arc current set-point in figure 7.8

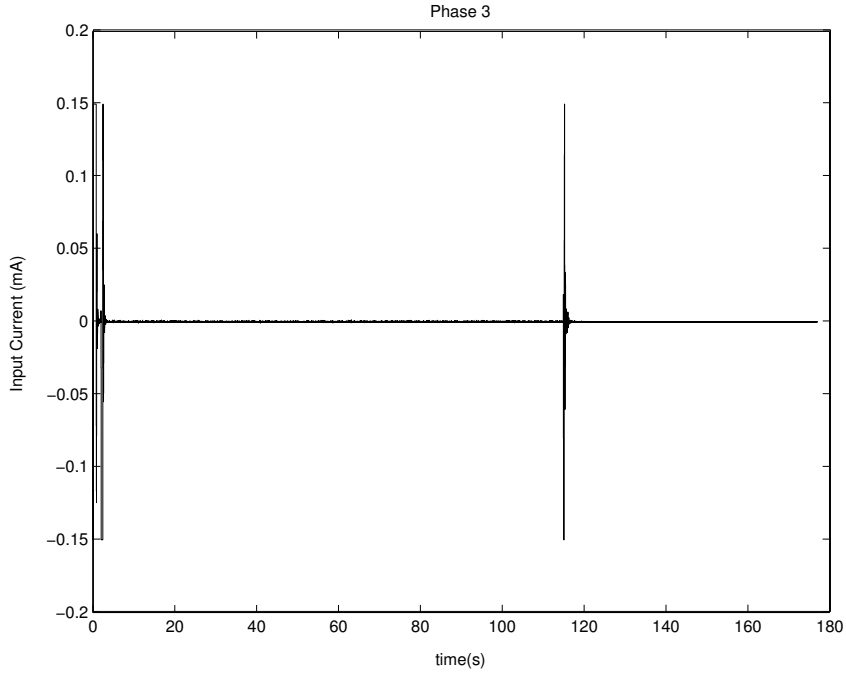

Figure 7.12: Simulated servo-valve input on phase 3, for the arc current set-point in figure 7.9

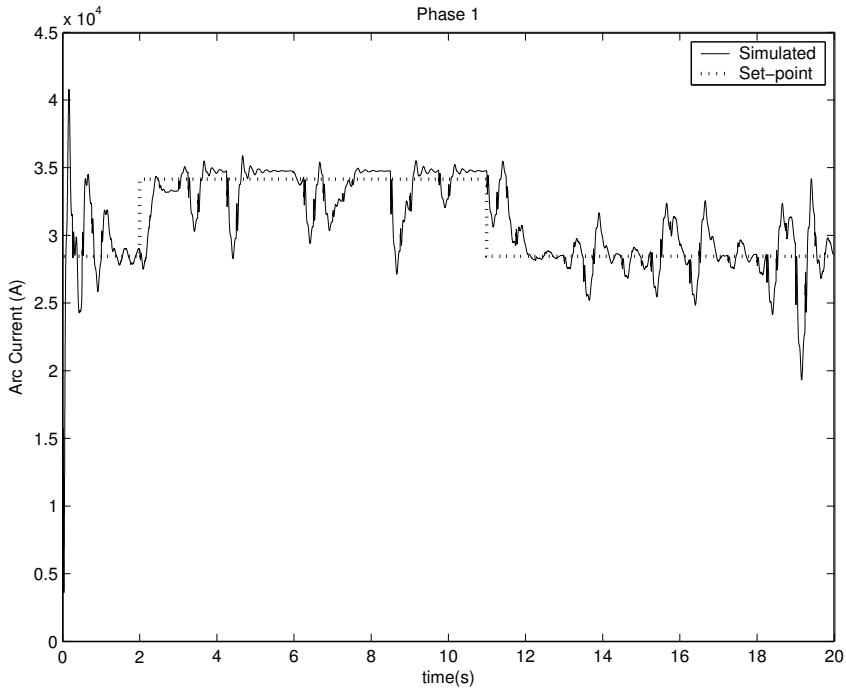

Figure 7.13: Simulated arc currents with random disturbances on the arc lengths, phase 1

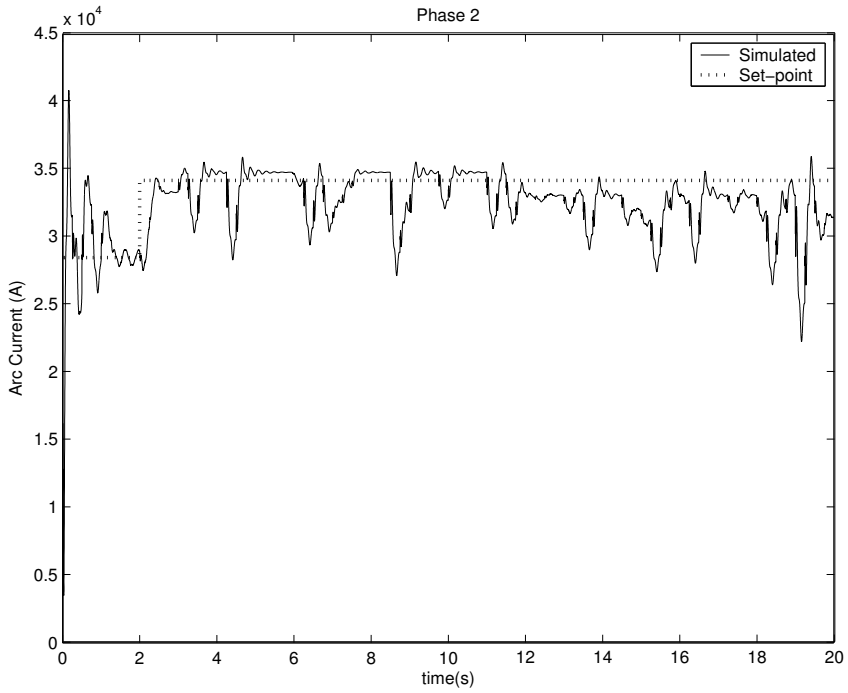

Figure 7.14: Simulated arc currents with random disturbances on the arc lengths, phase 2

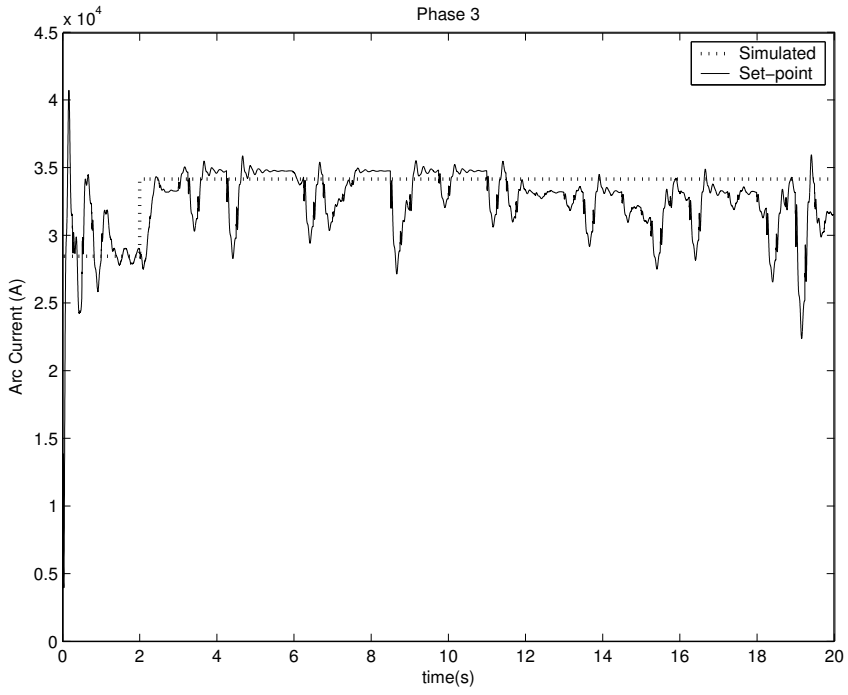

Figure 7.15: Simulated arc currents with random disturbances on the arc lengths, phase 3

Chapter 8

Conclusion and Recommendations

8.1 Introduction

This chapter concludes the work done in this dissertation. The steps followed to model and control an electric arc furnace are given. Recommendations for further research in the field of electric arc furnace control are given.

8.2 Conclusion

The electrode system modelled in this dissertation is motivated by the need for constant electrical power input. Constant electrical power input is assumed to be the case in an existing electric arc furnace model, developed at the University of Pretoria. Three-phase electrical arc current is used as outputs for the derived model. Measured arc current is continuously compared with desired set-points for control purposes. The controlled electrical arc current, together with arc impedance and arc voltage, was used to investigate the electrical properties of a three-phase electric arc furnace.

The modelling of the non-linear electrode system was carried out in chapter 3. The complete model consist of the electrical supply, three hydraulic actuators and, the three-phase electric arcs. The electrical supply was modelled as a three-phase circuit. Three separate hydraulic actuator models were derived, one for each phase. These models are mostly based on laws relating to science.

Both, literature as well as practical measurements relating to a three-phase electrical arc furnace are limited. This made the validation procedure for the arc furnace model extremely hard, especially for sub-models individually. The three-phase electrical supply, integrated together with the electric arc model, compared well with literature. One of the most important factors to note is the re-ignition of the highly nonlinear three-phase electric arc each time the current goes through a zero crossing. This phenomenon has significant impact on the specific waveform shape of the three-phase electrical current. This nonlinearity of the electric arc effects the waveforms of all the remaining electrical variables, which include the arc voltage and the arc resistance/conductance.

Integration of the electrical supply, the electrical arc and the hydraulic actuators were required for the purpose of controller design and to perform a closed-loop simulation on the electrode system. In practice, amplitude measurements are preferred rather than obtaining complete waveforms. This phenomenon had to be included into the derived model and proved to be very sufficient for controller design. This allowed for simulation results to be compared efficiently with industrial measurement.

Linearization of the three-phase electrical arc furnace model was needed for controller design. The obtained linear model compared sufficient enough with the nonlinear arc furnace model and was used for controller design. PID as well as model predictive controllers were designed and compared. Both controller strategies showed similar results but PID control is much more simple compared to MPC. An interesting phenomenon that was found is the 0.25s dead times of the hydraulic pistons. This resulted in oscillations on the model outputs. Both control strategies were used and after tuning and some adjustments the oscillations were almost completely rejected. For PID control, band rejection in the frequency domain was firstly used. A second well known method was used during the design of the PID controllers. This method is simply to include the dead time in the linear model via an approximation. Both these methods proved to be effective for the rejection of the oscillations. The last mentioned method however placed less strain on the actuators, which makes it the preferred method. Similar results and conclusions hold for the implementation of model predictive control on the electric arc furnace model. Both strategies rejected disturbances, caused by three-phase interaction, effectively.

Measured data obtained from the arc furnace industry were used to validate the modelled electric arc furnace. The disturbances present in the real process is impossible to mimic, which made the accuracy of the validation procedure very difficult. Random disturbances were placed on the lengths of the electric arcs which proved efficient for the purpose of validation. Another problem encountered during validation is that faster industrial sampling were required to make the obtained measurements sufficient enough to use. These fast measurements were affected significantly by the slow conversion between analog and digital in the electric arc furnace process. This had quite an effect on the validation procedure as the simulations are almost continuous. However, the model performance, as far as possible, compared well with that of the industrial measurements and some insight was gained in the ability to improve arc furnace efficiency.

8.3 Recommendations

One of the main variables used in the derived electrical arc furnace model is the length of the electric arc. Accept for arc photography, there is not many known methods to measure the length of an electric arc in industry. The absence of measured arc length makes it difficult to run the model developed here in parallel with the industrial process. Running the model and the industrial process in parallel will prove the performance of the derived model more thoroughly. Contribution towards arc length measurements will help to improve the accuracy of the derived model and maybe the efficiency of the electric arc furnace process.

Measurements of known disturbances and applying them to the present simulation will contribute significantly to the ability to validate the model thoroughly.

The designed control strategies simulated in this dissertation can be applied to a real electric arc furnace process to evaluate its true performance and efficiency. This will also allow for economic evaluation of the controller performances and also the accuracy of the simulations.

The electrical supply model on the primary side of the furnace transformer is neglected in this dissertation. These neglected components can be modelled and applied to the derived model to increase the accuracy of the simulation results. This will add quality aspects such as harmonic distortion and voltage flicker to the model.

The derived model in this dissertation must be added to the existing electric arc furnace process model. This will improve the accuracy of the existing model. The more complete the entire electric arc furnace model is, the more efficiently it can contribute to the improvement of industrial electric arc furnace processes.

Bibliography

[1] S. A. Billings and H. Nicholson, "Modelling a three-phase electric arc furnace: a comparative study of control strategies," *Applied Mathematical Modelling*, vol. 1, pp. 355–361, December 1977.

[2] C. R. Taylor, *Electric furnace steelmaking*. Iron and Steel Society, 1985.

[3] S. A. Billings, F. M. Boland, and H. Nicholson, "Electric arc furnace modelling and control," *Automatica*, vol. 15, pp. 137–148, 1979.

[4] D. J. Oosthuizen, I. K. Craig, and P. C. Pistorius, "Economic evaluation and design of an electric arc furnace controller based on economic objectives," *Control Engineering Practice*, vol. 12, no. 1, pp. 253–265, 2004.

[5] G. Bisio, G. Rubatto, and R. Martini, "Heat transfer, energy saving and pollution control in ultra-high-power electric-arc furnaces," *Energy*, vol. 25, pp. 1047–1066, November 1999.

[6] P. Brown and R. D. Langman, "Simulation of closed-loop energy control applied to arc furnaces," *Journal of the Iron and Steel Institute*, pp. 837–847, August 1967.

[7] L. Zi-qiang, G. Xing-yuan, and B. Yu-an, "Modelling and identification of an electrode position controller in electric arc furnace," *International Conference On Control*, vol. 1, pp. 434–439, March 1991.

[8] G. Holmes and F. Memoli, "Operational improvements achieved in Davsteel, a division of Cape Gate (Pty) Ltd, South Africa, utilizing the new Techint KT injection system and TDR digital regulation: a case study," in *Electric Furnace Conference Proceedings, Iron and Steel Society*, 2001.

[9] G. Carpinelli, M. DiManno, P. Verde, E. Tironi, and D. Zaninelli, "AC and DC arc furnaces: a comparison on some power quality aspects," *IEEE, Power Engineering Society Summer Meeting*, vol. 1, pp. 499–506, July 1999.

[10] H. Trenkler and W. Krieger, *Gmelin handbook of inorganic chemistry: practice of steelmaking 2*, 8th ed., Gmelin-Durrer, Ed. Springer-Verlag, 1985, vol. 8a.

[11] E. Acha and M. Madrigal, *Power system harmonics*. New York: John Wiley & Sons, 2001, ch. 12.

[12] E. Scholtz, *Modelling for control of a Steckel hot rolling mill*. South Africa: Master's dissertation, University of Pretoria, 1999.

[13] H. Nicholson and R. Roebuck, "Simulation and control of electrode position controllers for electric arc furnaces," *Automatica*, vol. 8, 1972.

[14] A. S. Hauksdttir, A. Gestsson, and A. Vsteinsson, "Current control of a three-phase submerged arc ferrosilicon furnace," *Control Engineering Practice*, vol. 10, Issue 4, pp. 253–258, April 2002.

[15] J. G. Bekker, *Modeling and control of an electric arc furnace off-gas process*. South Africa: Master's dissertation, University of Pretoria, 1998.

[16] D. J. Oosthuizen, J. H. Viljoen, I. K. Craig, and C. P. Pistorius, "Modeling of the off-gas exit temperature and slag foam depth of an electric arc furnace process," *ISIJ*, vol. 41, no. 4, pp. 399–401, 2001.

[17] R. F. Fruehan, *The making, shaping and treating of steel: steelmaking and refining volume*, 11st ed. Association of Iron and Steel Engineers, 1998.

[18] W. E. Stalb and R. B. Staib, "The intelligent arc furnace controller: a neural network electrode position optimization system for the electric arc furnace," *International Joint Conference on Neural Networks*, vol. 3, 1992.

[19] J. G. Bekker, I. K. Craig, and P. C. Pistorius, "Modeling and simulation of an electric arc furnace process," *ISIJ*, vol. 39, no. 1, pp. 23–32, 1999.

[20] J. G. Bekker, P. C. Pistorius, and I. K. Craig, "Model predictive control of an electric arc furnace off-gas process," *Control Engineering Practice*, vol. 8, pp. 445–455, 2000.

[21] G. Manchur and C. C. Erven, "Development of a model for predicting flicker from electric arc furnaces," *IEEE Transaction on Power Delivery*, vol. 7, No. 1, pp. 416–426, Jan. 1992.

[22] C. W. Lu, S. J. Huang, and C. L. Huang, "Flicker characteristic estimation of an ac electric arc furnace," *Electric Power Systems Research*, vol. 54, pp. 121–130, Sep 1999.

[23] G. C. Montanari, M. Loggini, and A. Cavallini, "Arc-furnace model for the study of flicker compensation in electrical networks," *IEEE Transaction on Power Delivery*, vol. 9, no. 4, Oct. 1994.

[24] S. A. Billings and H. Nicholson, "Identification of an electric-arc furnace electrode-control system," *Proceedings of the Institution of Electrical Engineers, Control and Science*, vol. 122, No.8, pp. 849–859, August 1975.

[25] I. K. Craig and R. G. D. Henning, "Evaluation of advanced industrial control projects: a framework for determining economic benefits," *Control Engineering Practice*, vol. 8, pp. 769–780, 2000.

[26] "World steel in figures by the Iron and Steel Institude," *See web site: http://www.worldsteel.org/media/wsif/wsif2004.pdf.*

[27] Y. Sakamoto, Y. Tonooka, and Y. Yanagisawa, "Estimation of energy consumption for each process in the Japanese steel industry: a process analysis," *Energy Conversion and Management*, vol. 40, pp. 1129–1140, 1999.

[28] R. T. Jones, Q. G. Reynolds, and M. J. Alport, "DC arc photography and modelling," *Minerals Engineering*, vol. 15, pp. 985–991, March 2002.

[29] J. Westly and L. T. Kvassheim, "Electric control of ferrosilicon submerged-arc funaces," *Metallurgical Processing and Control*, pp. 413–421, 1984.

[30] A. Gosiewski and A. Wierzbicki, "Dynamic optimization of a steel-making process in electric arc furnace," *Automatica*, vol. 6, pp. 767–778, 1970.

[31] S. R. Mendis and D. A. Gonzlez, "Harmonic and transient overvoltage analyses in arc furnace power systems," *IEEE Transactions on Industry Applications*, vol. 28, No.2, pp. 336–342, March 1992.

[32] K. Janson and J. Jrvik, "High power factor converter for normalizing flicker of arc furnaces," *IEEE Conference on Power Quality*, pp. 111–116, 1998.

[33] C. S. Chen, H. J. Chuang, C. T. Hsu, and S. M. Tseng, "Mitigation of voltage fluctuation for an industrial customer with arc furnaces," *Power Engineering Society Summer Meeting, IEEE*, vol. 3, pp. 1610–1615, July 2001.

[34] H. Mokhtari and M. Hejri, "A new three phase time-domain model for electric arc furnaces using MATLAB," *IEEE Transmission and Distribution Conference and Exhibition*, vol. 3, pp. 2078–2083, October 2002.

[35] C. Surapong, C. Y. Yu, D. Thukaram, T. Nipon, and K. Damrong, "Minimization of the effects of harmonics and voltage dip caused by electric arc furnace," *Power Engineering Society Winter Meeting, IEEE*, vol. 4, pp. 2568–2576, Jan 2000.

[36] A. Akdag, I. Cadirci, E. Nalcaci, M. Ermis, and S. Tadakuma, "Effects of main transformer replacement on the performance of an electric arc furnace system," *IEEE Transactions on Industry Applications*, vol. 36, Issue 2, pp. 1298–1307, March 1999.

[37] B. N. Ramos and J. L. deCastro, "An EMTP study of flicker generation and transmission in power systems due to the operation of an AC electric arc furnace," *Proceedings, Ninth International Conference on Harmonics and Quality of Power*, vol. 3, pp. 942–947, October 2000.

[38] A. Chofr, M. Pinilla, and J. M. Romero, "Connection of a plant with arc furnaces to the andalucian network," *16th International Conference and Exhibition on Electricity Distribution, IEE*, vol. 2, p. 5, June 2001.

[39] B. Boulet, G. Lalli, and M. Ajersch, "Modeling and control of an electric arc furnace," *Proceedings of the 2003 American Control Conference*, vol. 4, pp. 3060–3064, June 2003.

[40] K. Heinen, *Elektrostahl-Erzeugung*. Germany: Stahl Eisen, 1998.

[41] R. Sesselmann, "Improving EAF energy utilization with electrode controllers based on neural networks," *IFAC Automation in Mining, Mineral and Metal Processing*, pp. 61–67, 1998.

[42] D. Raisz, M. Sakulin, H. Renner, and Y. Tehlivets, "Recognition of the operational states in electric arc furnaces," *In the Proceedings of the 9th International Conference on Harmonics and Quality of Power*, vol. 2, pp. 475–480, Oct. 2000.

[43] U. Pinsopon, T. Hwang, S. Cetinkunt, R. Ingram, Q. Zhang, M. Cobo, D. Koehler, and R. Ottman, "Hydraulic actuator control with open-centre electrohydraulic valve using a cerebellar model articulation controller neural network algorithm," *Poceedings for the Intitution of Mechanical Engineers*, vol. 213, Part 1, pp. 33–48, 1999.

[44] D. P. Newell, H. Dai, and B. F. Spencer, "Nonlinear modelling and control of a hydraulic Seismic simulator," *Proceedings American Control Conference*, pp. 801–805, June 1995.

[45] J. A. T. Jones, "Electric arc furnace steelmaking," www.steel.org/howmade/eaf.htm, January 2004.

[46] C. E. Solver, "Electric arcs and arc interruption," *Chalmers University of Technology, Department of Electric Power Engineering*, June 2002.

[47] "Electric arcs and flicker," *see web site: www.robicon.com*, January 2004.

[48] M. A. Reuter, M. Oosthuizen, I. J. Barker, M. S. Rennie, and A. de Waal, "The dynamic response of submerged-arc furnaces to electrode movement," *Mintek, Randburg, South Africa*, pp. 97–102, 2002.

[49] W. Ting, S. Wennan, and Z. Yao, "A new frequancy domain method for the harmonic analysis of power systems with arc furnace," in *Proceedings of 4th International Conference on Advances in Power System Control, Operation and Management*, Hong Kong, November 1997, pp. 552–555.

[50] B. Bowman, G. R. Jordan, and F. Fitzgerald, "The physics of high-current arcs," *Journal of the Iron and Steel Institute*, pp. 798–805, 1969.

[51] B. Bowman, P. A. Stafford, and S. Alameddine, "Unuasual arcing phenomena in modern arc furnaces," *Iron and Steelmaker*, pp. 57–66, 2003.

[52] A. E. Emanual and J. A. Orr, "An improved method of simulation of the arc voltage-current characteristics," in *Proceedings of Ninth International Conference on Harmonics and Quality of Power*, vol. 1, October 2000, pp. 148–154.

[53] S. S. Venkata and B. Lee, "Development of enhanced electric arc furnace models for transient analysis," *see web site: www.pserc.wisc.edu*, 2004.

[54] O. Ozgen and A. Abur, "Development of an arc furnace model for power quality studies," *Power Engineering Society Summer Meeting, IEEE*, vol. 1, pp. 507–555, July 1999.

[55] T. Zheng and E. B. Makram, "An adaptive arc furnace model," *IEEE Transactions on Power Delivery*, July 2000.

[56] E. B. M. T Zheng and A. A. Girgis, "Effect of different arc furnace models on voltage distortion," *In Proceedings of the 8th International Conference on Harmonics And Quality of Power*, vol. 2, pp. 1079–1085, October 1998.

[57] L. van der Sluis and W. R. Rutgers, "The comparisons of test circuits with arc models," *IEEE Transactions on Power Delivery*, vol. 10, No. 1, pp. 280–285, Jan. 1995.

[58] K. J. Tseng, Y. Wang, and D. M. Vilathgamuwa, "An experimentally verified hybrid Cassie-Mayr electric arc model for power electronics simulations," *IEEE Transactions on Power Electronics*, vol. 12, Issue 3, pp. 429–436, May 1997.

[59] S. Chirattananon and Z. Gao, "A model for the performance evaluation of the operation of electric arc furnace," *Energy Conversion and Managment*, vol. 37, No.2, pp. 161–166, 1994.

[60] C. J. Wu, C. P. Huang, T. H. Fu, T. C. Zhoa, and H. S. Kuo, "Power factor definition and effect on revenue of electric arc furnace load," *Proceedings, International Conference on Power System Technology*, vol. 1, pp. 93–97, October 2002.

[61] S. R. Mendis, M. T. Bishop, and J. F. Witte, "Investigations of voltage flicker in electric arc furnace power systems," *Industry Applications Magazine, IEEE*, vol. 2, Issue 1, pp. 28–34, 1996.

[62] R. M. Guo, "Evaluation of dynamic characteristics of HACG system," *Iron and Steel Engineer*, pp. 52–61, 1991.

[63] E. B. M. S Varadan and A. A. Girgis, "A new time domain voltage source model for an arc furnace using EMTP," *IEEE Transactions on Power Delivery*, vol. 11, Issue 3, pp. 1685–1691, July 1996.

[64] G. C. Goodwin, S. F. Graebe, and M. E. Salgado, *Control system design*. Prentice Hall, 2001.

[65] M. N. Horenstein, *Microelectronic circuits and devices*. Prentice Hall, 1996.

[66] SACAC, *Process automation in a nutshell*. South African Council for Automation and Computation, 2004.

[67] M. Barreras and M. Garcia-Sanz, "Model identification of a multivariable industrial furnace," *In Proceedings of the 13th IFAC Symposium on System Identification*, pp. 449–454, 2003.

[68] A. R. Sadeghian and J. D. Lavers, "Application of radial basis function networks to model electric arc furnaces," *International Joint Conference on Neural Networks*, vol. 6, pp. 3996–4001, July 1999.

[69] D. E. Seborg, T. F. Edgar, and D. A. Mellichamp, *Process dynamics and control*. John Wiley and Sons, Inc., 2003.

Appendix A

Controller Tuning and Controller Inputs and Outputs

A.1 Initial PID Controller Outputs

PID controllers were designed for the three-phase electric arc furnace with a close loop pole placement strategy which proved to be very efficient. The simulation results are illustrated in chapter 6. The outputs of the three respective controllers serve as the electric current inputs to the hydraulic servo-valves.

The controller outputs for the initial PID controllers implemented on the nonlinear arc furnace model are illustrated in figures A.1, A.2 and A.3. The on/off responses of these controller outputs are due to the oscillations on the furnace outputs. It is also partly due to high close loop gain. This is one of the main reasons why tuning on the controllers were carried out in section 6.2.3.2.

A.2 Controller Tuning via Frequency Domain Analysis

The close loop frequency response obtained with the initial controllers take the shape of a low pass filter with 0dB gain. This is a typical close loop controlled response. This response is illustrated in figure A.4. From this response, note that all signals with fre-

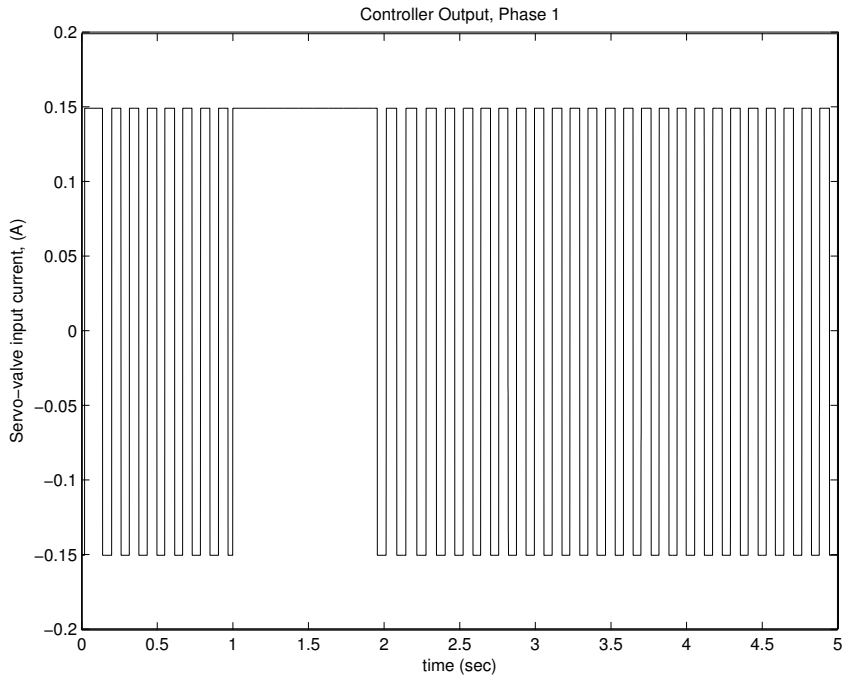

Figure A.1: Phase 1, PID controller output with no disturbance rejection.

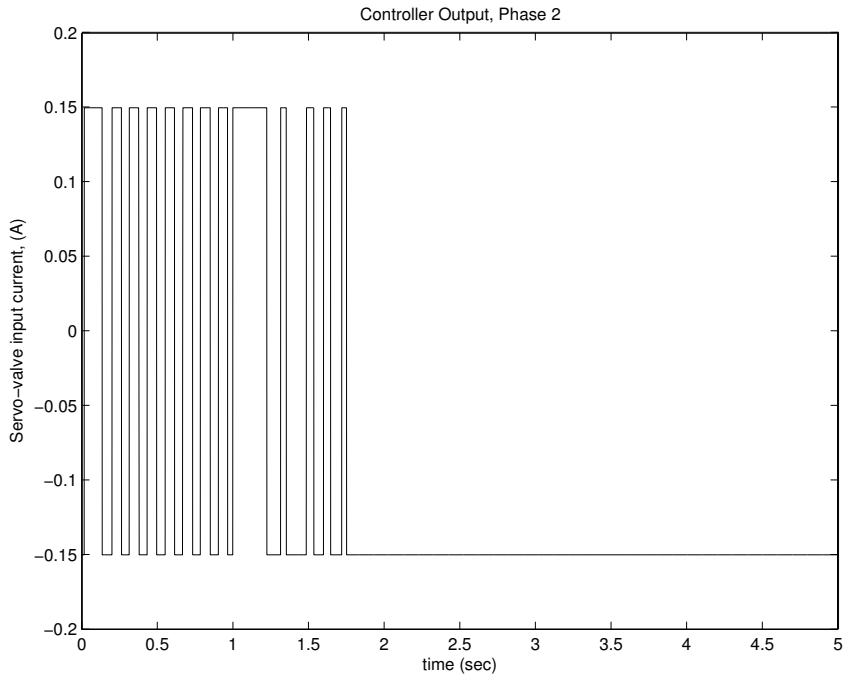

Figure A.2: Phase 2, PID controller output with no disturbance rejection.

quencies smaller than 1×10^4rad/s will not be rejected. To reject the oscillations on the controlled arc current responses with a low pass filter configuration will be difficult. The desired frequency response to do so will have a significant effect on the system response

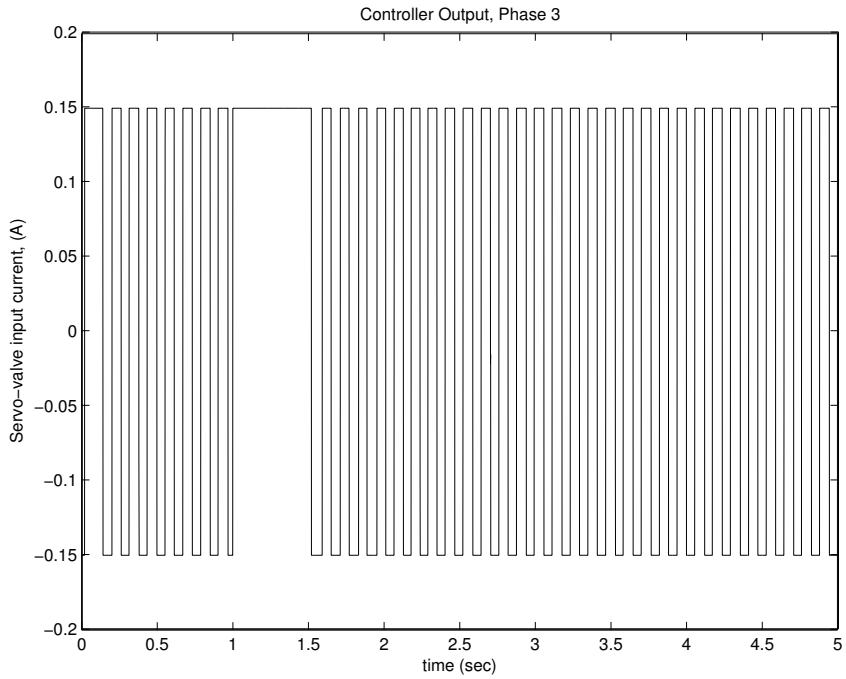

Figure A.3: Phase 3, PID controller output with no disturbance rejection.

time. This is because of the dominant pole which has to be very small and is highly undesirable for this specific control problem.

The method used here to reject the oscillations (disturbances) is to adjust the control configuration such that the frequency response still represents that of a low pass filter but with rejection in the band around 50rad/sec. The addition of a band reject response in the feedback control loop has a significant effect on the stability of the system. This is mainly due to an additional phase response introduced to the close loop which can force the system beyond the critical stability points on the frequency response. The result is that the designed PID controller, used in the previous section, has to be tuned to ensure that the system remains stable. The new frequency response obtained with this additional band rejection implemented in the loop is illustrated in figure A.5.

A 3rd order chebyshev filter was used to reject the undesired frequency band at 50rad/sec. Detail on the filter design is not discussed in this dissertation. The designed filter is represented by the following transfer function:

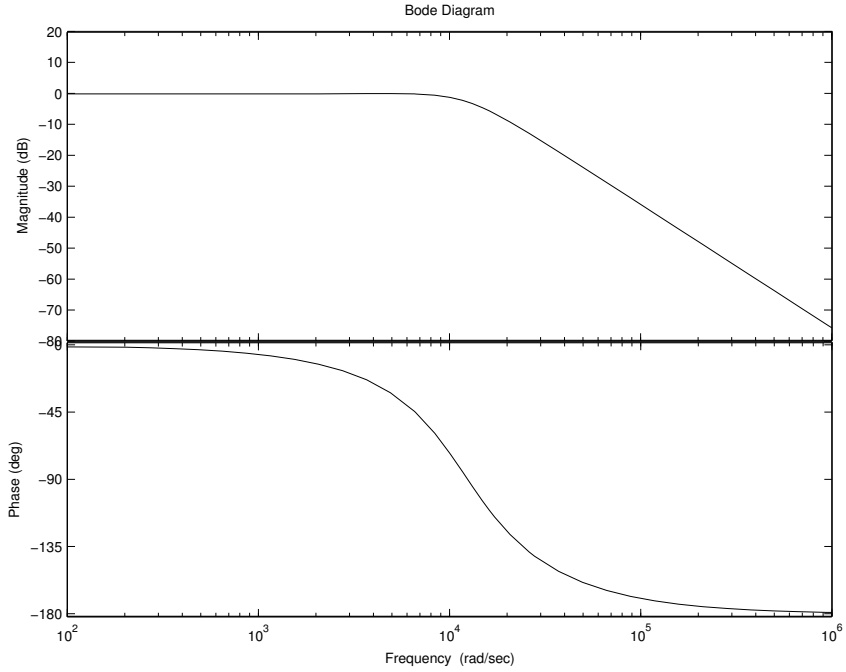

Figure A.4: Close loop frequency response with the initial PID controller implemented on the linear model. This is a typical low pass filter response.

$$F(s) = \frac{s^6 + 6300s^4 + 1.323 \times 10^7 s^2 + 9.261 \times 10^9}{s^6 + 85.79s^5 + 9101s^4 + 4.497 \times 10^5 s^3 + 1.911 \times 10^7 s^2 + 3.783 \times 10^8 s + 9.261 \times 10^9}. \tag{A.1}$$

The frequency response in figure A.5 represents the nominal complementary sensitivity function as given in 6.15. The addition of the band reject filter is not illustrated in 6.15. Another well known method to investigate the rejection of output disturbances is with the use of the nominal sensitivity, $S_o(s)$, which is given in A.2. The frequency response for this sensitivity function is illustrated in figure A.6.

$$S_o(s) = \frac{1}{1 + C(s)G(s)}. \tag{A.2}$$

This tuned control strategy via frequency domain analysis is next implemented on the nonlinear arc furnace model. The reference inputs together with the simulated outputs

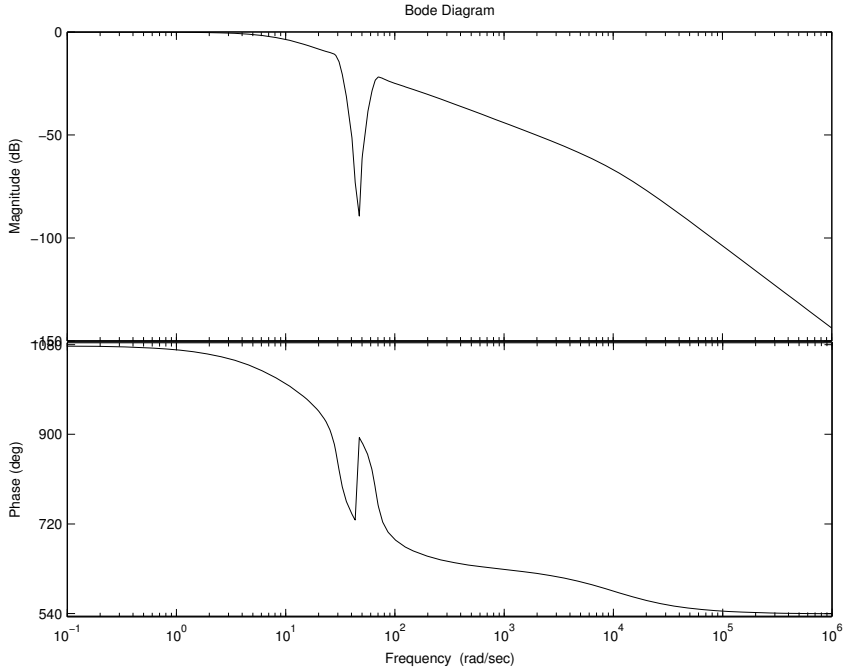

Figure A.5: Close loop frequency response with the tuned PID controller implemented on the linear model

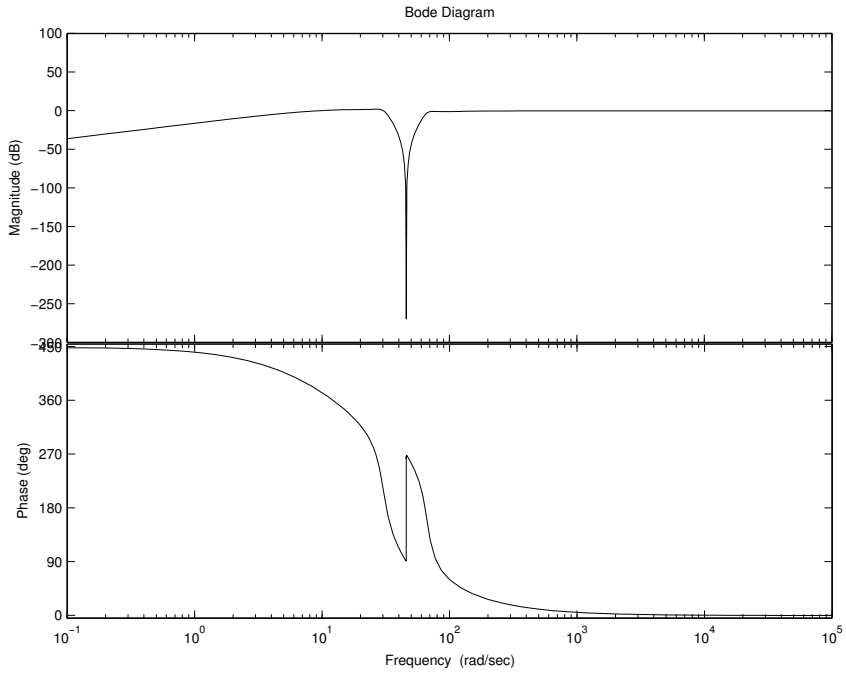

Figure A.6: Frequency response for the nominal sensitivity function.

are illustrated in figures A.7, A.8 and A.9. The controller inputs and outputs are illustrated in figures A.10 to A.15.

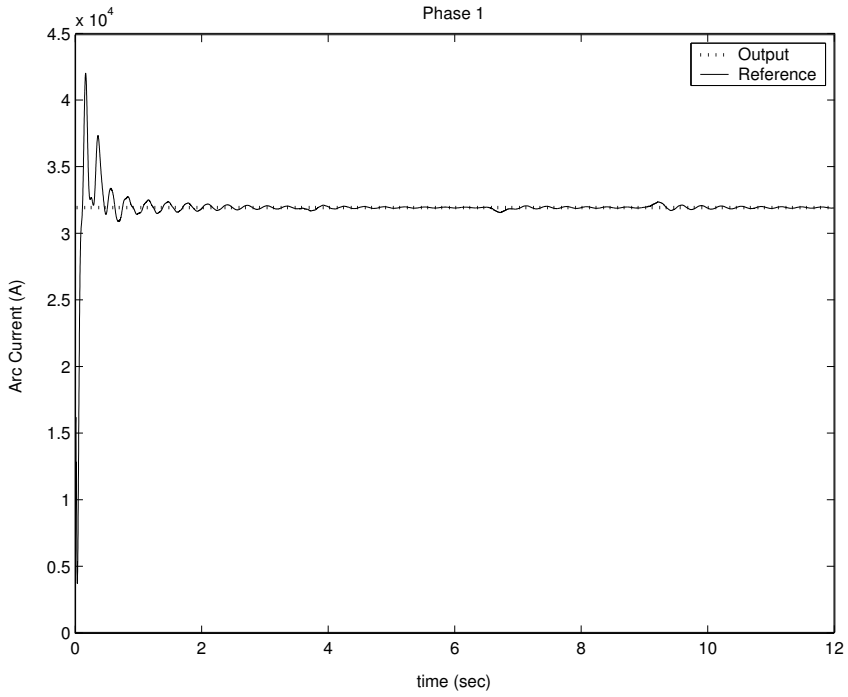

Figure A.7: Controlled arc current, phase 1, for the close loop system in figure A.6.

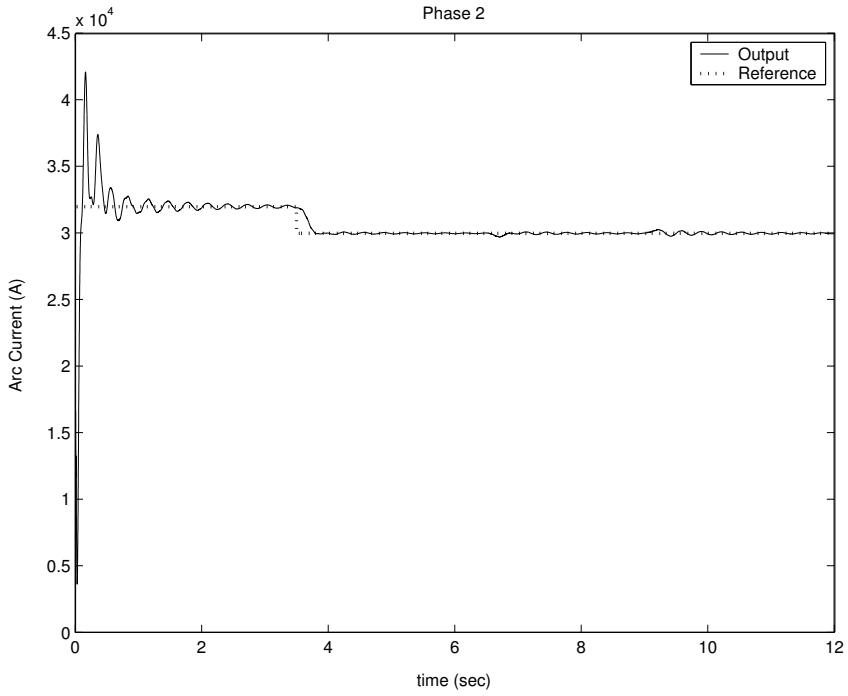

Figure A.8: Controlled arc current, phase 2, for the close loop system in figure A.6.

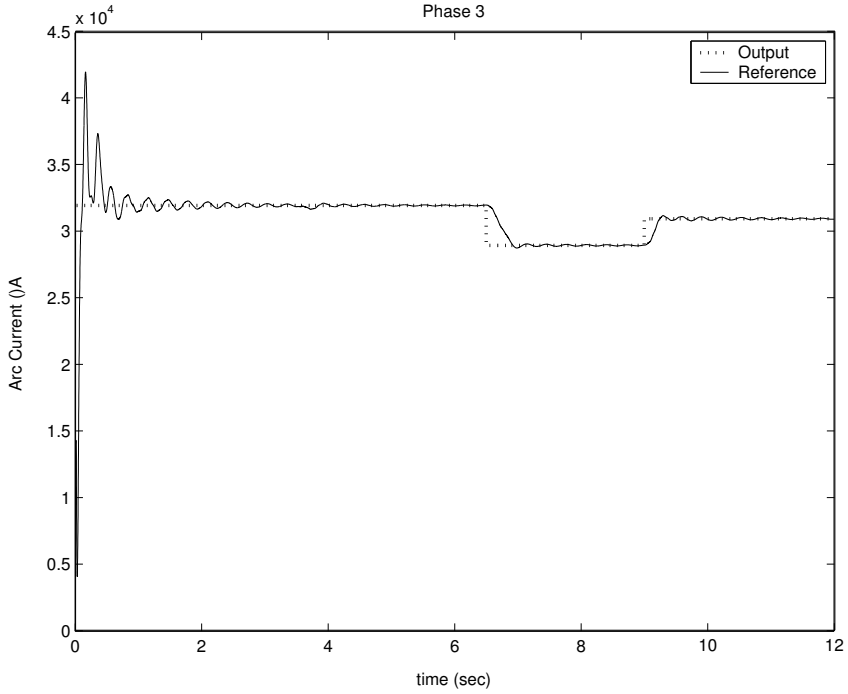

Figure A.9: Controlled arc current, phase 3, for the close loop system in figure A.6.

From these results we can see that the oscillations are almost completely rejected at steady state. The additional oscillations at the beginning of the simulation is due to initialization of all the model parameters. The reaction time of the close loop system remains the same and the rejection of disturbances on other phases are also very successful. This concludes that PID control is a very good choice for the regulation of arc current in a three-phase electric arc furnace.

A.3 Inputs and Outputs for the Tuned PID Controllers

Disturbance rejection was firstly carried out on the close loop system to reject the 8Hz oscillations on the arc currents for the three respective phases. Another method where proposed where the 0.25s dead time was included in the linear model before controller design. The simulation results with the tuned PID controllers are following the set-points with none or little oscillations, which prove the efficiency of the control strategy.

The respective controller inputs and outputs are illustrated in figures A.10 to A.21. From this it is clear that the inputs to the servo-valves is not switching continuously between its minimum and maximums as was the case with the initial PID controllers.

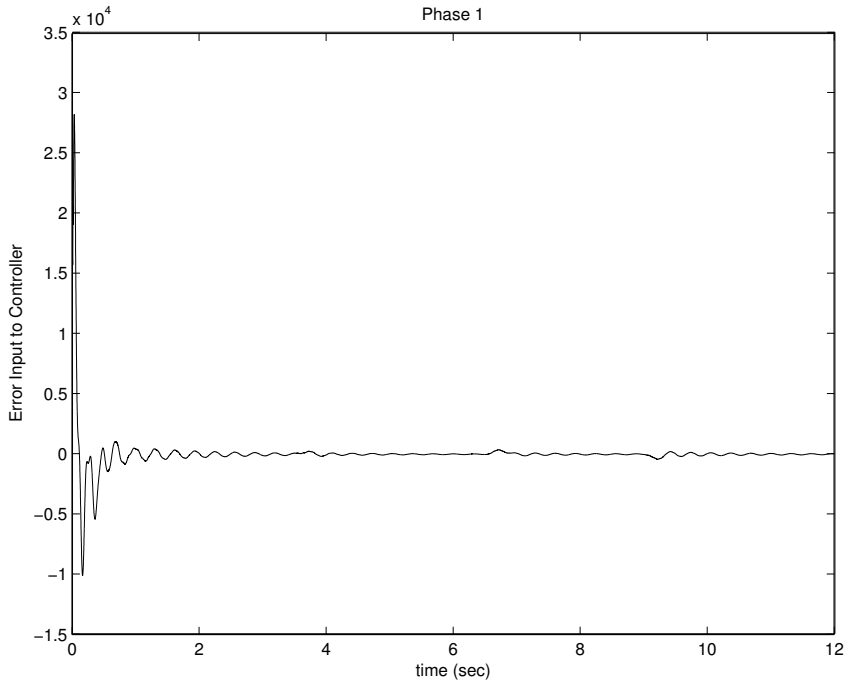

Figure A.10: Phase 1, PID controller input with disturbance rejection employed via frequency domain analysis.

A.4 Model Predictive Controller Outputs without Disturbance Rejection

After PID control was implemented on the electric arc furnace model, a multi-variable control strategy was needed to carry out some comparisons. Model predictive control was chosen as this is an effective method for multi-variable systems with input and output constraints.

Initially no disturbance rejection was done for this strategy. The simulation results again showed 8Hz oscillations on the outputs. The respective controller outputs are illustrated in figures A.22, A.23 and A.24.

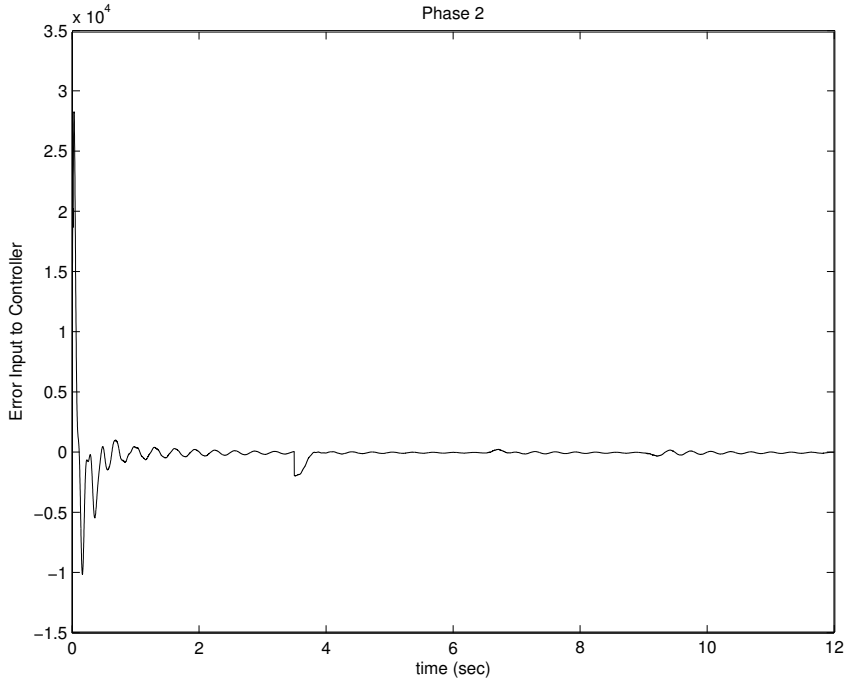

Figure A.11: Phase 2, PID controller input with disturbance rejection employed via frequency domain analysis.

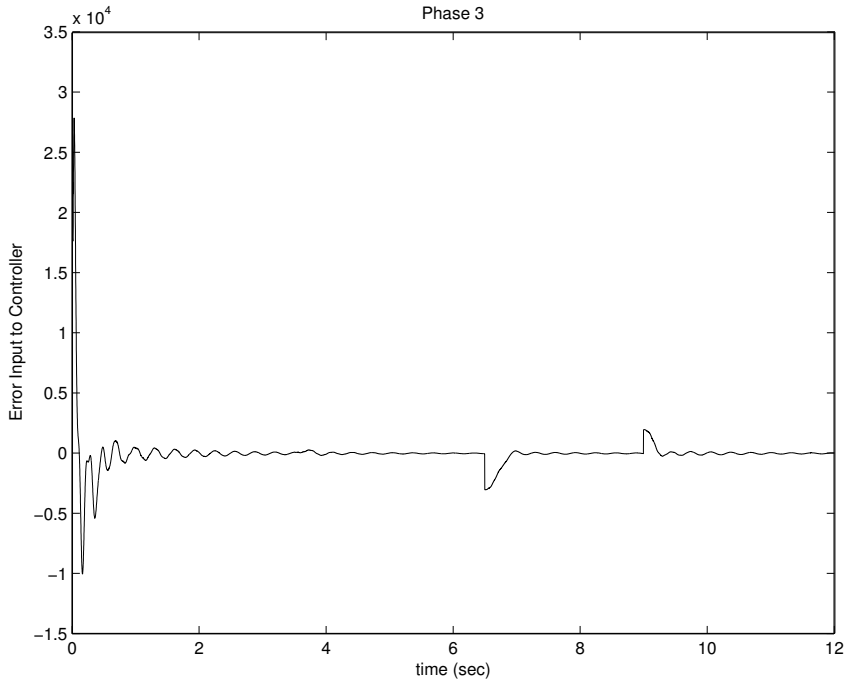

Figure A.12: Phase 3, PID controller input with disturbance rejection employed via frequency domain analysis.

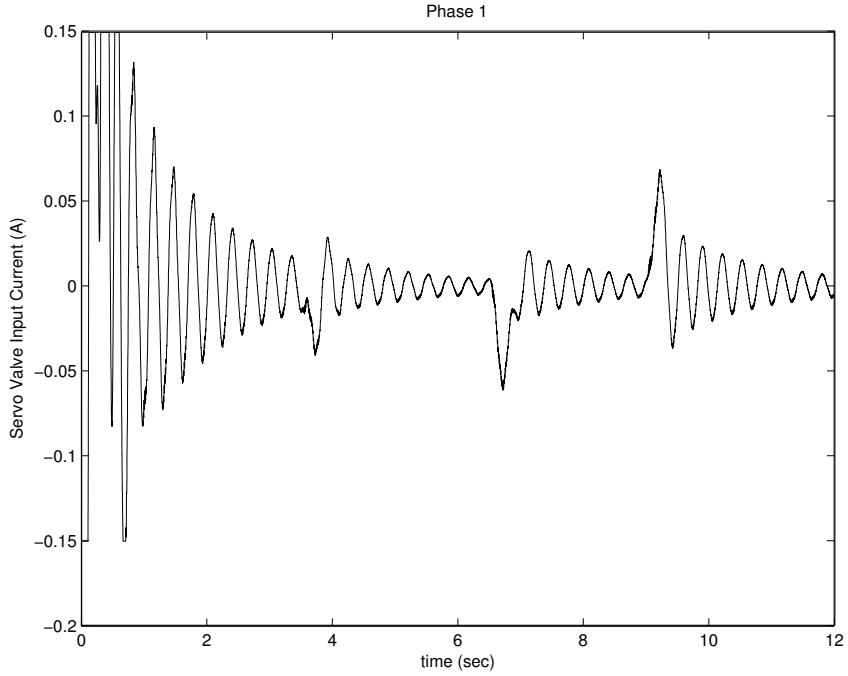

Figure A.13: Phase 1, PID controller output with disturbance rejection employed via frequency domain analysis.

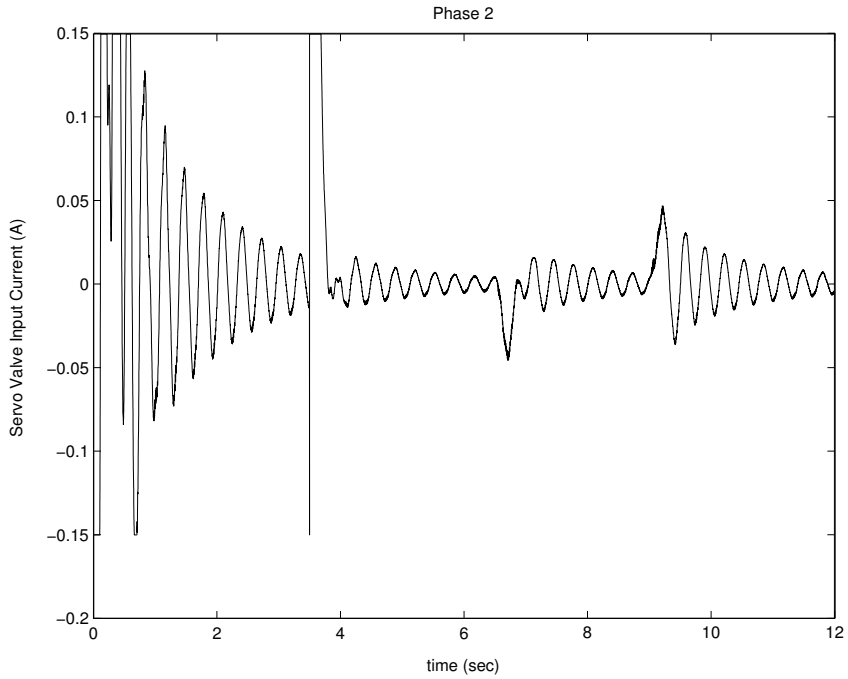

Figure A.14: Phase 2, PID controller output with disturbance rejection employed via frequency domain analysis.

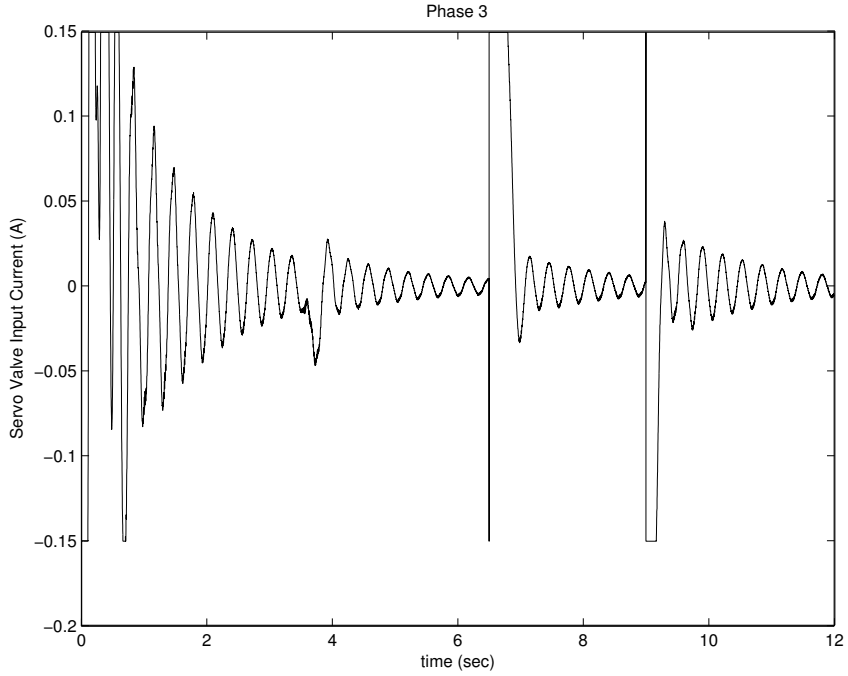

Figure A.15: Phase 3, PID controller output with disturbance rejection employed via frequency domain analysis.

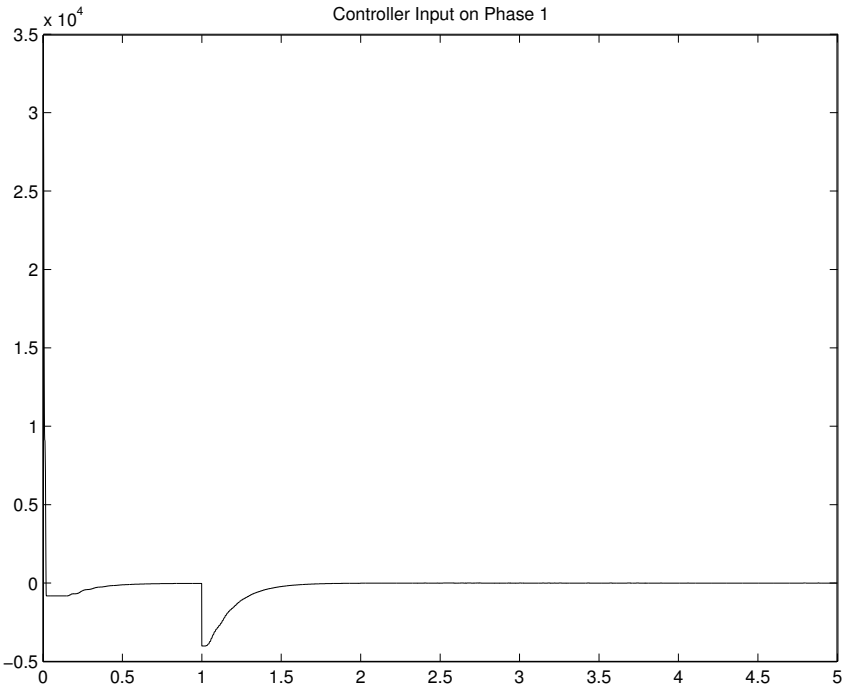

Figure A.16: Phase 1, PID controller input (Design with dead time included in linear model).

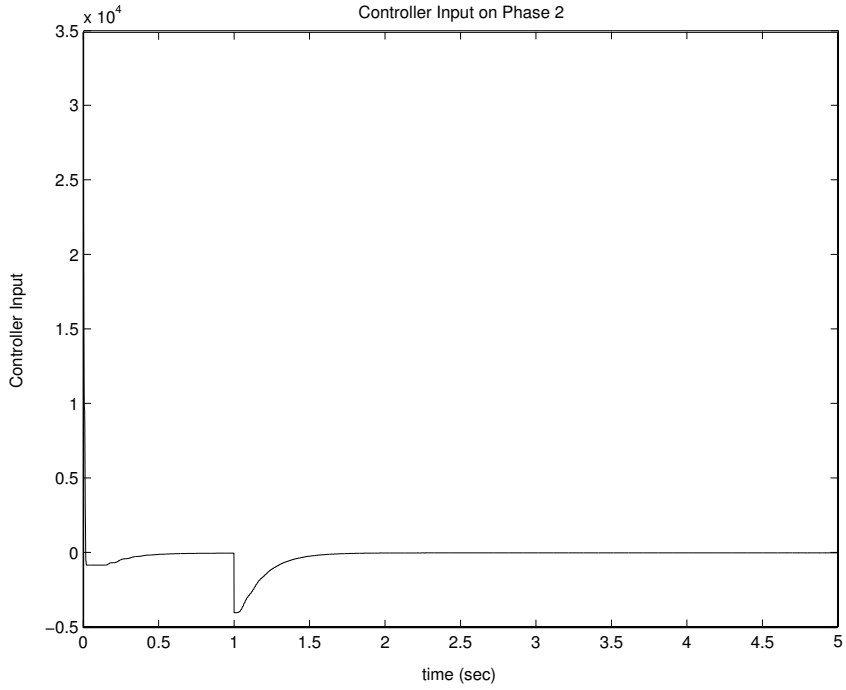

Figure A.17: Phase 2, PID controller input (Design with dead time included in linear model).

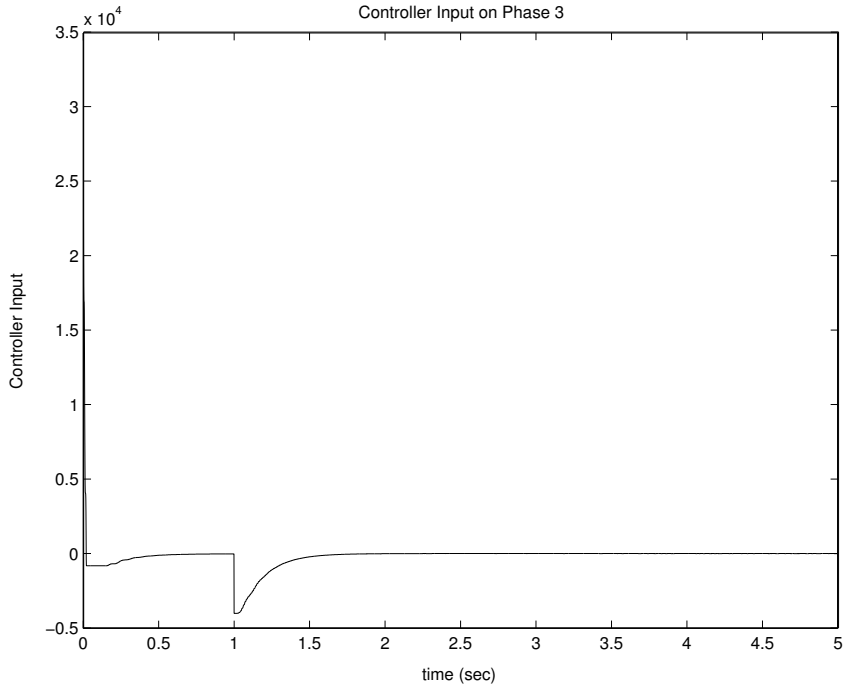

Figure A.18: Phase 3, PID controller input (Design with dead time included in linear model).

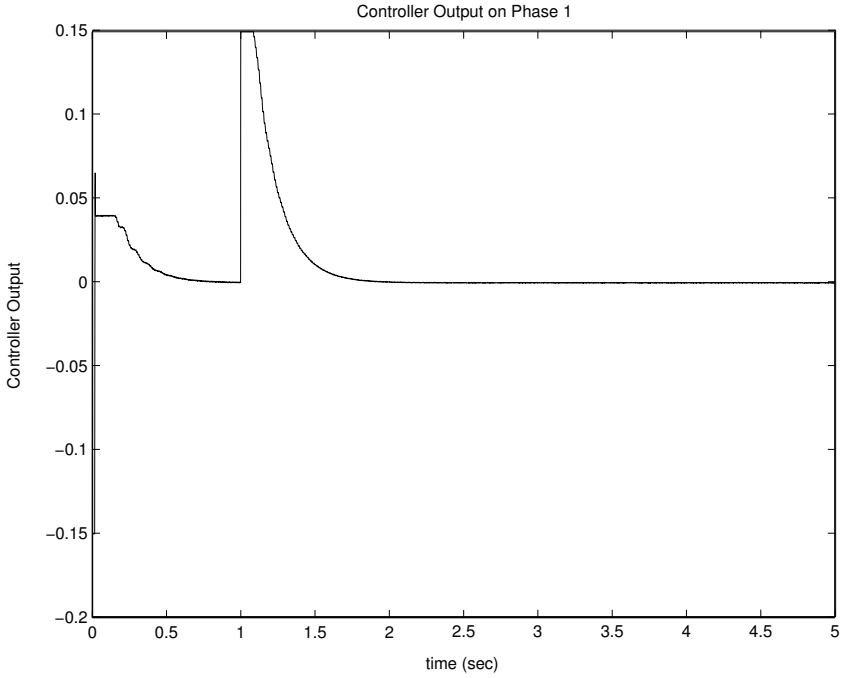

Figure A.19: Phase 1, PID controller output (Design with dead time included in linear model).

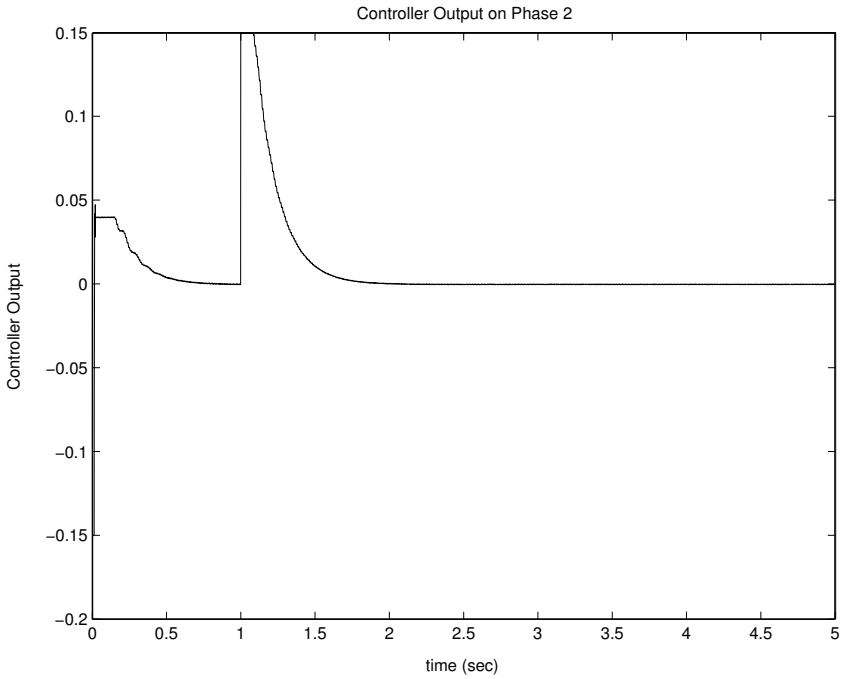

Figure A.20: Phase 2, PID controller output (Design with dead time included in linear model).

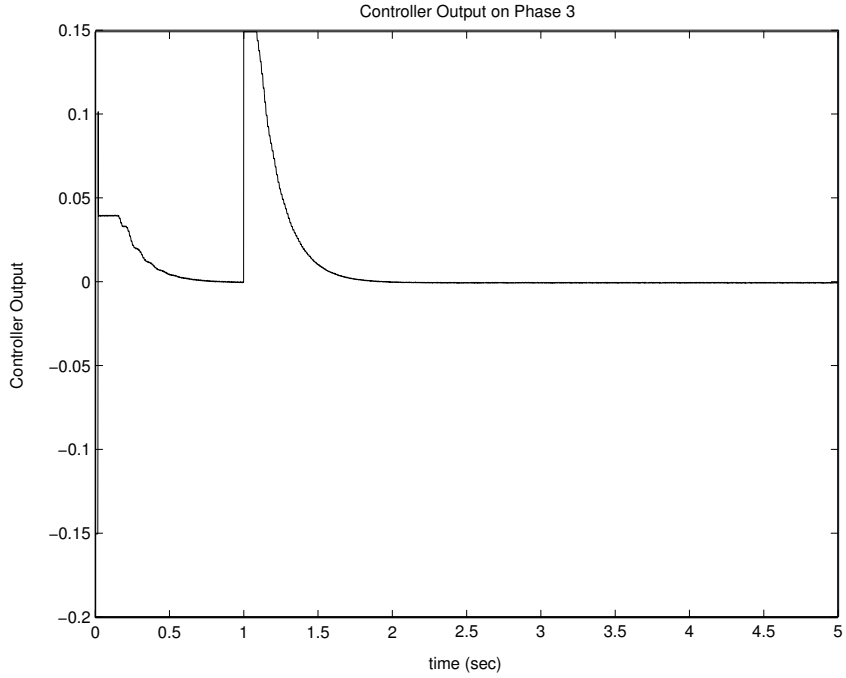

Figure A.21: Phase 3, PID controller output (Design with dead time included in linear model).

The continuous switching between the minimum and maximum values for the servo-valve inputs was also found in this simulation and served once again as the motivation to tune the controllers.

A.5 Model Predictive Controller Outputs with Disturbance Rejection

With disturbance rejection employed the controller outputs are illustrated in figures A.25, A.26 and A.27. These results prove to be most efficient as the switching between positive and negative servo-valve inputs are kept to a minimum.

Note the 0mA inputs to the hydraulic actuator inputs when the piston is required to be at a constant position. Its only when a disturbance occur on one of the phases that the controller outputs are adjusting the position of the hydraulic piston.

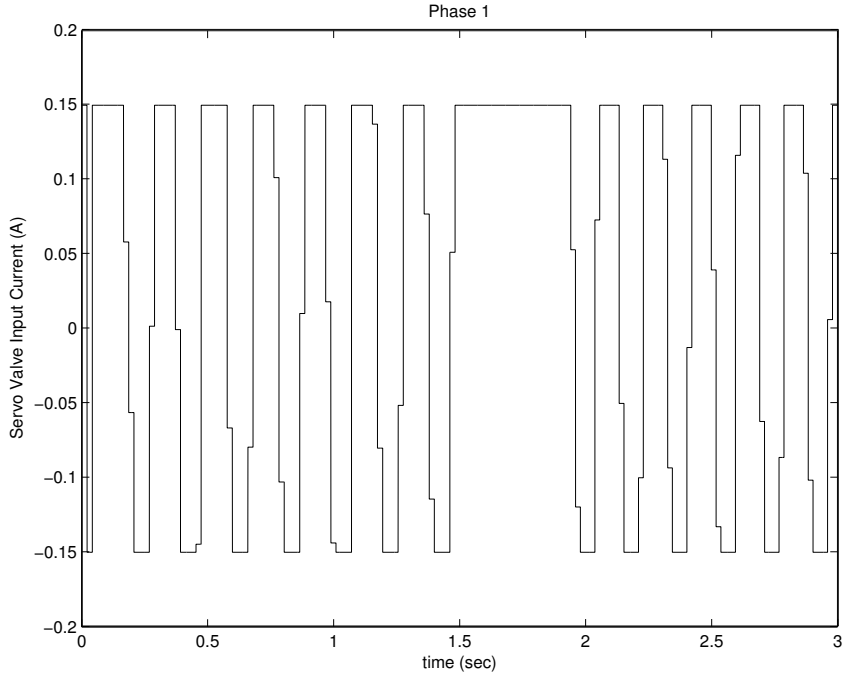

Figure A.22: Controller output for phase 1 with MPC without disturbance rejection employed.

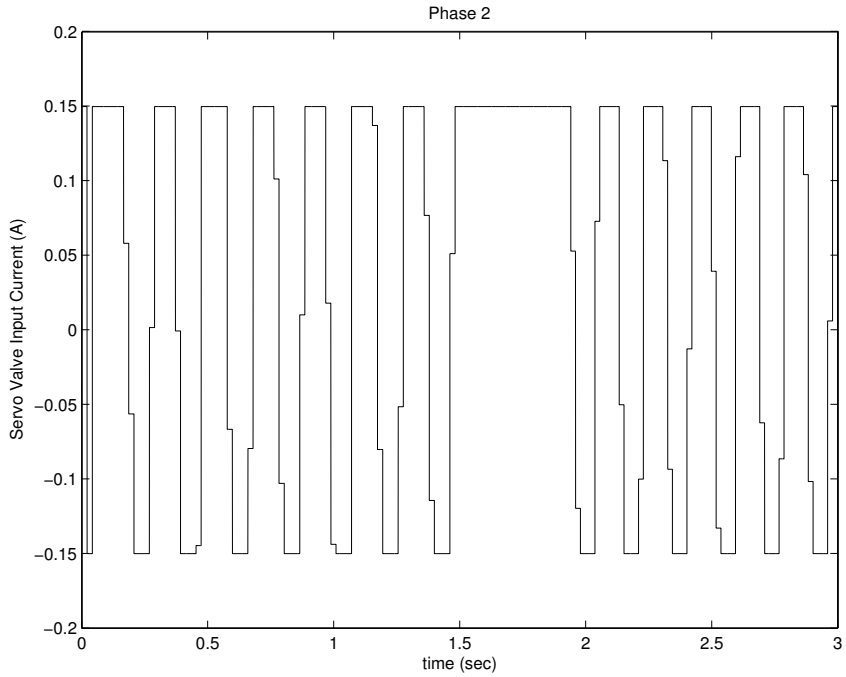

Figure A.23: Controller output for phase 2 with MPC without disturbance rejection employed.

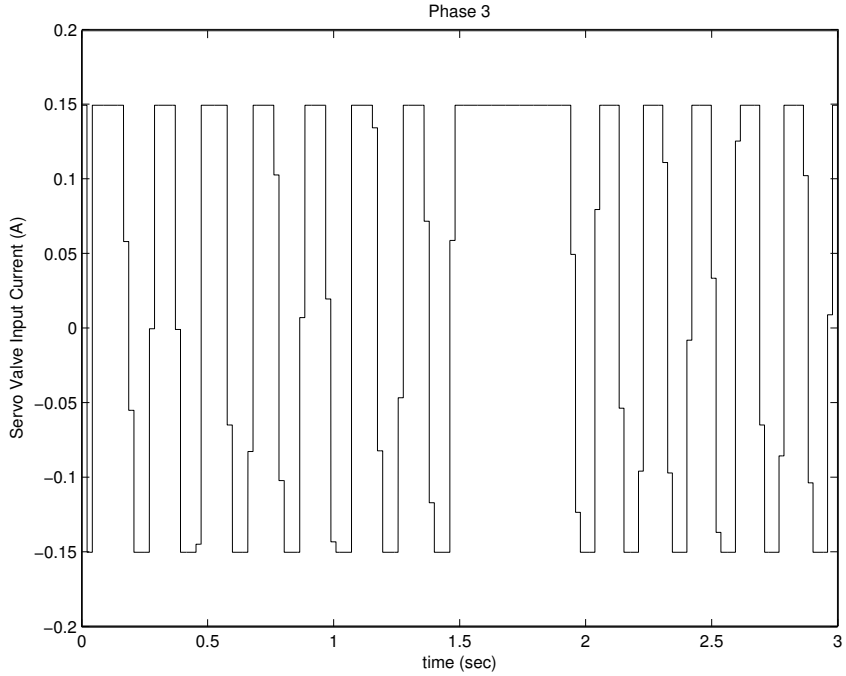

Figure A.24: Controller output for phase 3 with MPC without disturbance rejection employed.

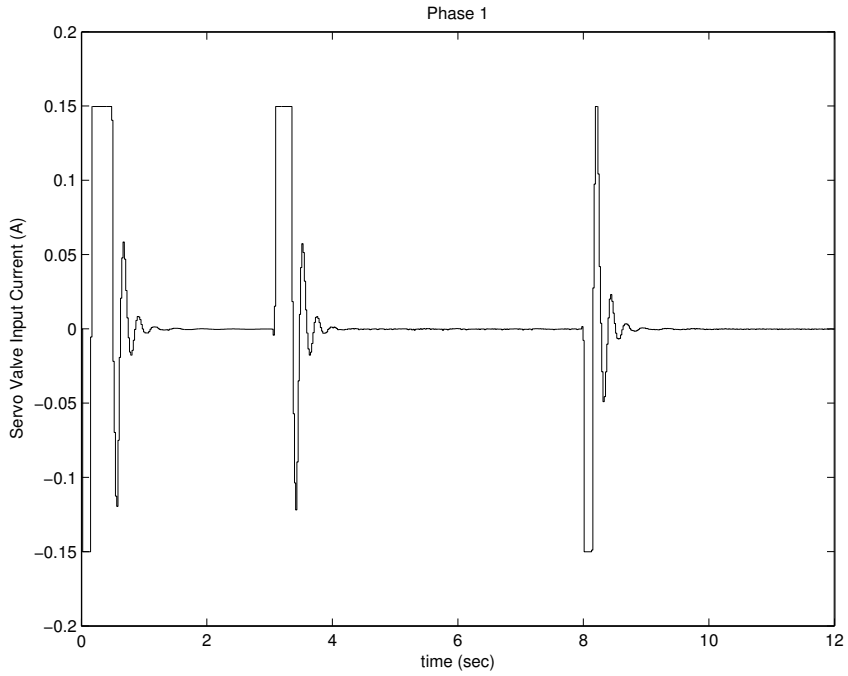

Figure A.25: Controller output for phase 1 with MPC and disturbance rejection employed.

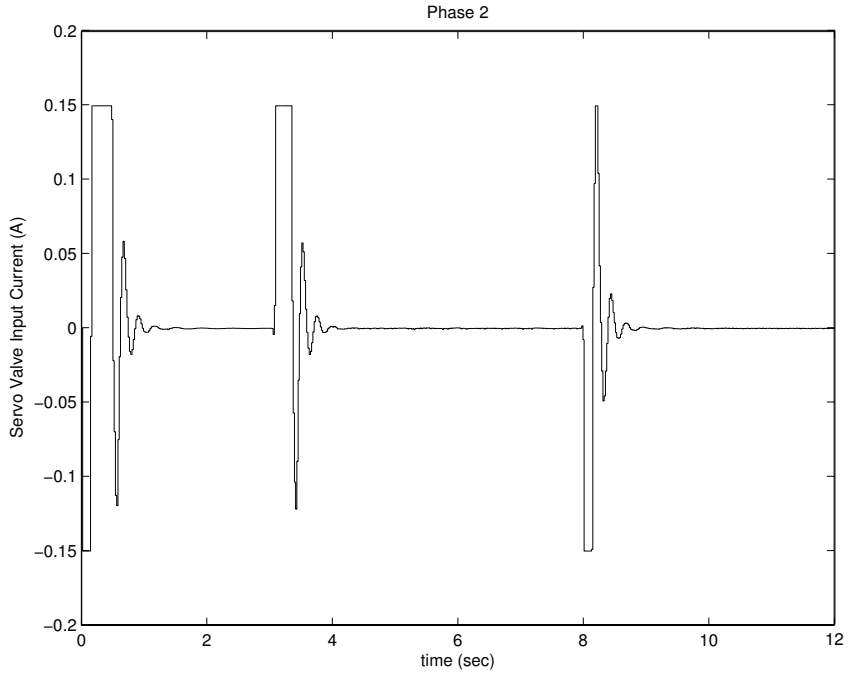

Figure A.26: Controller output for phase 2 with MPC and disturbance rejection employed.

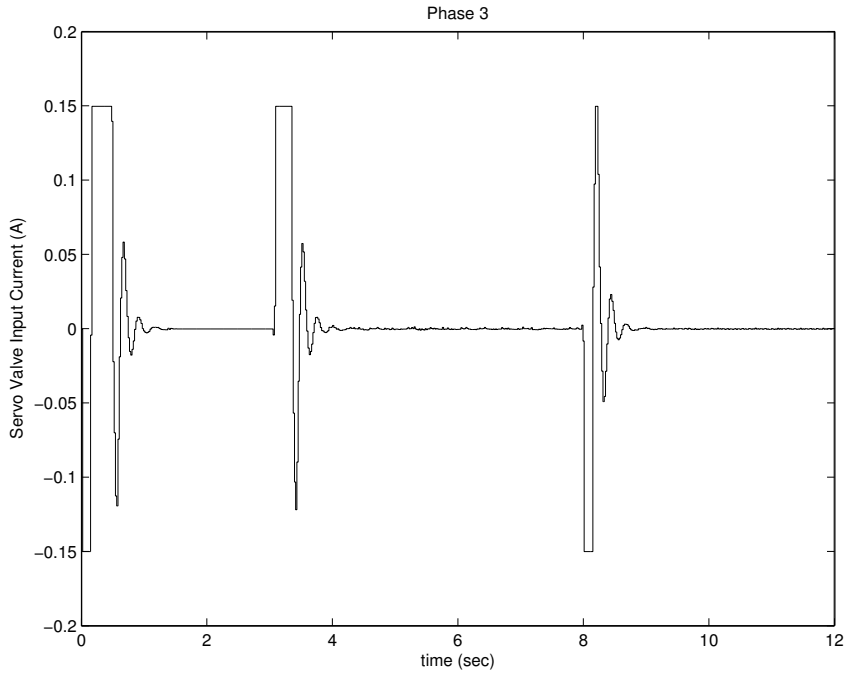

Figure A.27: Controller output for phase 3 with MPC and disturbance rejection employed.

List of Figures

1.1 Flow diagram for the general control problem used in this dissertation [25]. 7

2.1 World crude steel production, 2003/2004. 13
2.2 A typical three-phase electric arc furnace configuration [30]. 14
2.3 Top view of a furnace bath, with the triangular configuration of the graphite electrodes in the center. Also visible is auxiliary burners through the sides of the bath [10], pp. 120b. 15
2.4 Schematic arrangement of a tap changer connected to the primary winding of the furnace transformer [17]. 17
2.5 Delta-connection on the secondary windings of the three-phase furnace transformer ($\sqrt{3}i$ denotes the transformation from the primary to the secondary side) [17]. 17
2.6 Typical power transformation from the high voltage line to the arc furnace and other sectors in a steel plant [17]. 18
2.7 A typical step change in the arc length caused by the melting of scrap steel [40]. If h remains constant and h_0 increases with Δh_0, then the arc length, u_B, will change accordingly. 19
2.8 Electrode position control system to move the electrodes up or down. . . . 20
2.9 Schematic representation of the electrode arms connected to the graphite electrodes [10], pp. 101b. 21
2.10 Typical configuration used for voltage and current measurements in a three-phase electric arc furnace [17]. 22
2.11 Typical flow diagram for a single electric arc furnace heat (constructed from an industrial training manual). 23

3.1 Arcs discharging with a) cathode half-wave and b) anode half-wave. This illustrates the extreme nonlinearity in an electric arc furnace process due to the relative polarity of the electrodes [40]. 30
3.2 Simplified three-phase electrical circuit diagram used to model the supply system. 34
3.3 Hydraulic actuator system for electrode control (Constructed from various industrial data documents). 39

4.1 Connection between the hydraulic and electrical system in a three-phase electric arc furnace. 45

4.2 Supply voltages representing the secondary transformer voltage and also the electrical supply to the electrical system of the three-phase electric arc furnace. . . . 46
4.3 Simulated arc current on a single phase, obtained with the derived electrical model. . . . 47
4.4 Simulated arc resistance (Ω) on a single phase, obtained with the derived electrical model. . . . 48
4.5 Simulated arc conductance on a single phase, obtained with the derived electrical model. Arc conductance is the inverse of arc resistance. . . . 48
4.6 Simulated arc voltage on a single phase, obtained with the derived electrical model. . . . 49
4.7 Arc Voltage vs. Arc Current for a constant arc length of 1cm. . . . 50
4.8 Three-phase arc currents for a balanced system if constant arc lengths are applied to all the phases. This simulation illustrates the 120° phase difference between the respective phases. . . . 51
4.9 Variable arc length applied on phase 1. The arc lengths on phase 2 and 3 are constant at 1cm. The units for arc length above is also in cm. . . . 52
4.10 Simulated arc current obtained with the derived electrical model. . . . 52
4.11 Simulated arc resistance (Ω) obtained with the derived electrical model. . . 53
4.12 Simulated arc conductance obtained with the derived electrical model. . . . 53
4.13 Simulated arc voltage obtained with the derived electrical model. . . . 54
4.14 Arc voltage vs. arc current for variable arc length on phase 1. . . . 54
4.15 Simulated arc current on phase 1 with step changes on all 3 arc lengths. . 55
4.16 Simulated arc resistance on phase 1 with step changes on all 3 arc lengths. 56
4.17 Simulated arc conductance on phase 1 with step changes on all 3 arc lengths. . . . 56
4.18 Simulated arc voltage on phase 1 with step changes on all 3 arc lengths. . 57
4.19 Hydraulic distributor valve position for a servo-valve input of 150 mA for the first 1.5 s and -150 mA for the final 1.5 s. . . . 58
4.20 Hydraulic distributor valve velocity for the servo-valve input of 150 mA for the first 1.5 s and -150 mA for the final 1.5 s. . . . 59
4.21 Hydraulic piston position for the servo-valve input of 150 mA for the first 1.5 s and -150 mA for the final 1.5 s. . . . 59
4.22 Piston velocity for the servo-valve input of 150 mA for the first 1.5 s and -150 mA for the final 1.5 s. . . . 60
4.23 Pressure in chamber 1 for the servo-valve input of 150 mA for the first 1.5 s and -150 mA for the final 1.5 s. . . . 61
4.24 Pressure in chamber 2 for the servo-valve the input of 150 mA for the first 1.5 s and -150 mA for the final 1.5 s. . . . 61
4.25 Servo-valve input current to one of the hydraulic actuators. The inputs to the other two actuators are constant for this simulation. . . . 62
4.26 Piston position for the servo-valve input in figure 4.25. . . . 63
4.27 Arc Current with the electrode position as in figure 4.26. . . . 63
4.28 Arc conductance with the electrode position as in figure 4.26. . . . 64
4.29 Arc voltage with the electrode position in figure 4.26. . . . 64

5.1 Arc conductance as simulated with the electrical amplitude model. 72
5.2 Arc current as simulated with the electrical amplitude model. 73
5.3 Arc conductance simulated with the electrical amplitude model with variable arc length applied to a single phase. 74
5.4 Arc current simulated with the electrical amplitude model when a variable arc length is applied on a single phase. 74
5.5 Arc conductance simulated with the electrical amplitude model when variable arc lengths are applied on all three phases. 75
5.6 Arc current simulated with the electrical amplitude model when variable arc lengths are applied on all three phases. 76
5.7 Linear approximation for hydraulic piston position. 77
5.8 Arc current comparison between the linear and nonlinear model. The accuracy of this comparison is critical, because arc current is the control variable used to maintain constant arc length. Note that this is only a deviation from the operating value. 80
5.9 Arc conductance comparison between the linear and nonlinear model. The accuracy of this variable is not as critical as that of the arc current. 81
5.10 Piston position comparison between the linear and nonlinear model. 81

6.1 Step responses for G_{11} and G_{12}. 84
6.2 PID Control configuration for the linear arc furnace model. 85
6.3 Basic SISO feedback control loop. 86
6.4 Step responses for the SISO close loop system. G_{11} is used as the plant for this simulation. The interactions of other phases are not included here. . . 91
6.5 Frequency responses for the SISO closed loop system. G_{11} is used as the plant for this simulation. The interactions of other phases are not included here. 91
6.6 Close loop step response for the SISO system with limits placed on the controller output. G_{11} is again used as the plant model. The sharp change in the step response is due to the very high open loop gain. 92
6.7 Step response on phase 1 of the linear model. All three phases are stepped simultaneously. This is to illustrate the functioning of the controllers with the interactions of all three phases taken into account. 93
6.8 Step response on phase 2 with the linear model. 94
6.9 Step response on phase 3 with the linear model. 94
6.10 Phase 1, simulated arc current obtained with the nonlinear arc furnace model. The oscillations is due a time delay of approximately 0.25s. 95
6.11 Phase 2, simulated arc current obtained with the nonlinear arc furnace model. 95
6.12 Phase 3, simulated arc current obtained with the nonlinear arc furnace model. 96
6.13 Controlled arc current, phase 1, for the close loop system in figure A.6. . . 98
6.14 Controlled arc current, phase 2, for the close loop system in figure A.6. . . 99
6.15 Controlled arc current, phase 3, for the close loop system in figure A.6. . . 99
6.16 Block diagram for model predictive control [64]. 101
6.17 Simulated arc current on phase 1 with MPC. 103
6.18 Simulated arc current on phase 2 with MPC. 103
6.19 Simulated arc current on phase 3 with MPC. 104

6.20 Simulated arc current on phase 1 with MPC together with disturbance rejection filters. . . . 105
6.21 Simulated arc current on phase 2 with MPC together with disturbance rejection filters. . . . 105
6.22 Simulated arc current on phase 3 with MPC together with disturbance rejection filters. . . . 106

7.1 Arc current as measured on phase 1 together with the desired set-point. . . 109
7.2 Arc current as measured on phase 2 together with the desired set-point. . . 110
7.3 Arc current as measured on phase 3 together with the desired set-point. . . 110
7.4 Measured servo-valve input for phase 1 obtained with the arc current set-point in figure 7.1 . . . 111
7.5 Measured servo-valve input for phase 2 obtained with the arc current set-point in figure 7.2 . . . 112
7.6 Measured servo-valve input for phase 3 obtained with the arc current set-point in figure 7.3 . . . 112
7.7 Simulated and measured arc currents on phase 1 . . . 113
7.8 Simulated and measured arc currents on phase 2 . . . 113
7.9 Simulated and measured arc currents on phase 3 . . . 114
7.10 Simulated servo-valve input on phase 1, for the arc current set-point in figure 7.7 . . . 115
7.11 Simulated servo-valve input on phase 2, for the arc current set-point in figure 7.8 . . . 115
7.12 Simulated servo-valve input on phase 3, for the arc current set-point in figure 7.9 . . . 116
7.13 Simulated arc currents with random disturbances on the arc lengths, phase 1 116
7.14 Simulated arc currents with random disturbances on the arc lengths, phase 2 117
7.15 Simulated arc currents with random disturbances on the arc lengths, phase 3 117

A.1 Phase 1, PID controller output with no disturbance rejection. . . . 130
A.2 Phase 2, PID controller output with no disturbance rejection. . . . 130
A.3 Phase 3, PID controller output with no disturbance rejection. . . . 131
A.4 Close loop frequency response with the initial PID controller implemented on the linear model. This is a typical low pass filter response. . . . 132
A.5 Close loop frequency response with the tuned PID controller implemented on the linear model . . . 133
A.6 Frequency response for the nominal sensitivity function. . . . 133
A.7 Controlled arc current, phase 1, for the close loop system in figure A.6. . . . 134
A.8 Controlled arc current, phase 2, for the close loop system in figure A.6. . . . 134
A.9 Controlled arc current, phase 3, for the close loop system in figure A.6. . . . 135
A.10 Phase 1, PID controller input with disturbance rejection employed via frequency domain analysis. . . . 136
A.11 Phase 2, PID controller input with disturbance rejection employed via frequency domain analysis. . . . 137
A.12 Phase 3, PID controller input with disturbance rejection employed via frequency domain analysis. . . . 137

A.13 Phase 1, PID controller output with disturbance rejection employed via frequency domain analysis. . . . 138
A.14 Phase 2, PID controller output with disturbance rejection employed via frequency domain analysis. . . . 138
A.15 Phase 3, PID controller output with disturbance rejection employed via frequency domain analysis. . . . 139
A.16 Phase 1, PID controller input (Design with dead time included in linear model). . . . 139
A.17 Phase 2, PID controller input (Design with dead time included in linear model). . . . 140
A.18 Phase 3, PID controller input (Design with dead time included in linear model). . . . 140
A.19 Phase 1, PID controller output (Design with dead time included in linear model). . . . 141
A.20 Phase 2, PID controller output (Design with dead time included in linear model). . . . 141
A.21 Phase 3, PID controller output (Design with dead time included in linear model). . . . 142
A.22 Controller output for phase 1 with MPC without disturbance rejection employed. . . . 143
A.23 Controller output for phase 2 with MPC without disturbance rejection employed. . . . 143
A.24 Controller output for phase 3 with MPC without disturbance rejection employed. . . . 144
A.25 Controller output for phase 1 with MPC and disturbance rejection employed. 144
A.26 Controller output for phase 2 with MPC and disturbance rejection employed. 145
A.27 Controller output for phase 3 with MPC and disturbance rejection employed. 145

List of Tables

2.1 Continuously-Cast steel outputs, worldwide and in South-Africa, (Million Metric Tons per Annum). 12
2.2 Steel production via different production routes, 2003/2004. 12

3.1 Typical melting program and the constants affected by the various tap settings on the transformer windings (Obtained from industrial data documentation). 38
3.2 Constants in the electric arc model. These are all constants not affected by the tap settings on the transformer windings. 39
3.3 Constants and variables in the hydraulic model. 42

6.1 Variables used for the implementation of MPC on the electric arc furnace. 102